LUT
Lappeenranta
University of Technology

John Bruzzo Escalante

DYNAMIC SIMULATION OF CROSS-COUNTRY SKIING

Thesis for the degree of Doctor of Science (Technology) to be presented with due permission for public examination and criticism in the Auditorium of the Student Union House at Lappeenranta University of Technology, Lappeenranta, Finland on the 19th of December, 2017, at noon.

Acta Universitatis
Lappeenrantaensis 784

Supervisor Professor Aki Mikkola
LUT School of Energy Systems
Lappeenranta University of Technology
Finland

Reviewers Professor Bernhard Schweizer
Institute of Applied Dynamics
Technische Universität Darmstadt
Germany

Associate Professor José Luis Escalona Franco
Department of Engineering
Aarhus University
Denmark

Opponent Associate Professor Kari Tammi
Department of Mechanical Engineering
Aalto University
Finland

ISBN 978-952-335-190-5
ISBN 978-952-335-191-2 (PDF)
ISSN-L 1456-4491
ISSN 1456-4491

Lappeenranta University of Technology
Yliopistopaino 2017

Abstract

John Bruzzo Escalante
Dynamic Simulation of Cross-country Skiing
Lappeenranta, 2017
120 pages

Acta Universitatis Lappeenrantaensis 784
Dissertation. Lappeenranta University of Technology

ISBN 978-952-335-190-5
ISBN 978-952-335-191-2 (PDF)
ISSN-L 1456-4491
ISSN 1456-4491

The application of simulation techniques in different sport disciplines have become an important asset to coaches, teams and public in general due to the detailed information that different types of simulation techniques can provide. This dissertation work focuses on the study of cross–country skiing from a point of view different than those usual research fields. It studies cross–country skiing from the point of view of the mechanical engineering by applying the concepts of kinematics and dynamics to understand better the biomechanics involved in the skier's movement. There are three main aspects that this dissertation addresses. Firstly, how to simulate the movement of a skier by applying simplified simulation models. Secondly, how to compare the evolution of the skier's technique irrespectively from the variability of the body movement. Finally, how to incorporate to the analysis toolbox other measurement devices such as inertial measurement units which allow for the acquisition of data in a more vast range of conditions such as the study of the effect of the ski pole on the skier's propulsion force. Experiments to validate each one of these three main aspects presented in this dissertation work were carried out in multiple locations with the support of different teams with expertise in fields of sport physiology, physiotherapy and human performance quantification. The main findings showed that the techniques applied and the methodology employed to address the tasks were sound and the numerical results obtained were closed to results acquired in the set of experiments.

Keywords: biomechanics, cross–country skiing, inertial measurement units, multibody modeling, simulation,

Acknowledgments

The research work of this dissertation was carried out during the years 2012–2017 in the laboratory of Machine Design at Lappeenranta University of Technology. Also, during part of 2016 in the laboratory of Dynamics of Human Motion in the University of Michigan, Ann Arbor, USA. The research was funded by the laboratory of Machine Design, Aalto Graduate School of Mechanical Engineering, Lappeenranta University of Technology Research Foundation, and several other research projects. Their support is highly appreciated.

I would like to thank my supervisor Professor Aki Mikkola for providing me the opportunity and means to pursue my doctoral studies in his research team. It was a pleasure to have the opportunity to work with you and learn that the academic life is full of interesting nuances that makes it a pleasing and fulfilling line of work. Also, I would like to thank Professor Noel Perkins from the University of Michigan, USA, for hosting my research exchange in one of the top research groups in the field of human motion performance assessment.

The comments from the preliminary examiners Professor Bernhard Schweizer from Technische Universität Darmstadt, Germany, and José Luis Escalona Franco from Aarhus University, Denmark are highly appreciated. The participation and comments of the opponent of the public examination, Associate Professor Kari Tammi from Aalto University, is also highly appreciated.

Big thanks to all the members, former and actual, of the laboratory of Machine Design over the years for the valuable support in different fields. Special thanks to D.Sc. Marko Matikainen for his extended support during my stay in the laboratory team.

To my loving family, my wife Saricer, my children Shamira, Shamir, Sarah and Saricer, thanks for all your love, support, and for the faith your have in me. Life is easier and with a purpose when you are near me.

Finally, I would like to dedicate this work to the memory of my loved mother. I treasure all your efforts and sacrifices to raise me.

Lappeenranta, December 2017

John Bruzzo Escalante

Symbols

$\boldsymbol{A}$	Rotation matrix
A	Frontal area
a_{max}	Track maximum height
a_{min}	Track maximum height
b	Body
$\boldsymbol{C}$	Vector of constraints
$\boldsymbol{C_q}$	Jacobian matrix of the constraints
$\boldsymbol{C_{qt}}$	Vector differentiated with respect to the constraints and time
$\boldsymbol{C_t}$	Vector of time differentiated constraints
$\boldsymbol{C_{tt}}$	Vector of time twice differentiated constraints
c_d	Dimensionless drag friction coefficient
$\boldsymbol{F}$	Force vector
F_d	Air drag force
F_y	Force component in Y direction
F_z	Force component in Z direction
f	Total friction coefficient, time dependent function
f_d	Dry friction coefficient
f_s	Capillary friction coefficient
f_w	Lubricated friction coefficient
G	Acceleration unit of measurement
h	Time step
$\boldsymbol{i}$, $\boldsymbol{j}$, $\boldsymbol{k}$	Unit vectors aligned with the reference coordinate axes
i	Numbered index, inertia tensor component
j, k	Numbered indexes
l	Leg extension
LS	Left skate mass
$\boldsymbol{M}$	Symmetric mass matrix, vector of moments
$\boldsymbol{N}$	Normal force
n	Number of generalized coordinates
n_a	Integer
n_c	Number of holonomic constraint equations
n_f	Number of force application points
n_{hc}	Number of non–holonomic constraint equations
n_m	Number of applied moments
$\boldsymbol{O}$, $\boldsymbol{G}$, $\boldsymbol{I}$	Reference coordinate system origin
P	Point on body
$\boldsymbol{Q}_e$	Vector of generalized external forces

$\boldsymbol{Q}_v$	Quadratic velocity force vector
$\boldsymbol{q}$	Vector of generalized coordinates
$\dot{\boldsymbol{q}}$	Vector of generalized velocities
$\ddot{\boldsymbol{q}}$	Vector of generalized accelerations
R	Position vector scalar component, Pearson correlation coefficient
$\boldsymbol{R}$	Position vector represented in the absolute reference system
$\boldsymbol{r}$	Position vector represented in the absolute reference system
RS	Right skate mass
t	Time
t_{cycle}	Time length of a stroke
$\boldsymbol{u}$	Position vector
V1, V2	Variations of skate ski technique
$\boldsymbol{v}$	Linear velocity, forward velocity
$\boldsymbol{X}_1$, $\boldsymbol{X}_2$, $\boldsymbol{X}_3$	Reference coordinate axes
$\boldsymbol{X}$, $\boldsymbol{Y}$, $\boldsymbol{Z}$	Reference coordinate axes
X, Y	Time series
x, y, z	Cartesian coordinate scalar
$\boldsymbol{x}$, $\boldsymbol{y}$, $\boldsymbol{z}$	Cartesian coordinate vector
z	Height of the path

Greek letters

α, β	Baumgarte parameters
Δ	Bland–Altman difference
∂	Partial derivative operator
θ	Euler angle
$\boldsymbol{\lambda}$	Lagrange multiplier vector
μ	Sliding friction coefficient
λ	Lagrange multiplier
ρ	Air density, mass density
φ	Euler angle
ψ	Euler angle
$\boldsymbol{\omega}$	Angular velocity vector represented in the absolute reference system
$\bar{\boldsymbol{\omega}}$	Angular velocity vector represented in the body reference system

Abbreviations

3D	Three–dimensional
ANOVA	Analysis of variance
B.C.	Before Christ

CoM	Center of mass
DoF	Degree of freedom
DTW	Dynamic time warping
FBD	Free body diagram
IMUs	Inertial measurement units
ODEs	Ordinary differential equations
SD	Standard deviation, secure digital
SLIP	Spring–loaded–inverted–pendulum
USB	Universal serial bus
ZXY	Euler angle sequence

Chapter 1

Introduction

Skiing has been an important part of life in cultures inhabiting regions where the snow occupies the land for long periods during the year. Where did skiing originate and who was the first skier? The topic is still debated by historians dedicated to finding out the origins of this activity.

Some Chinese archaeologists claim that skiing originated around 8000 B.C. in Altay, China [33]. Others say that skiing came to that area at a later date. Nevertheless, it would be safe to assign an antiquity of 8000 - 10000 years to skiing relying on the discovery of one of the most valuable pieces of evidence, the ski found in Vis, Russia. To date, it is the oldest ski found and it is estimated to date from 6000 B.C. [80].

Pictographs found in Scandinavian and Russian caves support the estimated age of skiing. These rock paintings and carvings dating back to 5000 B.C. confirm the importance of skiing to the people of that time. Figure 1.1 shows the famous rock carving found in a cave in Rødøy, Norway. Figure 1.2 shows another aspect of the daily life of the inhabitants of Alta, Norway. This is the only painting in the Alta area where a skier is represented.

It is interesting to examine the evolution of skiing: how such an ancient practice, normal in the daily facets of old Nordic cultures, continues to evolve from its rudimentary beginnings to its finest technical development seen today. It is even more interesting to see that an activity that originated as a means of subsistence became a social practice reserved for a certain elite during the 1800s in the United States. Figure 1.3 shows a group of people, presumably of a high social class, posing for the photograph in Wasatch, Utah, in 1890.

Skiing definitively continues to be important in countries with snowy winters – now with the added nuance of enjoyment and recreation for the whole family in

Figure 1.1. Rock carving of a skier found in a cave in Rødøy, Norway, circa 4000 B.C. This carving depicts a skier using a stick and a pair of skis. Photo: Nordland County.

Figure 1.2. Pictograph of a skier chasing an elk. Rock painting found in Alta, Norway. This painting is dated circa 5000 B.C. Photo: Ralph Frenken 2012.

any social stratus. This 10000–year–old activity is more than ever in the pinnacle of public interest.

One segment that is continuously striving to learn more about skiing is high–level competitors and their supporting teams. These teams need research–based knowledge on the physiology of different skiing techniques, working to unveil the secrets of the trade. How to be more efficient? How to leverage the physiological differences between the athletes? How to produce more useful propulsion force? These are just a few questions commonly found between the lines of ski literature abstracts.

Figure 1.3. Ski outing in Wasatch, Utah. 1890 (Photos courtesy Special Collections, J. Willard Marriott Library, University of Utah).

1.1 Motivation for the study of cross–country skiing

The topic for this dissertation originated from the research on speed skaters done in 2011 by Fintelman et al. [19] at the Technical University of Delft, the Netherlands. Fintelman's research, led by Prof. Arend L. Schwab, produced a simple two–dimensional multibody model of a speed skater on the straights based on three lump masses: **B** to represent the skater's body mass, and **LS** and **RS** to represent the left and right skates' masses, respectively. This simple model, shown in Figure 1.4, was able to mimic propulsion forces and movements from the center of mass and skates, among other variables, of a speed skater.

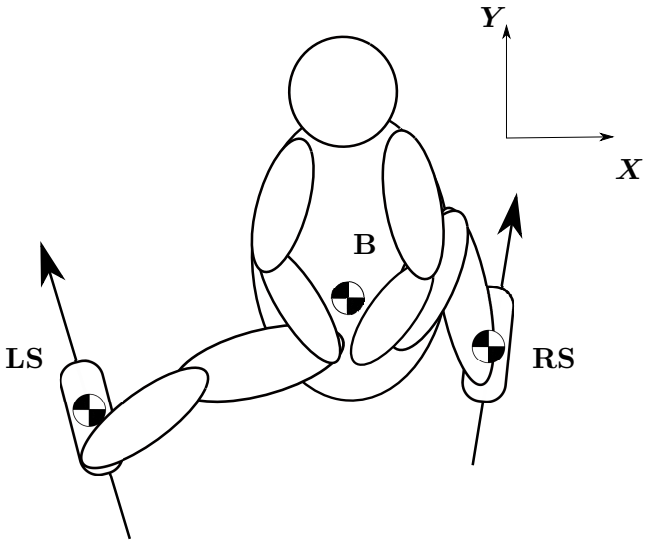

Figure 1.4. Speed skater model proposed by Fintelman et al. [19].

To reduce the complexity of the biomechanics of the speed skater's movement, Fintelman et al. postulated a few simplifications. Among these, the following considerations were made:

- The skater's movement is restricted to two dimensions. This consideration comes from the fact that speed skaters try to maintain the movement of their center of mass on one plane.
- The contact between the ice and skate is modeled as a holonomic constraint in the vertical direction and as a non–holonomic constraint in the lateral direction of this contact.
- A leg extension constraint was used to couple the position of both skates and the center of mass.

To validate the skater's forces and movements, a force measurement system installed on the skates and a combination of motion capture systems were used.

After seeing the results from this simple model, the idea of applying the same concepts to the skier came up. If one compares the movement of the skater to that of the skier performing the skate technique in cross–country skiing, the similitudes are obvious. One of the most relevant differences is that the skier uses poles and the skater does not. A visual comparison can be made using Figure 1.5.

(a) Speed skater [86] (b) Skate skier [42]

Figure 1.5. Techniques performed by speed skaters and skiers: visual similitudes and differences.

After intuitively inferring that the likelihood of using the speed skater model to produce a similar type of multibody model for the skier was high, the scope of the study topic was outlined. In the first phase, the initial concept in mind was to create a simple multibody model of the lower limbs of a skier able to reproduce the skier's center of mass movement by proposing assumptions and simplifications on the lower limbs dynamics.

With this first thought in mind, a literature review on ski multibody models was carried out. However, little information was found on dynamic models applied to cross–country skate style technique. Some of the most relevant articles related to ski modeling will be presented briefly in the following section.

1.2 Review of cross–country skate skiing models

Skate ski style multibody models

The skate style is one of the main techniques present in cross–country skiing. Figure 1.6 shows a high level classification according to Rusko [63] of the techniques and sub–techniques found within cross–country skiing.

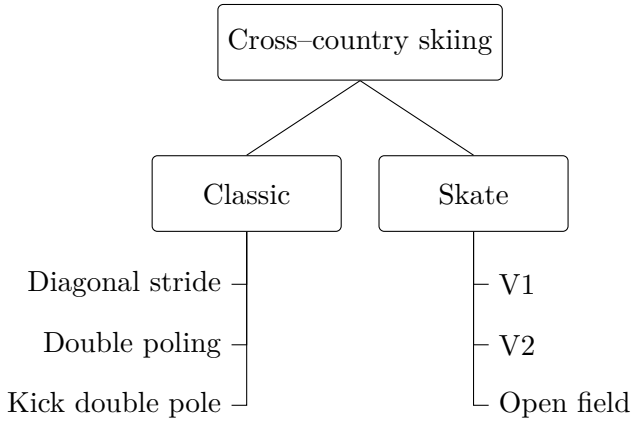

Figure 1.6. Cross–country ski technique classification [63].

The skate style made its official appearance in the 1980s [6,25]. Although the skate technique was not classified as a technique of its own before that, it was already part of the classic skiing technique. Classic skiers skated in step turns, or when certain terrain conditions allowed it. The advent of machinery to mechanically groom snow for the tracks at the end of the 1970s, together with the evolution of the skis' gliding properties, facilitated the debut of the skate skiing technique as a discipline.

The skate style has been around for almost 40 years. However, multibody simulation models describing this specific technique are non existent. This opened an area of opportunity to contribute to the vast amount of scientific literature dedicated to the study of cross–country skiing in other topics as skiing physiology, muscle fatigue, injuries, snow friction, aerodynamics, ski gear design, just to mention a few of these topics.

In the case of the classic style, only a few dynamic simulation models studying some of the sub–techniques of the classic style can be found in the literature. One of the reasons behind the existent number of classic style dynamic models has been attributed to the well coordinated patterns taking place in the saggital plane found in this technique. Due to the symmetry of the skier's movement performing the classic style, it is possible to reduce the modeling complexity to a one dimensional problem [26, 28, 47].

In skate style, modeling this technique can be a daunting task due to the complexity of skiing movement patterns. As expressed in Smith and Holmberg [72], cross–country skate skiing is so rich from the point of view of human movement that researchers are still learning a great deal about human physiology, mechanics, and human motor control. What makes skiing such a special activity are the quadrupedal characteristics of its movement patterns, which are rarely found in other sports. Despite this inherent complexity, it is still possible to simplify the complex patterns in skate skiing to overcome the modeling challenges, as will be seen in the chapters dedicated to the modeling of skiing.

Although the main topic of this dissertation is focused on the skate style, a review of the approaches used to model the classic style is important as some of the assumptions used in classic models can be applied to skate models.

To the best of the author's knowledge, one of the first models of the classic style correspond to upper–body model presented in 2003 by Holmberg and Wagenius [26], followed by another upper–body model published in 2007 by Lund and Holmberg [36] and a full–body model published by Holmberg and Lund [27] in that same year. Later in 2008, Holmberg and Lund [28] modeled again the double poling technique with a full–body model and Moxnes and Hausken [47] proposed a one dimensional model based on differential equations of one particle to simulate the diagonal stride of the classic style.

In 2009, Chen and Qi [11] studied the skier performing simple movements in a two dimensional model consisting of six bodies to represent the skier and in 2010, Oberegger et al. [18] used an inverse dynamic problem to investigate the skier's reaction forces originating from an purely gliding downhill. Table 1.1 summarizes details present in the aforementioned models.

Table 1.1. Published studies in cross–country skiing dynamic models. Papers published by the author of this dissertation are not included.

Reference	Data used	Aim	Method	Findings
Holmberg and Wagenius (2003) [26]	Kinematic data from video recordings and pole forces measured with ergometer.	Propose a first biomechanical skier model which could assist in studying common injuries and muscle activation in double poling.	Two–dimensional inverse dynamic model of the right upper–body. Friction, air drag not considered in the study. Field test done on a tread mill.	Good agreement concerning muscle activation data. However, not good agreement between experimental and simulated power data.
Lund and Holmberg (2007) [36]	Kinematic data from Vicon Motion capture system.	Try to find antagonists to the pectoralis major for a specific movement in cross–country skiing.	Three–dimensional inverse dynamic model of the upper–body of a skier. No pole, friction or ground reaction forces were included in the study.	New method for finding antagonists to a muscle for a specific motion.
Holmberg and Lund (2007) [27]	Two–dimensional motion capture data from a video recorder and pole forces measured with ergometer.	Study the load distribution between the teres major (TD), latissimus dorsi (LD) in double–poling technique.	Three–dimensional inverse dynamic model of the full body of a skier. No friction or ski ground reaction forces were used.	It is possible to study load distribution between TM and LD.
Holmberg and Lund (2008) [28]	Two–dimensional motion capture data from a video recorder and pole forces measured with ergometer.	Create a three–dimensional full–body that can handle realistic external loads and to test the use of inverse dynamics and static optimization in this kind of models.	Three–dimensional inverse dynamics multibody model of the right upper–body and pole. Constrained Newton–Euler equations. No friction or ski ground reaction forces were used.	Muscle forces output which are used for comparison with data obtained from the literature.

Table 1.1. Continued.

Reference	Data used	Aim	Method	Findings
Moxnes and Hausken (2009) [47]	Two–dimensional video analysis, electromiography (EMG), and joint angles measured by goniometers. Planar forces taken from [81].	Formulate a mathematical model to increase skier performance based on the study the effect of the kicking forces, friction and ski waxing on the diagonal stride skiing.	One–dimensional forward dynamic model based on Newton's equations. Hill muscle model was used to represent kicking forces. Ski–snow friction modeled as Coulomb friction force.	The kicking angle, terrain and waxing affect the velocity achieve by the skier. Additionally, the optimal mechanic characteristics of the skis used have to adapt to the conditions find in the terrain.
Chen and Qi (2009) [11]	Data from ski movement simulations.	Two–dimensional inverse dynamic model based on Newton–Euler equations.	The forces considered by this model are the ski–snow interaction (penetration), air drag and ski–snow friction introduced as a Coulomb friction force. Ski–snow contact simulated as a planar joint.	The model mimics simple types of movements and can provide kinematic and kinetic data (not shown) such as the skier's displacement, velocity, acceleration, joint moment and force, and ground reaction forces. Focused on the behavior of the ski.
Oberegger et al. (2010) [18]	Video camera systems is used to acquired kinematic data and force plates installed under the two and heel of the right ski are used to obtaining the force validation data.	Three–dimensional inverse dynamic model based on constrained Newton–Euler equations. Air drag was neglected and ski–snow friction introduced as a Coulomb friction force.	Slope, track of the right ski, and driving constraint for the right ski specified by the user. This one degree of freedom three dimensional model is represented by seven bodies. The forces considered are gravity and ski–snow friction modeled as Coulomb friction. Kicking forces are not considered in this model.	The model yields reaction forces comparable with those obtain from force plates fixed under the toe and heel of the right ski.

Estimation of orientation of ski poles

In some techniques, ski poling is essential. As an example, in the double poling technique of the classic style, poling is one of the largest producers of forward motion [25, 32, 46, 88]. To measure the forward propulsion forces that ski poles

add to the skier, a set of four variables are needed: pole ground contact force and its direction, pole orientation in space, and pole–ground contact intervals. Figure 1.7 shows a simple body diagram of the pole forces generated in the double poling technique and Figure 1.8 shows the poling forces in the skate style.

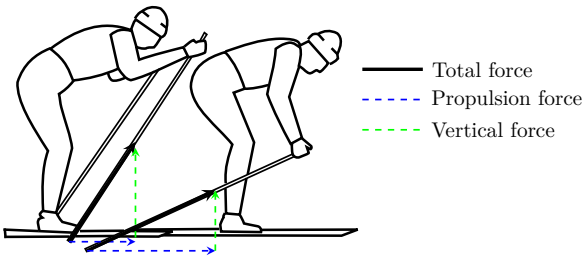

Figure 1.7. Progression of the forces produced in the double poling technique represented in the sagittal plant [63].

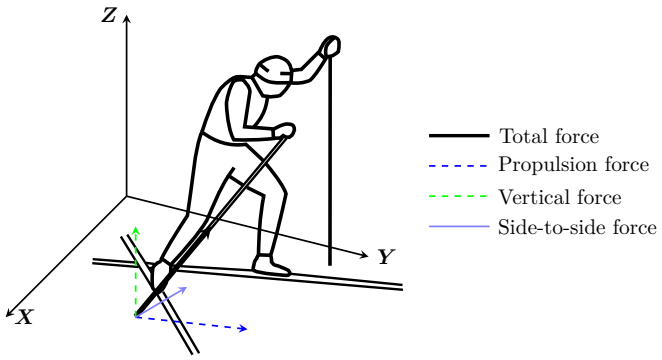

Figure 1.8. Forces produced by the poles in skate skiing [63].

In this dissertation, the researcher is interested in investigating and proposing a new technique to estimate the orientation of the ski pole in space. In the case of the measurement of the pole force, researchers have measured them using different techniques such as: force plates [32, 52, 81], ergometers [26–28], or force transducers installed on the poles [5, 15, 25, 45, 53, 55, 57, 58, 74, 76, 77, 88].

Each of these force estimation methods come with certain advantages and disadvantages. The amount of validated studies demonstrate that depending on the method, they might be suitable for long–run applications. However, methods for measuring the orientation of the pole and pole–ground contact intervals or pole plant and pole lift have an interesting area of opportunity for further development.

In the scientific literature, three methods are commonly used to estimate the orientation of the pole. These methods can be grouped into optical motion capture systems, video recording, and goniometers. To detect the pole–ground contact

intervals, methods based on optical motion capture systems, force value threshold, video camera recorders, and inertial measurement unit (IMU) systems are used. Table 1.2 presents a summary of the scientific literature related to estimating pole orientation and pole–ground contact.

Table 1.2. Published studies related to ski pole orientation estimation and pole–ground contact detection.

Reference	Orientation estimation	Pole – ground contact detection	Comments
Smith et al. (1989) [73]	Pole orientation was estimated by inspection of video recordings.	Pole–ground contact detection was done by inspection of video recordings.	Pole data was used to correlate V1 technique cycle variables among participants of the 1988 Calgary Games.
Millet et al. (1998) [45]	Not performed.	Pole–plant occurred when force was greater than 27 N and pole–lift occurred when force had a negative value (pole extension).	Experiments done in the skate style V2 technique.
Canclini et al. [10]	Pole orientation was estimated by inspection of video recordings.	Pole–ground contact detection was done by inspection of video recordings.	Pole data was used to analyze the different variants among skiers performing the same technique. Experiments done in the classic style.
Nilsson et al. (2003) [51]	Optical motion capture system.	Not performed.	It was possible to calculate pole angles in the sagittal plane by utilizing the positions of the reflective markers. Experiments done in the classic style double poling technique.
Holmberg et al. (2005) [25]	Not performed.	Force data was used to determine ground–pole contact. Threshold values were not specified.	Pole data was used to analyze the poling cycle rate within the experiment. Experiments done in the classic style double poling technique.

Table 1.2. Continued.

Reference	Orientation estimation	Pole – ground contact detection	Comments
Zory et al. (2009) [88]	Pole orientation was estimated by inspection of video recordings.	Pole–ground contact detection was done by inspection of video recordings.	Pole data was used to analyze poling cycle rating and technique to understand the effect of kinematic parameters in the fatigue of professional skiers. Experiments done in the classic style, double poling.
Stöggl and Holmberg (2011) [74]	Optical motion capture system.	The vertical position of the pole tip was used to detect the pole–ground contact.	Pole data was used to analyze the correlation between pole angles and skiing speed. Experiments done in the classic style, double poling technique.
Pellegrini, Bortolan and Schema (2011) [57]	Optical motion capture system.	A force threshold of 10 N was used to detect the pole–ground contact.	Pole angles were used as part of the calculation of the mechanical work for each of the experiments when varying the inclination of the track. Experiments were done in the classic style diagonal stride.
Stöggl and Karlöf (2013) [75]	Optical motion capture system.	The vertical position of the pole tip was used to detect the pole–ground contact.	The three–dimensional kinematics of the ski poles were used to assess the bending behavior of ski poles with different cross–sections. Softer poles demonstrated greater bending resulting in lower performance for some skiers. Experiments done in the skate style V1 technique.

Table 1.2. Continued.

Reference	Orientation estimation	Pole – ground contact detection	Comments
Pellegrini et al. (2014) [58]	Optical motion capture system.	A force threshold of 10 N was used to detect the pole–ground contact.	Pole angles were used as part of the calculation of the mechanical work for each of the experiments. Experiments were done in the classic style diagonal stride, double poling, and double poling with kick.
Federolf et al. (2014) [17]	Orientation was estimated by video recordings.	Pole–ground contact detection was done by inspection of video recordings.	Pole data was used to analyze the different variants among skiers performing the same technique.
Myklebust, Losnegard, and Hallén (2014) [50]	Not performed.	Jerk, span and acceleration data obtained from IMUs are used to locate the pole–ground contact events. Validation was made by means of video recording.	This algorithm allows to detect pole cycle ratings that can be used to automatically detect V1 to V2 technique changes in the skate style.
Fasel et al. (2015) [16]	Not performed.	IMUs acceleration values were used to detect pole–ground contact. Validation was made by meas of optical motion capture system.	IMU data–based algorithms were used to automatically detect pole–ground contact events. Experiments done in the classic style, diagonal stride technique.
Stöggl and Holmberg (2016) [76]	Optical motion capture system.	The vertical position of the pole tip was used to detect the pole–ground contact.	The three–dimensional kinematics of the ski poles were used to assess the differences in the classic style double poling technique in flat and uphill conditions.

After analyzing the information found in the scientific publications, two hypotheses were postulated on the topics of ski pole orientation estimation and pole–ground contact detection. The first hypothesis referred to be able to estimate the ski pole orientation using the information obtained from the IMU system: acceleration and angular velocity by means of a sensor fusion algorithm.

The second hypothesis pointed out to utilize a generalization of the ski pole's movement during skiing. The ski pole movements can be roughly seen as two different phases: swing phase when the ski pole is not in contact with the ground, and inverted pendulum phase while the ski pole is contacting the ground. The researcher considered that it would be possible to develop a different method to detect pole–ground contacts taking advantage of the kinematic relationships occurring during the phases of the the ski pole movements.

1.3 Objective and scope of the dissertation

The objective of this dissertation is to present three main components of a dynamic analysis system for cross–country skiing. Firstly, cross–country skiing is viewed from the perspective of the multibody dynamics theory. As commented in the section dedicated to the motivation to study cross–country skiing, this research started from the multibody model of a speed skater done in the Netherlands. The author of this dissertation produced two simple multibody models during his doctoral studies. However, as also previously mentioned, these models involved an important simplification: the skier performs the technique without poles.

Secondly, to compare results from different athletes and measurement systems, the dynamic time warping (DTW) method widely used in voice recognition systems was adapted as a comparison tool in skiing dynamics. DTW allows forming a baseline which serves as a comparison line between athletes' results and the measurement systems' accuracy. Baselines are not commonly seen in scientific literature, but they help in monitoring the evolution of an athlete's technique and provide us with a comparison tool to understand the specifics of the performance of different athletes.

Lastly, the poles, which were excluded from the initial multibody models, are studied independently using IMUs.

1.4 Outline of the dissertation

This dissertation comprises the following chapters.

Chapter 1: Introduction

The introductory chapter concisely presents, the origins of this research topic. It briefly describes the history of skiing and its importance to certain countries in the world and the study that served as foundation to develop the first skate skiing dynamic models. A literature review on the relevant areas contemplated by this dissertation form an important section of the introductory chapter. The objectives and scientific contribution are also outlined in this chapter.

Chapters 2 and 3: Cross–country skiing multibody models

These chapters present two multibody models and their results. The first simple model provides a simplified version of the skier's leg movement, which is presented as if it were a hydraulic cylinder. In the second model, extension of the first simple model, a configuration closer to reality is introduced.

Chapter 4: Assessment of the skier technique's evolution

This chapter describes the DTW and its use to compare results from two different motion capture systems. This method is also proposed to create baselines to evaluate the evolution of the athlete's technique.

Chapter 5: Dynamics and kinematics of ski poles

This chapter introduces a new method for calculating kinematic parameters of ski poles. Two important variables are studied here: the pole–ground contact detection and the estimation of the ski pole relative orientation in space.

Chapter 6: Conclusions

Conclusions on the work done in the dissertation are provided here. Additionally, lines of action for future work related to the subjects covered in this dissertation work are outlined.

1.5 Scientific contribution and published articles

This dissertation provides the following scientific contributions:

- A simple skate skiing model able to mimic the movements of the center of mass of a skate skier during several strides. The importance of this simple model is that with a system of three bodies, the simplification of the skier's leg joints, and a set of non–natural leg movement prescriptions, the center of mass trajectory and the skier's overall velocity can be estimated to a certain

extent. The skier's leg joints are represented as follows: the foot–shank constraint is represented as a spherical joint, and the shank–thigh relative movement is described using a prismatic joint. The movement of the skier is considered symmetrical, which introduces the first differences with respect to the actual movement of the skier, which may be asymmetrical. The differences found in the trajectory lie in the amplitude of the movement. The frequency of the skier's movement matches that of the real experiment. The resultant velocity differs from the real skier's velocity in values around 10.78%.

- A extended second ski–skating dynamic model consisting of a more detailed description of the skier's leg which allows to estimate leg propulsion forces. This leg model uses two spherical joints to describe the relative movements of the foot–shank and shank–thigh relative movements. Similarly to the first model above, this dynamic model employs three bodies to represent the totality of the skiers body. The inertia parameters of the leg are constructed from statistical data found in the literature. This allows the automatic generation of these parameters without the cumbersome detailed measurement of the typical topological landmarks to calculate precisely the mass and inertia of the body segments. The leg force obtained from this model resembles the force measured using dedicated force sensors installed in the ski bindings. The closeness of the simulated and measured leg force is presented using the Pearson correlation factor, which for the case presented in this dissertation is 0.94. The additional use of Bland–Altman plot reinforces the affinity of the simulated and measured force data by showing 95% agreement between the analyzed data sets.

- A tool is needed to monitor the evolution of the technique in different athletes or to compare the execution of the technique among different practitioners and thus understand where the differences lie. For this case, a method widely used to analyze sounds is implemented. The method is based on the dynamic time warping (DTW) approach that compares two time–based data sets indistinctly of the amount of sample points within the same time frame. The method based on imposing constraints to select which pair of data sets should be compared uses a distance cost function to estimate how far apart those points are in the data set pair. This cost function depends on the type application and the careful selection of this cost function is key to produce outputs for easy comparison. For the studied data sets, it was observed that using the definition of the Manhattan distance works best for most cases in human gait.

- Lastly, one of the important components of the skier gear set are the ski poles that provide the skier with propulsion force originating in the arms

and trunk. The influence of the ski poles has been assessed in highly controlled conditions mainly because of the diversity of movements in the use of poles and the complex level of measurement instrumentation required. As the poles are located away from the skier's body and can be detached from the skiers hands, the data collection becomes difficult. To overcome these limitations and to employ a system able to provide data not only in controlled conditions but in the long run, IMUs are exploited. Using IMUs, the orientation (roll and pitch angles) of the poles is estimated during movement. Tests performed on Nordic walking confirmed the possibility of estimating the ski pole orientation, and with the additional use of a force sensor it would possible to propose an algorithm to calculate the component of the ski pole force influencing the skier's forward movement positively.

Part of the results presented in this dissertation were published in the following conferences and journal:

- Bruzzo, J. Schwab A. L., Mikkola, A., Ohtonen, O., and Linnamo V. A simple Multibody Dynamic Model of Cross–Country Ski–Skating. ASME 2013 International Design Engineering Technical Conferences and Computers and Information. Portland, Oregon, August, 2013.
- Bruzzo, J., Schwab, A. L., Mikkola, A., Valkeapää, A., Ohtonen, O., and Linnamo, V. A Simple Mechanical Model for Simulating Cross–Country Skiing Propulsive Force. ASME 2015 International Design Engineering Technical Conferences and Computers and Information in Engineering Conference, 2015.
- Bruzzo, J., Schwab, A. L., Valkeapää, A., Mikkola, A., Ohtonen, O., and Linnamo, V. A simple mechanical model for simulating cross–country skiing, skating technique. Sports Engineering, 1 - 14.

Chapter 2

First simple skier simulation model

This chapter describes a simple multibody model of a cross–country skier employing the skate skiing technique on a flat surface with a slight incline. The formulation process will be described starting from the selection of the multibody approach, following with experiments to obtain data for the validation process, and the final results.

2.1 Assumptions in the description of the multibody model

The objective of this first model is to mimic the skier's center of mass movement by utilizing an equivalent body configuration to that of the skier. This model proposes to simplify the skier's body configuration – number of body segments – by considering three bodies and a set of arbitrarily selected motion laws. The ski, lower leg, and upper leg serve as a simplification for this purpose. One special characteristic of this proposed model is that the interactions between these three parts are represented differently from the real physiological relationships.

Studying the cross–country skate skiing technique through simple models is a useful approach to describing and evaluating general questions, ideas, and the specific phenomena under investigation. Also, they can be used as a means of evaluating the different paths to follow when the decision of increasing the complexity of the model is considered [84].

The following key points have been addressed to build and limit the skier model:

- Selection of the multibody dynamic theory to develop the equations of motion of the skier model.

- Construction philosophy and objectives of the skier model.
- Details on the construction of the skier equations of motion.

2.2 Multibody dynamic theory selected

The multibody dynamics formulation used in this research is based on the augmented Lagrangian formulation [65, 69, 70]. Some of the advantages of the augmented formulation are [7, 14, 20, 70]:

- The augmented formulation is widely used in multibody simulation models.
- Multibody models based on the augmented formulation allow the systematic introduction of non-linear constraints or force functions and thus the automation of the equations of motion formulation process.
- The motion of the bodies are often described using absolute Cartesian and orientation coordinates.
- Using similar sets of coordinates makes it easy to add and remove bodies and joints to the model.
- The constraint forces appear in the final form of the equations of motion.
- The equations of motion can be solved when the system is close to a singular position or when in presence of redundant constraints.

One of the most important drawbacks of the augmented formulation is the increasing number of generalized coordinates and equations to be solved. Despite of this, sparse matrix structures can be used to solve efficiently the simple set of differential algebraic equations product of using this redundant set of generalized coordinates.

2.3 Construction and objectives of the skier model

One of the simplest form that the skier model can have is the form adopted by Fintelman in the speed skater model [19]. One of the main differences between the speed skater model and the skier model is the number of axes where the models are constructed. In the case of the speed skater model, Fintelman limited the study to a two–dimensional plane. The hypothesis used to consider only a planar representation was that the planarity of the movement of the center of masses of speed skaters is equivalent to a better throughput in their performance. This statement seems to be taken from experienced coaches and athletes in this

discipline. Further validation of the planarity statement is at the moment not available in scientific reports.

In the case of the skier model, common knowledge of experienced athletes and coaches exclude the planarity hypothesis and focus more on the resultant gliding direction of the ski in skate skiing or force–kick coordination in classic skiing. Then, the planarity hypothesis used in the speed skater model is left out of the consideration in the skier model.

Taking into account a three–dimensional or three axes representation for the skier model, one of the simplest forms this model can have is presented in Figure 2.1.

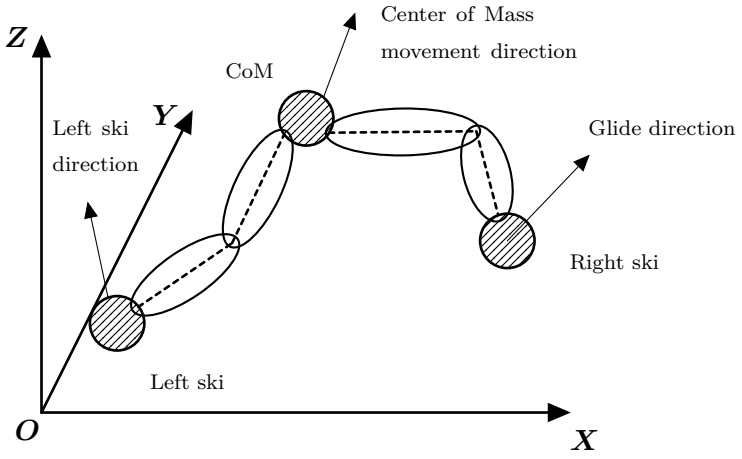

Figure 2.1. Simplest version of a skier model taking as a reference the speed skater model from Fintelman.

As this model is analyzed in a stroke–by–stroke basis, meaning that the dynamic analysis is done for every half of one skiing cycle, it is possible to identify two modeling stages. One of these stages can be when the left leg is pushing while the right leg is gliding and the second stage is the complementary action to this first stage which is when the right leg is pushing while the left leg is gliding. These stages are clearly divided by the instants when the pushing ski is not longer in contact with the snow. Figure 2.2 shows the equivalent model representation for a half phase or one stroke. Additionally, it is assumed that in the skiing cycles, the strokes mirror each other symmetrically. Figure 2.3 shows this assumption.

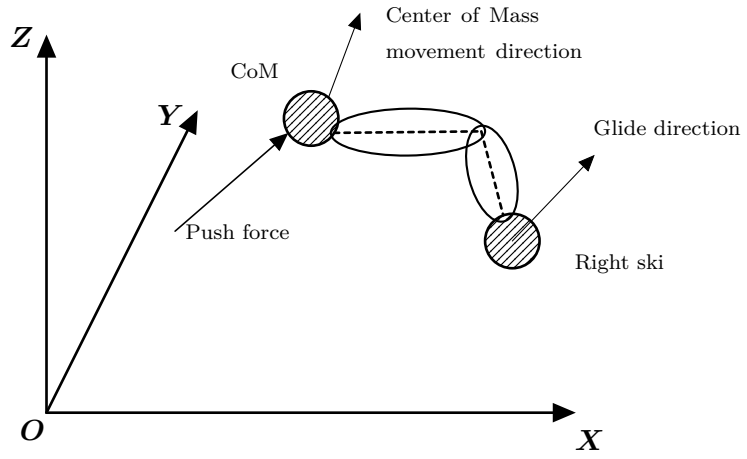

Figure 2.2. Reduced model considering just one stroke or half skiing cycle. The left ski is substitute by its pushing force applied in the CoM of the skier.

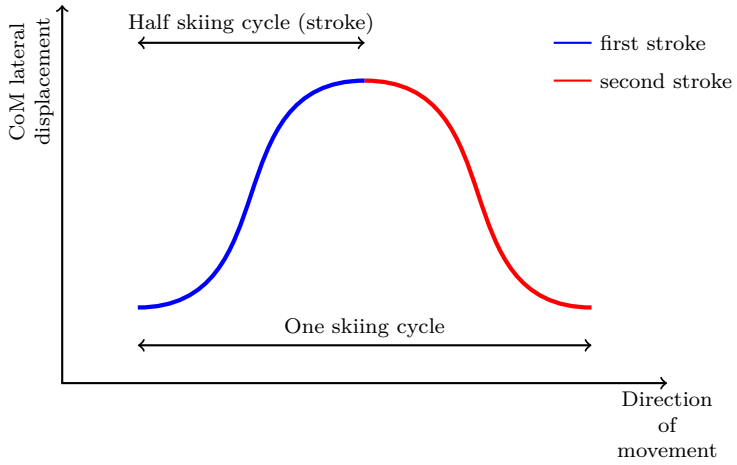

Figure 2.3. Description of the mirror–symmetric skiing cycles considered in the assumptions of the ski model.

The model presented in Figure 2.2 could be described with six generalized coordinates: three generalized coordinates x, y, and z to describe the position of the right ski and three coordinates that describe the position of the center of mass. The three generalized coordinates that represent the position of the CoM correspond to two orientation angles θ and ψ of the line formed between the CoM point and the right ski, and the distance l of the CoM with respect to the right ski. Figure 2.4 represents graphically these six coordinates.

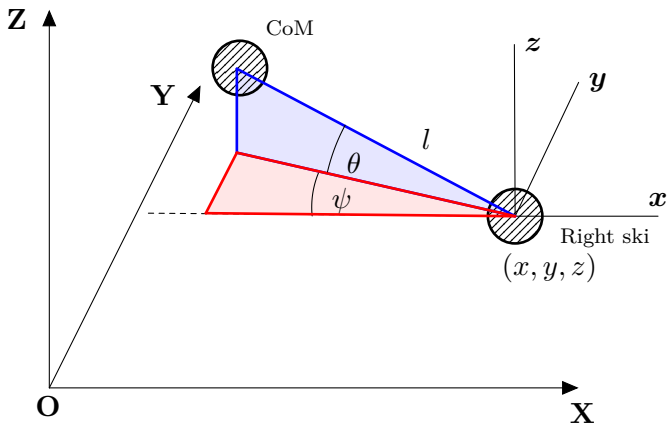

Figure 2.4. Representation of the minimum set of generalized coordinates that can be used to describe the simple skier model.

Considering future developments of this initial skier model, a similar case to the SLIP (spring–loaded–inverted–pendulum) gait simulation model first proposed by Full [22] and lately developed further by Poulakakis [61] and Millard [44] was adopted. The SLIP model is a technique to model gait in the sagittal plane. Figure 2.5 shows the SLIP model presented by Poulakakis.

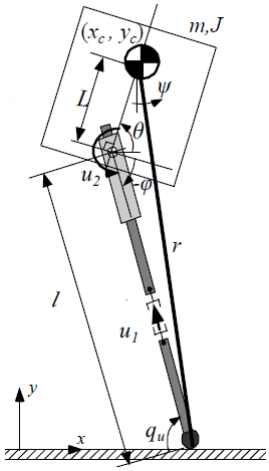

Figure 2.5. SLIP model proposed by Poulakakis [61]. The terms presented in this figure are defined in the original manuscript by Poulakakis.

The final three–dimensional representation of the simple skate skier model adopted resembles the one presented in Figure 2.5 with variations in the number of generalized coordinates used to describe the laws of motion of the skier. Figures 2.6 and 2.7 present the adopted skier model and how it resembles the skier's lower limbs, respectively.

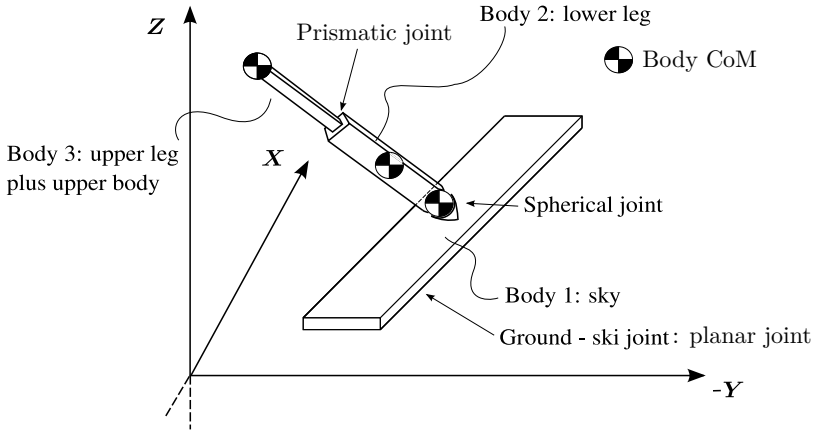

Figure 2.6. Description of the simplified multibody model of the skate skier.

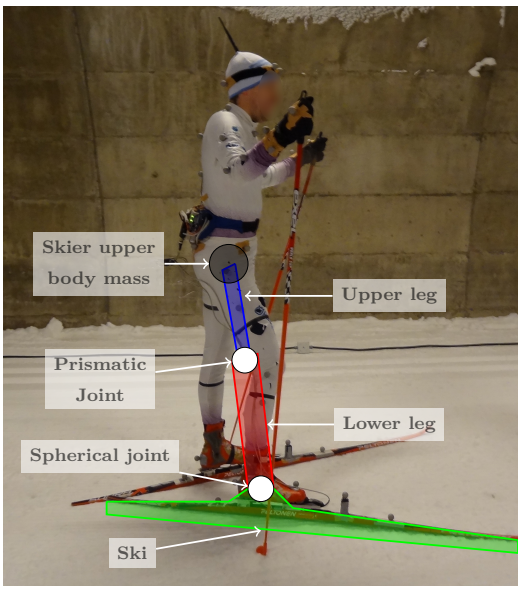

Figure 2.7. Description of the lower leg configuration in the first skier model. The joints utilized in this model are a simplification of the natural relative movements in the human leg.

The initial objective of this model was to mimic the movement of the CoM of the skate skier. The number of generalized coordinates in the skier model was 18. This corresponds to account for six degrees of freedom in each of the three bodies used to represent the skier's lower leg. Due to the configuration selected for the skier model, the resultant number of DoF is one. This DoF represents the movement of the ski on the gliding direction. The model is a mixture between a kinematically driven system and a force driven system. Five rheonomic constraints are imposed in the model in addition to the 12 geometric constraints used to represent the movement relations between the model's bodies.

At the present stage, the model produces the trajectory and velocity of the skier's CoM as a direct output from integrating the equations of motion of the model. Indirectly, it could output the constraint forces from which, some interesting data might appear.

2.4 Equations of motion of the skier model

The skier's equations of motion formulated according to the augmented formulation can be written as follows:

$$\begin{bmatrix} \boldsymbol{M} & \boldsymbol{C}_{\boldsymbol{q}}^{\mathrm{T}} \\ \boldsymbol{C}_{\boldsymbol{q}} & \boldsymbol{0} \end{bmatrix} \begin{bmatrix} \ddot{\boldsymbol{q}} \\ \boldsymbol{\lambda} \end{bmatrix} = \begin{bmatrix} \boldsymbol{Q}_e + \boldsymbol{Q}_v \\ \boldsymbol{Q}_d \end{bmatrix}. \tag{2.1}$$

In Equation (2.1), $\boldsymbol{M}$ is the mass matrix of the system, $\boldsymbol{C}_{\boldsymbol{q}}$ is the constraint Jacobian matrix, $\ddot{\boldsymbol{q}}$ is the vector of generalized accelerations, $\boldsymbol{\lambda}$ is the set of Lagrange multipliers, $\boldsymbol{Q}_e$ and $\boldsymbol{Q}_v$ are, respectively, the vector of external forces and the quadratic velocity vector, and $\boldsymbol{Q}_d$ is the vector that arises after taking the second differentiation of the vector of constraints.

In the remaining part of this section, the terms comprising the skier's equations of motion will be described starting with the vector of generalized coordinates of the system.

Vector of generalized coordinates $\boldsymbol{q}$

Each body conforming the skier model has six generalized coordinates. Equation (2.2) presents the vector of generalized coordinates $\boldsymbol{q}$ of the whole model.

$$\boldsymbol{q} = \begin{bmatrix} \boldsymbol{q}^{1\mathrm{T}} & \boldsymbol{q}^{2\mathrm{T}} & \boldsymbol{q}^{3\mathrm{T}} \end{bmatrix}^{\mathrm{T}} \tag{2.2}$$

In Equation (2.2), $\boldsymbol{q}^i = \begin{bmatrix} R_x^i & R_y^i & R_z^i & \varphi^i & \theta^i & \psi^i \end{bmatrix}^{\mathrm{T}}$ with $i = 1, 2, 3$ representing the bodies of the model, R_x^i, R_y^i, and R_z^i are the translational coordinates of

the origin of the body i reference system with respect to the absolute reference system, and φ^i, θ^i and, ψ^i are the Euler angles used to represent the orientation of the body reference system.

The applied sequence of Euler angles is ZXY. This Euler angle sequence allows introducing some similar leg angular movements during the performance of the active phase of the skier in accordance with the data obtained from the Vicon motion capture system. Figure 2.8 presents how the body reference systems are oriented.

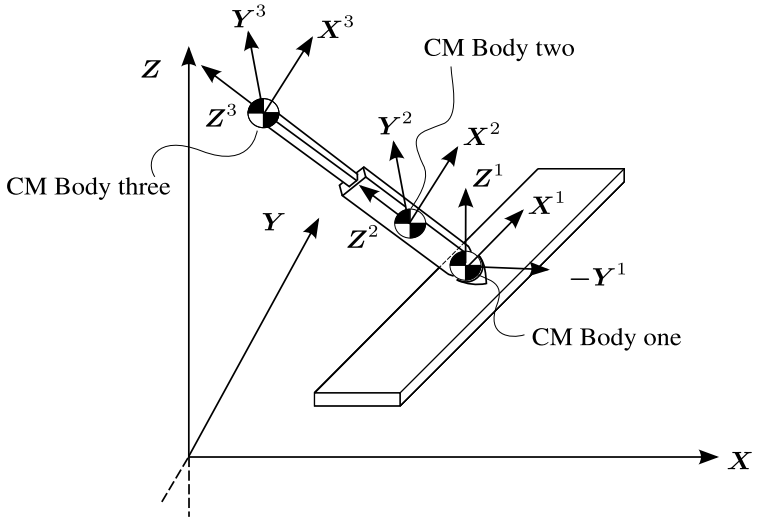

Figure 2.8. Body reference system orientation.

Jacobian matrix of the constraints C_q

The Jacobian matrix of the constraints is formed by studying first the constraints of the system. These constraints dictate the interaction between the bodies of the model, and also between and the bodies and environment. Table 2.1 summarizes the constraints already shown in Figure 2.6 and presents the restrictions caused by these constraints and the resultant DoF.

Table 2.1. Summary of the skier model's constraints. Initial number of DoF in the model = 18.

Constraints	Generalized coordinates involved	Constraints imposed
Geometrical constraints		
Ground–snow planar joint	R_x^1, R_y^1, φ^1, θ^1, ψ^1	4
Spherical joint	R_x^1, R_y^1, R_z^1, R_x^2, R_y^2, R_z^2 φ^1, θ^1, ψ^1, φ^2, θ^2, ψ^2	3
Prismatic joint	R_x^2, R_y^2, R_z^2, R_x^3, R_y^3, R_z^3 φ^2, θ^2, ψ^2, φ^3, θ^3, ψ^3	5
Rheonomic constraints		
Ground steepness change	R_z^1	1
Leg extension	R_x^1, R_y^1, R_z^1, R_x^3, R_y^3, R_z^3	1
Leg orientation	φ^2, θ^2, ψ^2	3
	Total constraints imposed	**17**
	Total DoF left	**1**

The constraints presented in Table 2.1 are introduced in the model under the following reasoning:

Geometrical Constraints:

- **Planar constraint**: used to model the ski–snow contact with the following particularities:
  - The rotation of the ski around any of the perpendicular axes is kept fixed. The three constraint representing the no rotation are expressed in Equations (2.3), (2.4), and (2.5).

$$C1 = \varphi^1 - c_{\varphi^1} = 0 \tag{2.3}$$

$$C2 = \theta^1 - c_{\theta^1} = 0 \tag{2.4}$$

$$C3 = \psi^1 - c_{\psi^1} = 0 \tag{2.5}$$

    In Equations (2.3), (2.4), and (2.5), c_{φ^1}, c_{θ^1}, and c_{ψ^1} are predetermined fixed angles that the ski should maintain.
  - The ski does not slip laterally. The movement is only present in the ski gliding direction. Figure 2.9 shows graphically the physical meaning of this constraint, and Equation (2.6) describes mathematically this condition.

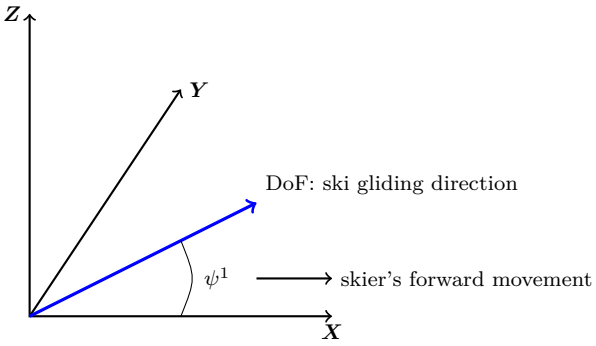

Figure 2.9. Description of the skier model's DoF

$$C4 = R_x^1 \sin\psi^1 - R_y^1 \cos\psi^1 = 0. \tag{2.6}$$

- **Spherical constraint**: used to model the joint between the ski and the foot of the skier.
  - The real effect of the skier's boot binding system used by the skier was not considered.
  - The spherical constraint is located in the ankle of the skier and lying directly on the ski.
  - The necessary condition to be fulfilled in the spherical joint is that two points, P^1 and P^2 on bodies 1 and 2, respectively, coincide throughout the motion. This condition may be written as

$$\begin{bmatrix} C5 \\ C6 \\ C7 \end{bmatrix} = \boldsymbol{R}^1 + \boldsymbol{A}^1\bar{\boldsymbol{r}}_P^1 - \boldsymbol{R}^2 - \boldsymbol{A}^2\bar{\boldsymbol{r}}_P^2. \tag{2.7}$$

    In Equation (2.7), $\boldsymbol{A}^1$ and $\boldsymbol{A}^2$ are the rotation matrices of bodies one and two, respectively, and $\bar{\boldsymbol{r}}_P^1$ and $\bar{\boldsymbol{r}}_P^2$ are the local position vectors of the point P.

- **Prismatic constraint**: used to model the joint between the upper leg and lower leg. It substitutes the natural knee joint. Similar approach to the SLIP model [22].
  - Figure 2.10 shows the configuration used to formulate the constraint equations.

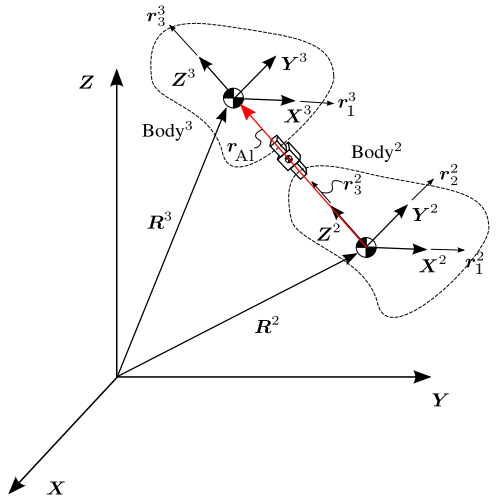

Figure 2.10. Prismatic joint construction vectors.

A prismatic joint in three dimensions has one DoF and five relative movement restrictions composed of two translations and three rotations. The use of this joint in the model is convenient for describing the vertical motion of the center of mass of the skier. In fact, this effect has not been considered in an analogous research project carried out for the speed skater [19], but it is a very important consideration because of the close relationship with the force exerted by the skier during the push–off phase.

The five constraint equations that arise from this joint are based on the following assumptions [70]:

- There is no relative rotation between the two bodies.
- There is no relative translation between the two bodies along an axis perpendicular to the axis of the prismatic joint.

Equations (2.8), (2.9), and (2.10) represent the non–relative rotation relative rotation between the bodies.

$$C8 = \boldsymbol{r}_1^{2\mathrm{T}} \boldsymbol{r}_3^3. \tag{2.8}$$

$$C9 = \boldsymbol{r}_2^{2\mathrm{T}} \boldsymbol{r}_3^3. \tag{2.9}$$

$$C10 = \boldsymbol{r}_2^{2\mathrm{T}} \boldsymbol{r}_1^3. \tag{2.10}$$

Constraints 11 and 12 represent the non–relative translation of the bodies in directions different than the joint axis direction.

$$C11 = \boldsymbol{r}_1^{2\mathrm{T}} \boldsymbol{r}_{\mathrm{Al}}. \tag{2.11}$$

$$C12 = \boldsymbol{r}_2^{2\mathrm{T}} \boldsymbol{r}_{\mathrm{Al}}. \tag{2.12}$$

Up to this point, the model contains 18 (generalized coordinates) minus 12 (constraints) = six degrees of freedom. It is necessary to specify additional constraints controlling the physiological parameters of the leg extension and range of angles.

Rheonomic Constraints: five rheonomic constraints are used to drive part of the model. The five rheonomic constraints used in the model are described by linear relationships between the studied variables R_z^1, φ^2, θ^2, ψ^2 and time, and the distance of the CoM to the ski.

The maxima and minima ranges were obtained by direct observation of the motion capture system data. The linear representation used is an over simplification to the natural movement of the leg. The reason to assume this simple form lies on developing a model able to predict the skier's CoM movement with initially simplified movements but opened to include more complex movement patterns.

Changes in the skier's technique can be included in this simple model with a specific time function representing the desired movement patterns. Then, the skier could try to perform similar patterns to study the real effects of these changes. The model is considered trivial but with opportunities to exploit simplicity to obtain a rough draft of outputs under diverse situations.

These constraints are:

- **Track stepness**: The plane inclination or steepness is modeled with a custom time function that represents this inclination.
  - For the case presented in this dissertation, the custom function used is

$$z(t) = z_{t-1} + \frac{(a_{max} - a_{min})}{t_{cycle}} t. \tag{2.13}$$

    In Equation (2.13), z represents height of the path at a determined time t within one skiing half–cycle (this describes the characteristics of the terrain of the ski tunnel where the tests were conducted). $a_{max} = 0.14$m and $a_{min} = 0$ represent the initial and final height of the track at the beginning and end of the half–cycle, respectively. Finally, t_{cycle} represents the time length of the stroke. It is important to mention that any other function could be used to model the irregular change of elevation of the terrain.

– The time dependent function presented in Equation (2.13) is introduced as a constraint as follows:

$$C13 = R_z^1 - z. \tag{2.14}$$

- **Leg Orientation**: Two other custom time functions are used to prescribe the orientation of the lower leg. This assumes a huge simplification on the way the leg behaves in terms of orientation parameters. These two custom time functions represent the change in the roll and pitch angle of the skier leg according to an arbitrary law proposed by the researcher. **Note**: although the Euler angles convention was used to represent the orientation of the system the researcher names two of these Euler angles as roll and pitch angle due to the simplicity assumed of the leg movement.

  – The roll angle change is limited to a span of 0° – 45° (φ_{min} to φ_{max}). This change is represented under the law presented in Equation (2.15):

$$\varphi^{law}(t) = \varphi_{t-1}^{law} + \frac{(\varphi_{max} - \varphi_{min})}{t_{cycle}} t. \tag{2.15}$$

  In Equation (2.15), φ^{law} is the leg roll angle. The rest of the terms are similar to those introduced in Equation (2.13).

  – The pitch angle change is limited to a span of -20° – 20° (θ_{min} to θ_{max}). For this angle, the change is represented by the law described in Equation (2.16):

$$\theta^{law}(t) = \theta_{t-1}^{law} + \frac{(\theta_{max} - \theta_{min})}{t_{cycle}} t. \tag{2.16}$$

  In Equation (2.16), θ^{law} is the leg pitch angle. The rest of the terms are similar to those introduced in Equation (2.13).

  – The leg yaw angle is considered a fixed value ψ^{fixed} during the skier movement.

  – To use the arbitrary rotation functions previously constructed the following relationships are applied in the model.

$$C14 = \varphi^2 - \varphi^{law}. \tag{2.17}$$

$$C15 = \theta^2 - \theta^{law}. \tag{2.18}$$

$$C16 = \psi^2 - \psi^{fixed}. \tag{2.19}$$

- **Leg Extension**: The fifth rheonomic constraint is related to the combined glide–push action performed by the skier on the gliding phase. This is represented as a leg extension constraint. It is assumed in the model, that the leg extends in a range of 0.5 – 0.9 m (l_{min} to l_{max}). The leg extension follows the law presented in Equation (2.20):

$$l^{law}(t) = l^{law}_{t-1} + \frac{(l_{max} - l_{min})}{t_{cycle}} t. \tag{2.20}$$

  In Equation (2.20), l^{law} is the distance of the CoM of the skier with respect to the center of the ski (origin of the ski body reference system). The rest of the parameters are similar to those introduced in Equation (2.13).

- The final constraint can be expressed as in the following equation.

$$C17 = \left\| \boldsymbol{R}^3 - \boldsymbol{R}^1 \right\| - l^{law}. \tag{2.21}$$

After defining these set of constraints, the equations representing the constraints $C1$ to $C17$ are collected into the vector of constraints

$$\boldsymbol{C} = \left[C1\, C2\, \ldots\, C17 \right]^{\mathrm{T}}. \tag{2.22}$$

Vector of generalized forces

The forces used to drive the model consist on the pushing force produced by the pushing leg, the friction force in the ski–snow contact and the air drag force. Figure 2.11 shows the points of application of these three previously mentioned forces.

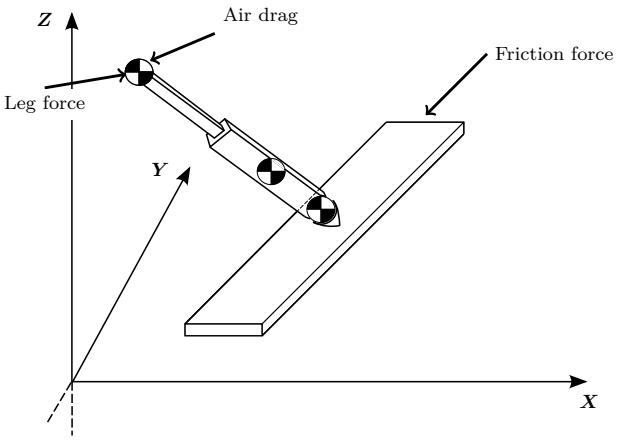

Figure 2.11. External forces applied to the model.

Leg force

To illustrate the forces produced during the propulsion phase, Figure 2.12 describes the active forces present during this phase.

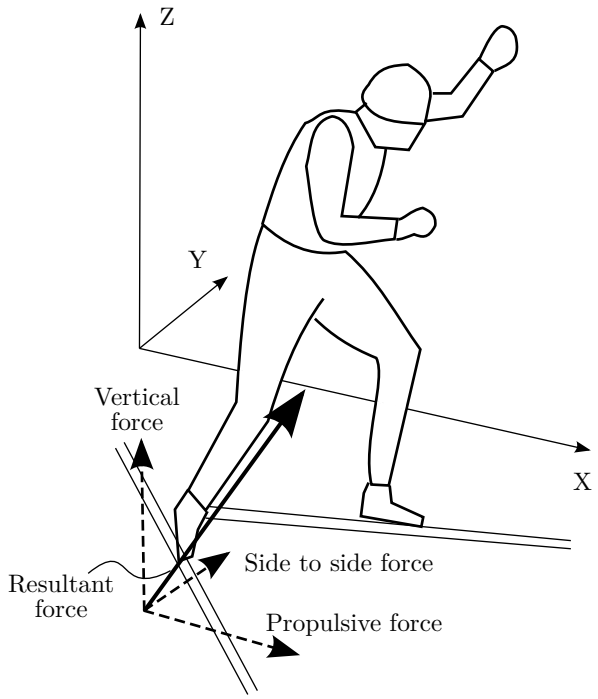

Figure 2.12. Forces acting during the propulsion phase. Figure adapted from [63].

Rusko [63] proposes that the resultant force exerted by the pushing leg can be defined as the vectorial sum of three main acting forces: the vertical force, the side to side force and the propulsive force. This propulsive force is the component that is actively related to the travel movement of the technique, thus affecting the output speed of the skier. Actions or improvements to increase this force will directly impact the performance of the skier.

The pushing force data originates from the system installed in the ski binding system rigidly attached to the ski. Figures 2.13 and 2.14 show the attachment device used to measure the leg forces. This system, validated by Ohtonen et al. [54, 55], provides information of the pushing force decomposed in three axes oriented on the ski body reference system.

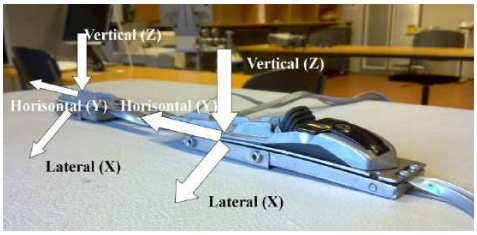

Figure 2.13. Force plates installed in the ski bindings [55].

Figure 2.14. Force plates on the ski bindings [54].

Figure 2.15 shows an example signal obtained from the force binding system utilized to acquire the leg force data. One important information that the leg force measurement system produces is the ski–snow friction coefficient. By considering a ratio between two of the components of the leg force, the z and y components according to the reference system described in Figure 2.13, Ohtonen et al. [55] estimated the gliding properties of a number of different skis.

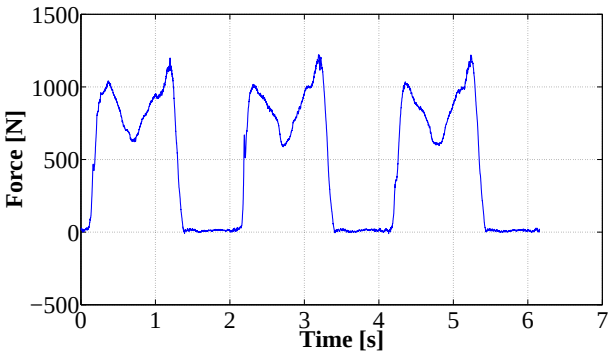

Figure 2.15. Vertical force exerted by the skier during the active phase.

Additionally, Figure 2.16 present the leg force of a skiing half cycle or stroke together with the correspondent fitted curve used in the skier model. To fit the set of discrete data produced by the force measurement system, the procedure based on Fourier series employed by Fintelman et al. [19] was used.

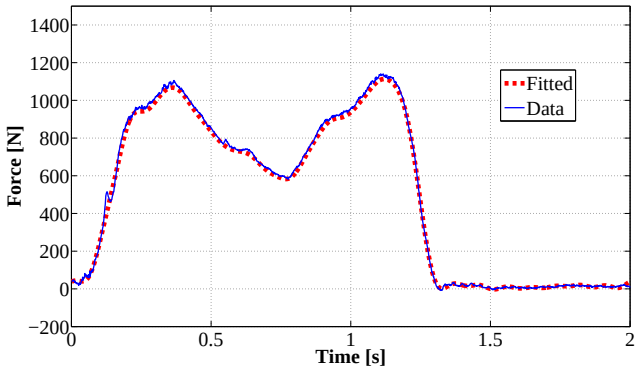

Figure 2.16. Results of the vertical force fitting process to obtain a continuous curve from a discrete data set.

It is of importance mentioning that to conveniently implement the Fourier series curve fitting procedure, it is necessary to segment the discrete data to be fitted. The Fourier series requires the target signal to be periodic and in the case of the skier model, the signal is input to the model in a stroke–by–stroke basis, that is, segmented. Other curve fitting methods could be applied to accomplish a similar outcome. However, because of the successful application of the Fourier series technique in the speed skater model [19], this methodology was adopted thorough the skier models presented in this dissertation.

Ski–snow friction force

Snow friction is a resisting force originating from by the interaction of the ski and snow on the ski–snow contact layer. This friction force has a negative correlation with the forward speed of the skier and has been studied over the past 100 years with the aim to diminish its effects on the process of gliding [62]. Although the small value of snow friction might seem deceiving when it is first taken into account, snow friction may have a tremendously harmful influence on the skiers' racing time.

To this day, one important fact has emerged from the different studies: the mechanisms that explain the behavior of the ski–snow relationship are complex. In addition, being the snow friction part of the field of tribology, is understandable

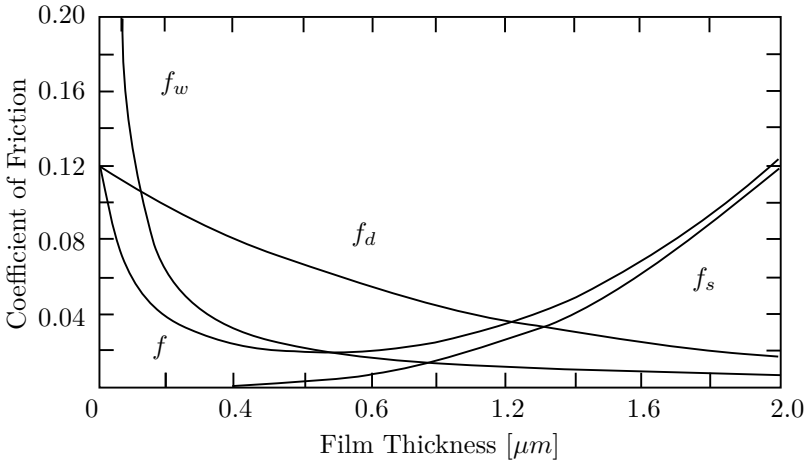

Figure 2.17. f total friction coefficient, f_d dry friction coefficient, f_w lubricated friction coefficient and f_s capillary friction coefficient. Extracted from [13].

that most of the knowledge is empirical. Researchers have been unmasking the complex relationships behind the observed snow friction phenomena by formulating or adapting theories able to explain or to predict, to a certain accuracy level, the behavior of sliding on snow.

The study of snow kinetics became a topic of special focus because of the increased interest in studying skiing [13]. Additionally, this interest in skiing involves understanding how the skier accommodates for the variable friction conditions [55]. Besides being a complex phenomenon, studying skiing in real conditions is even more complex because of the variable conditions of the snow on the competition tracks. Most of the research done to develop the tribology theory of snow friction have been done in confined or controlled conditions.

The value of the friction force in the ski–snow contact depends on several factors and mechanisms, such as the skier's total vertical force, snow and air temperature, snow hardness ski surface properties, and forward movement velocity [79]. Studies show that the total friction comprises at least three components: dry friction, lubricated friction and capillary friction. These three components affect the friction coefficient used to determine the friction force. Figure 2.17 shows the influence of the friction mechanisms in the total friction coefficients.

In the presence of very cold conditions, snow might reach frictional coefficient values close to 0.3 (similar to sand). However, in most natural conditions and because of the water layer beneath the skis, this frictional coefficients might be as low as 0.01 [79].

In the case of the skier model, these complex relationships between the snow and ski were not considered in totality. Conversely, the ski–snow friction force was introduced to the skier model as previously done by Moxnes and Hausken, Chen and Qi, and Oberegger et al. [11, 18, 47]. Equation (2.23) describes the mathematical form of the ski–snow friction used in the skier model.

$$\boldsymbol{f}_f = -\mu \|\boldsymbol{N}\| \frac{\boldsymbol{v}_{ski}}{\|\boldsymbol{v}_{ski}\|}. \tag{2.23}$$

In Equation (2.23), $\boldsymbol{f}_f$ is the friction force generated in the ski–snow contact, μ is the Coulomb friction coefficient, $\boldsymbol{N}$ is the normal force applied to the ski, and $\boldsymbol{v}_{ski}$ is the velocity of the gliding ski in contact with the snow. The value of the normal force applied to the ski used in the simulation was approximated to the body weight of the skier and the value of the friction coefficient was a calculated average following the approach employed by Ohtonen et al. [55] and presented briefly in Equation (2.24).

$$\mu = \frac{F_y}{F_z}. \tag{2.24}$$

In Equation (2.24), the leg force components F_y and F_z are time dependent and measured with respect to the binding system specific reference coordinate system.

Air drag forces

Air drag forces are the other existent resistive forces playing against the forward movement of the skier. A few studies showed that the negative effect of the air drag is seen more frequently in ski jumping [49, 68]. Other studies have concluded that for cases such as slalom and cross–country skiing, ski–snow friction is more detrimental to the skier's movement than air drag [78].

Although aerodynamics in general has been researched extensively, very little is known about the aerodynamic relationships affecting the complex structure of the skier [49]. As most of the skiing aerodynamic theory is based on the Navier–Stokes equations, it is impossible to escape major mathematical difficulties when computing its solution. Nevertheless, computational fluid dynamics is the best chance researchers have to estimate the value of these drag forces associated with different sports [49].

To obtain an idea of the air drag force value, researchers often use wind tunnels to precisely determine this force under controlled conditions [43]. Wind tunnels are the closest to an ideal environment to theorize about the experiment data obtained. Figure 2.18 shows a typical test procedure in a wind tunnel performed by Supej et al. [78].

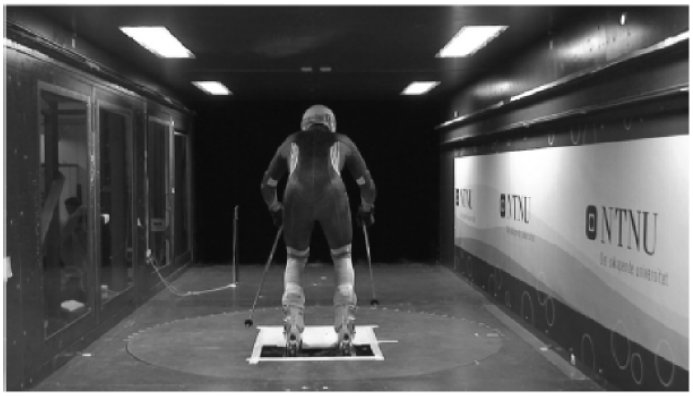

Figure 2.18. Typical wind tunnel setup [78].

To date, there are no validated systems to determine or measure the external forces affecting the skier's movement under race conditions or entire competitions [24]. Outdoors, 3D systems based on video cameras are commonly used to estimate the skier's forces. These camera systems monitor only one segment of the race track with limitations on the volume of information they can handle and the costly post–processing time [24]. One example of typical camera procedures is presented in Figure 2.19 found in the study by Gilgien et al. [24].

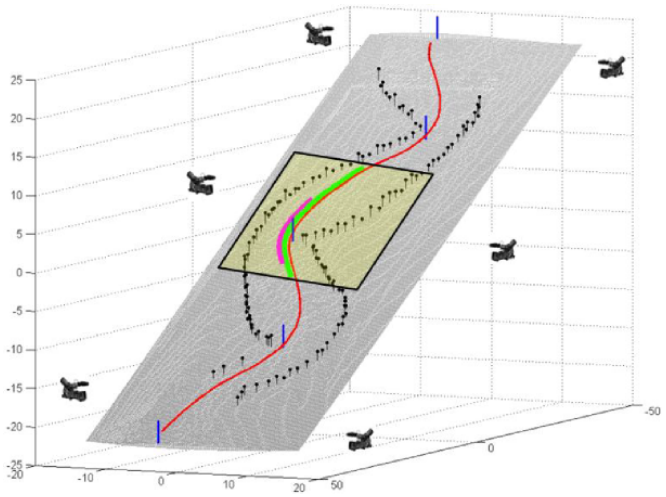

Figure 2.19. Typical 3D camera system set–up [24]. This setup was used to study one segment of a downhill track. It shows the complexity of using camera–based systems outdoors.

Air drag is based on the aerodynamics of the set conformed to the skier's physiognomy, clothing, and gear design. These three aspects are accounted

for in the air drag force value as two specific parameters: the air drag force, where the physiognomy is taken into account as a surface or more specifically as the skier's frontal area facing the movement, and the air drag coefficient to account for the the aerodynamics of the skier's clothing, equipment, and posture. This relationship can be seen in Equation 2.17.

$$\boldsymbol{f}_d = -\frac{\rho}{2}\|\boldsymbol{v}_{skier}\|^2 c_d A \frac{\boldsymbol{v}_{skier}}{\|\boldsymbol{v}_{skier}\|} \tag{2.25}$$

where $\boldsymbol{f}_d$ is the force drag acting on the skier, ρ is the air density, $\boldsymbol{v}_{skier}$ is the forward velocity of the skier, c_d is the dimensionless friction coefficient, and finally, A is the frontal area of the skier facing the movement. The value of c_d adopted for this simulation in Equation (2.25) is 0.5, taking as a reference the modeling done by Chen [11]. The projected area used for the inclusion of the air drag force was taken as a constant value similar to the rectangular dimensions of the upper body of the skier obtained from Yeadon's body model [85] (more details in the mass matrix quantification segment following). This area was also considered to be facing the main axis of displacement at all times.

Having the three major forces accounted for, the next step is to incorporate them into the vector of generalized forces. The total vector of generalized forces has the following form:

$$\boldsymbol{Q}_e = \left[\begin{array}{cccccc} \boldsymbol{Q}^1_{e_R}{}^{\mathrm{T}} & \boldsymbol{Q}^1_{e_\theta}{}^{\mathrm{T}} & \boldsymbol{Q}^2_{e_R}{}^{\mathrm{T}} & \boldsymbol{Q}^2_{e_\theta}{}^{\mathrm{T}} & \boldsymbol{Q}^3_{e_R}{}^{\mathrm{T}} & \boldsymbol{Q}^3_{e_\theta}{}^{\mathrm{T}} \end{array} \right]^{\mathrm{T}} \tag{2.26}$$

where the terms $\boldsymbol{Q}^i_{e_R}$, with $i = 1 \ldots 3$ being the number of the body, represent the individual vector of generalized forces applied to each one of the bodies, and $\boldsymbol{Q}^i_{e_\theta}$ represent the generalized moments also applied to each one of the bodies.

It is assumed that the lines of action of the forces pass through the respective CoM of the bodies where they are applied. This assumption reduces the formulation of the generalized forces by eliminating the possible torques ($\boldsymbol{Q}^i_{e_\theta}$) appearing when translating the real point of application of the forces. The components of the generalized force vector acquire the form presented in Equations (2.27) and (2.28):

$$\boldsymbol{Q}^1_{e_R} = \boldsymbol{A}^1 \overline{\boldsymbol{f}}_f \tag{2.27}$$

$$\boldsymbol{Q}^3_{e_R} = \boldsymbol{A}^3 \left(\overline{\boldsymbol{f}}_{leg} + \overline{\boldsymbol{f}}_d \right). \tag{2.28}$$

In this specific case, vector $\boldsymbol{Q}^2_{e_R}$ is equal to **zero** because no forces are applied to this body. The vector $\boldsymbol{Q}^1_{e_R}$ depends on the ski–snow friction force, and $\boldsymbol{Q}^3_{e_R}$ depends on the leg and air drag forces. Friction forces and leg force are represented in the body reference system.

Mass Matrix $\boldsymbol{M}$

- The inertia terms of the mass matrix of the system are obtained utilizing the statistical model proposed by Yeadon [85]. Yeadon's model requires two main inputs: the height and weight of the subject. These inputs are known and taken from the test subject's physiological data. Yeadon's model produces a full description of the human body according to a predefined segmentation. Each body segment is presented with its weight and inertia tensor represented in the segment's reference system. Body segmentation and body reference system positioning and orientation is a priori postulated by Yeadon. In the model, it is only visible the use of Yeadon's parameters for the lower and upper leg; Nevertheless, the mass contemplating the rest of the body was extracted from Yeadon's model.

- As the representation of the inertia terms in the mass matrix of the system are firstly introduced in the body reference system, kinematic relationships depending on time are used to represent these local systems in terms of the absolute reference frame.

- The masses of the skier's leg and ski are utilized in the model while the rest of the skier's body segments mass (trunk, head, arms, pushing leg) are considered to be located at the origin of the body reference system of the skier's upper leg as a concentrated mass.

Form of the equations of motion

The equation of motion is presented as a set of ODEs index-1 system that can be integrated using the built-in MATLAB (Math Works, Inc., Natick, MA, USA) function ODE45 to obtain the velocities and positions of the relevant points of the model during the simulation time. Equation (2.29) presents the matrix configuration of the equations of motion, including the terms of the Baumgarte stabilization method:

$$\begin{bmatrix} \boldsymbol{M} & \boldsymbol{C}_{\boldsymbol{q}}^{\mathrm{T}} \\ \boldsymbol{C}_{\boldsymbol{q}} & \boldsymbol{0} \end{bmatrix} \begin{bmatrix} \ddot{\boldsymbol{q}} \\ \boldsymbol{\lambda} \end{bmatrix} = \begin{bmatrix} \boldsymbol{Q}_e + \boldsymbol{Q}_v \\ \boldsymbol{Q}_d - 2\alpha \left(\boldsymbol{C}_{\boldsymbol{q}} \dot{\boldsymbol{q}} + \boldsymbol{C}_t \right) - (\beta)^2 \boldsymbol{C} \end{bmatrix}. \tag{2.29}$$

In Equation (2.29), $\boldsymbol{C}_t$ is the time derivative of the constraint vector of the system, and α and β are the Baumgarte stabilization parameters.

To select a convenient value for these stabilization parameters, the method proposed by Flores et al. [21] is used.

As a summary, the sources of data utilized to construct the skate skier model are presented next graphically. The equations of motion of the skier model together with its inputs and the desired output can be depicted as in Figure 2.20.

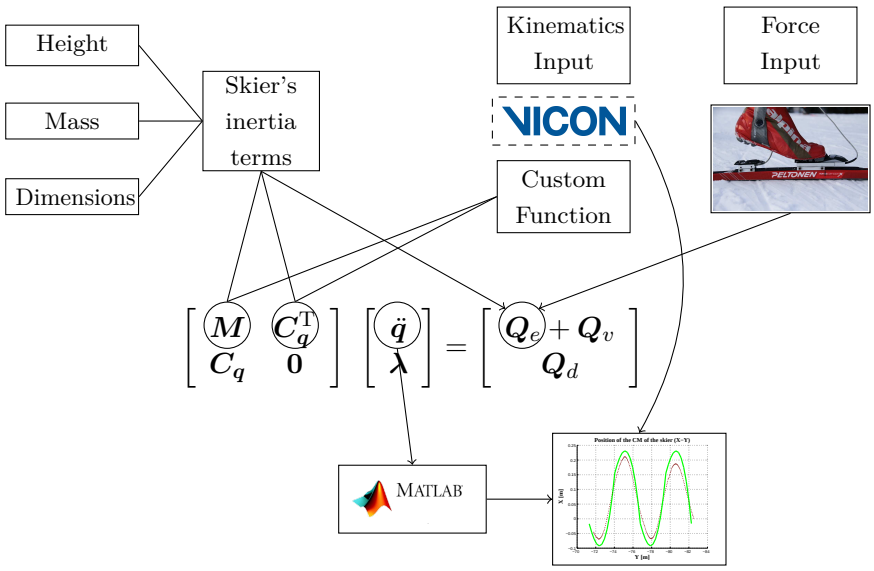

Figure 2.20. Inputs utilized to construct the skate skier model and their relationships with the components of the equations of motion of the model.

2.5 Experimental procedure

Skier

A professional skier, former member of the Finnish Olympic team, was the test subject to demonstrate the feasibility and validity of the simple mechanical model. The physiological parameters needed as inputs in the skier model are the mass and height of the skier, and the weight and dimensions of the ski and binding.

The different lengths of the leg segments were taken directly from the distance measurement of the markers positioned on the topological points of the legs (ankle, knee, and head of the femur). However, these data are only used at this stage of development of the model as a validation tool for comparison with simulation outputs. The model itself generates these data based on the physiological studies presented by Yeadon [85]. The purpose of this is to provide the model in the future with some generality to avoid adding more measurement procedures and ease the use of the model as a practical tool by teams with different scopes: high competitions, leisure activities, or beginners.

Parameters used in the model

Table 2.2 presents the detailed parameters used to produce the results in this first model.

Table 2.2. Parameters used in the first skier model

Parameter	Value	Units
Mass of the skier	80	kg
Weight of the skis plus force bindings	24	N
Length upper leg	0.4288	m
Length lower leg	0.4489	m
Height of the skier	1.83	m
Coefficient of friction	0.15	
Air drag coefficient	0.5	
Integration time	0 to 2.5	s
ρ_{air} @ -5°C	1.316	$\mathrm{kg\,m^{-3}}$
Skating angle ψ^1	14.3	°

Measurement equipment

All of the data was collected in the ski tunnel in the Vuokatti Sports Institute [82]. The length of this indoor ski track is about 1 km with different track steepnesses to perform tests and for skiing in general. The tunnel temperature is normally kept between -5 ℃ and -9 ℃. Updates on the conditions of the ski tunnel can be found on the Vuokatti website. All of the snow in the tunnel is maintained mechanically, and also fresh snow can be produced when needed. Due to the restrictions on the measurement length of the motion capture equipment, the test was limited to 16 m. This length allows capturing approximately three complete strokes of the skier.

The equipment can be divided into two important segments: the first is the equipment dedicated to performing the experiment in the tunnel and the second is used to develop the multibody dynamic model and the verification of the results. In the experiments, the Vicon System MX manufactured by Vicon Motion Systems, consisting of 16 cameras, was used to acquire the positions of the 37 markers set on the body. The markers were spheres attached to the body in the locations shown in Figures 2.21 and 2.22 defined the motion capture system at a sampling rate of 1000 Hz.

To measure the forces exerted by the foot on the ski, an in–house force measurement system was used. The validity of this force system has been reviewed by Ohtonen et al. [54, 55].

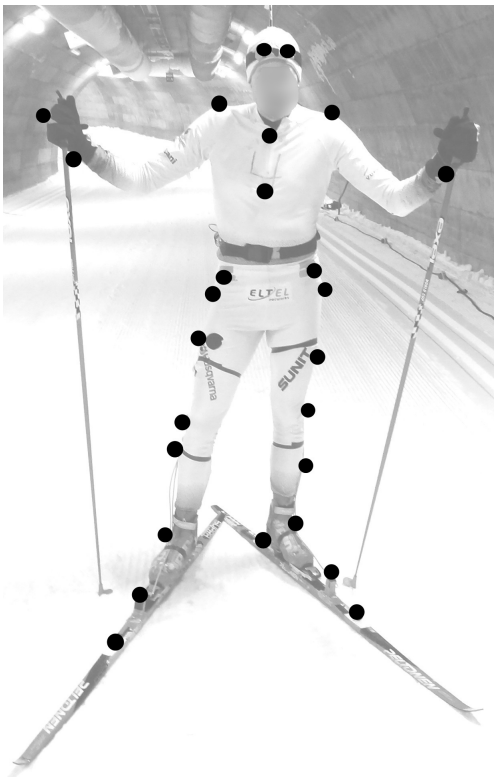

Figure 2.21. Marker positioning represented by black dots. Frontal view.

This measurement system allows obtaining the full resultant force exerted by the skier. It contains the sum of all forces produced during the propulsion phase independently of how they are produced. At this stage of development, this feature reduces the need for a detailed analysis of the role of the individual movements and parts of the leg and foot.

The system Protom–Light System, Model Con 12 was used as a visual speed indicator for the skier to carry out the test run. It is important to mention that the velocity used as compare against the velocity produced by the model was the real one calculated from the motion capture system data. The Protom–Light system was used only as a reference for the skier.

To collect and transmit the data to the computer used to pre–process the experiment data, the following equipment was used:

- Two custom–made small and lightweight (980 g) force plate pairs built by the Neuromuscular Research Center, University of Jyväskylä.
- An eight channel ski force amplifier built by the Neuromuscular Research

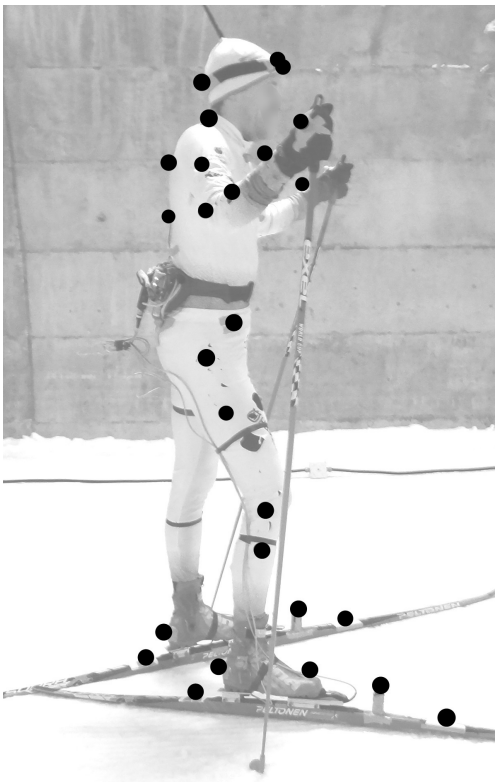

Figure 2.22. Marker positioning represented by black dots. Lateral view.

Center, University of Jyväskylä.

- An A/D converter with a sampling rate of 1 kHz, model NI 9205, National Instruments, Austin, Texas, USA.
- A wireless transmitter WLS-9163, National Instruments, Austin, Texas, USA.
- A PC laptop with a wireless receiver card and data collection software LabVIEW 8.5, National Instruments, Austin, Texas, USA.

The final weight of the measurement and collection system combined with the transmitting system was approximately 2030 g.

To manipulate the motion capture data from the experiments, the MATLAB 2013a software and the VICON Nexus software were used, respectively. MS Office was used to preview the result of the measured forces and to apply the necessary calibration offsets and conversion constants.

Measurement procedure

The measurement system was configured, set and calibrated according to the manufacturer's recommendations, and the force measurement system was calibrated using the internal existent protocol of the Neuromuscular Research Center of the University of Jyväskylä. Further specifications of the measuring system can be found in the work of Ohtonen et al. [54].

The test subject did not perform any structured warm–up prior to the tasks; however, the one kilometer skiing run to reach the test zone inside of the tunnel can be considered a warm-up. No other exercises were needed to get used to the equipment, as the same test subject has performed this test many times in the past. Then, a specific skiing speed was set as the only parameter to be followed by the skier during the execution of the skating technique without poles. The forward speeds used in the test were 5 and 6 m/s. For each specified speed, three runs were made to ensure the availability of clean raw data.

All of the marker positions and force data were collected and saved in usable formats to be input in the simulation model. The motion capture data was exported in the .c3d format, and in the case of the force, the format used was .txt. No synchronization issues between the position capture and force data appeared thanks to the Vicon Nexus software linking these two sets. After selecting the information of the markers to be input into the model, the forces exerted by the foot on the ski were calculated and compared against those measured with the force acquisition system.

Figure 2.23 shows the relationships of inputs and outputs of the skier simulation model.

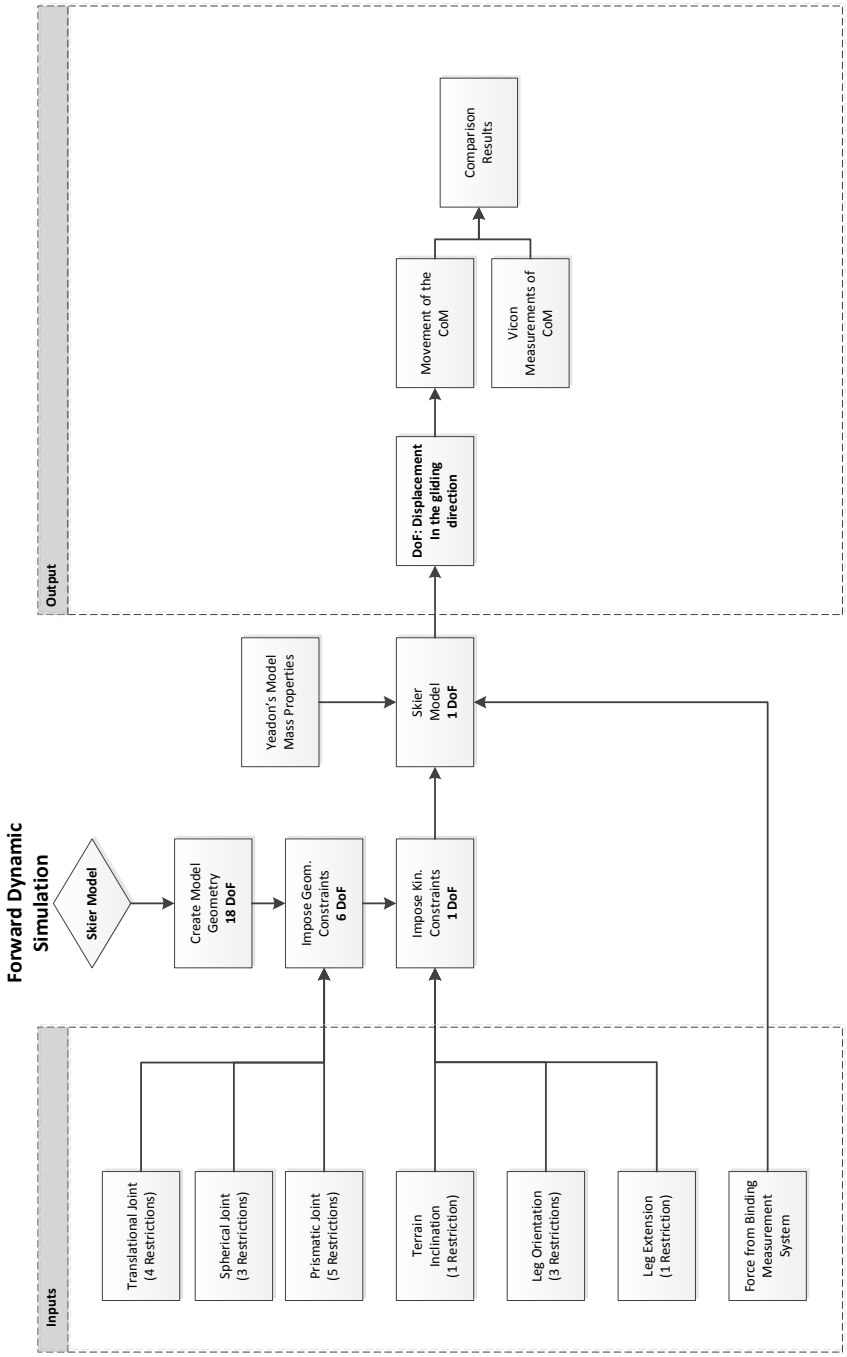

Figure 2.23. Model Algorithm

2.6 Results

To test the skier model, Table 2.3 presents the basic parameters selected to perform the simulation.

Table 2.3. Definition of the technique parameters.

Variable	Value
Phase Time (s)	0.59
Skating angle (°)	± 14.3
Initial velocity (m/s)	0
Number of strides	30

As the simulation is based on several strokes and changing the active leg (right or left) on every stroke, the skating angle can take a positive or negative value. After simulating the simplified model with the above–mentioned assumptions, the following results can be presented and discussed.

Figure 2.24 compares the skier's CoM position with the data obtained from the motion capture system (dotted line) and the results of the simulation after the velocity of the skier model remained constant (continuous line).

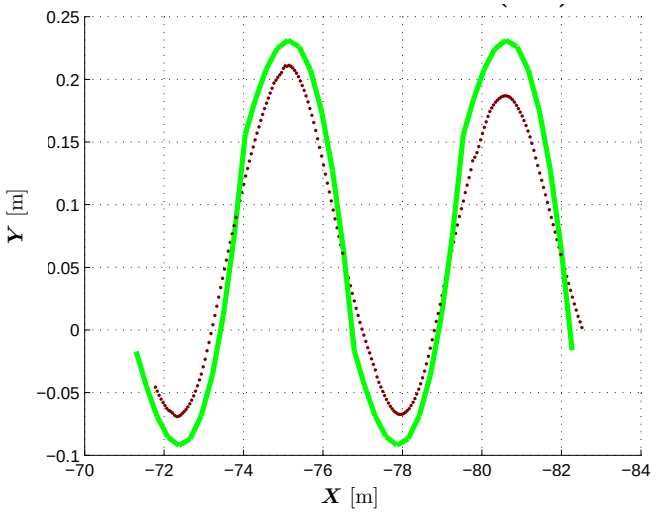

Figure 2.24. Skier's CoM displacement comparison. The green continuous line represents the simulated results and the brown dashed line represents the measured data.

Table 2.4 shows the differences between the trial run, motion capture, and simulated velocity.

Table 2.4. Resultant average travel velocity.

Velocity (m/s)	Value	Difference (Rel.)
Trial run set up velocity	5	–
Motion capture system travel velocity	4.83	3.52%
Simulation travel velocity	4.36	10.78%

2.7 Conclusions

The use of multibody dynamic models in real–life applications has been undoubtedly useful for enhancing the processes in which they are involved. The skate skiing technique does not escape this trend.

When developing this research, it became evident during the literature review about skate skiing multibody models that the number of studies related to multibody dynamic models of this technique is scarce. This leaves an interesting open area to be addressed in the near future.

One of the most interesting results is the reproduction of the skier's CoM position after the simulation. As the movement of the legs is introduced as a combination of data derived from the motion capture system and the capabilities of the constraints imposed on the model, it is possible to refine the study even further to obtain much closer results without converting the model into an inverse dynamic model.

Despite using a large set of redundant generalized coordinates, there were not singularity problems during the integration of the equations of motion. This evidences one of the advantages of adopting the augmented formulation to construct the model.

In the case of velocity, the forces acting on the model have proven to be of importance. In the present model and the environment where the trial runs were performed, more precise values of the air drag coefficient should be considered. It is also important to expand this model to recreate closer ski–snow interactions.

The comparison of the results was limited by the physical capacity of the Vicon Motion Capture System. The system is highly recommended for studies such as gait analysis in closed spaces. However, due to the characteristics of the skiing technique, only a trial run of 12 to 14 meters could be captured.

The author considers that this model can be used as step towards understanding the skate skiing technique and its integration with the multibody dynamics.

Further development of multibody dynamic models may support the research on muscle actuation, energy consumption, and stresses affecting bones. Also, the possible impact of the skate skiing technique on athletes' lower limb joints can be assessed, and common injuries that top competitive athletes may develop with the continued practice of this sport discipline can be studied better.

Chapter 3

Extension of the skier simulation model

This chapter focuses on extending the simple mechanical model developed in Chapter 2 for simulating and describing the general aspects of the skate technique in cross–country skiing. The use of a simplified model is justified when the output information is obtained within certain broad limits of accuracy, as is shown by Bruzzo et al. [9]. When more accuracy or more detailed information is needed, moving to complex models might seem the path to follow; however, as the model increases its complexity, other complications have to be considered. Among these are the computational burden if the model is used in real–time simulation, precise knowledge of all needed system parameters and input variables, and the appearance of unknowns which are difficult to estimate correctly and cannot be experimented with (see Liu and Popović [35]). The main objective of extending the skier model is to calculate the leg propulsion forces developed in the gliding leg on one half cycle.

The main assumptions and considerations made to create the skier model described in Chapter 2 remain valid. However, the following key aspects were addressed to extend the previously described simulation model:

- The selection of a more adequate representation of the leg of the skier. Specifically, the simulation of the knee joint.
- The input of the prescribed motion to represent the movement of the lower limb of the skier.
- Calculate the leg propulsion forces developing in the gliding leg on one half cycle.

3.1 Simulation model

The skier representation assumed in the second model is shown in Figure 3.1. The new shape of the skier's leg considered the joint as a revolute joint instead of a prismatic joint. Additionally, Figure 3.2 shows the new configuration of the skier model in a schematic form.

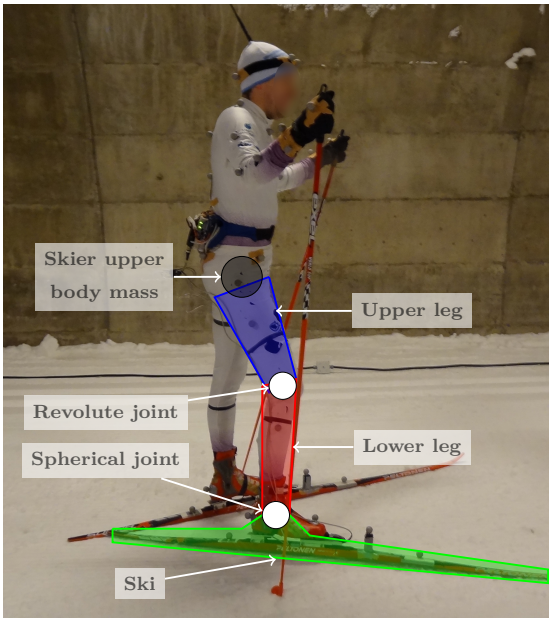

Figure 3.1. Description of the lower leg configuration in the second skier model. The joints utilized in this model more closely resembles the natural relative movements in the human leg.

Using a revolute or hinge joint to model the knee considers only the flexion and extension of the knee during the simulation process. The joint between the lower leg and the ski is remains as a spherical joint allowing only rotational movements of the ski with respect to the lower leg. And, the joint between the ski and the ground will have five constraints, such that, when on the snow, it is only able to move in the longitudinal or gliding direction of the ski.

3.2 Form of the model's equations of motion

The augmented formulation form of the equations of model of the skier model can be written as

$$\begin{bmatrix} \boldsymbol{M} & \boldsymbol{C}_q^{\mathrm{T}} \\ \boldsymbol{C}_q & \boldsymbol{0} \end{bmatrix} \begin{bmatrix} \ddot{\boldsymbol{q}} \\ \boldsymbol{\lambda} \end{bmatrix} = \begin{bmatrix} \boldsymbol{Q}_e + \boldsymbol{Q}_v \\ \boldsymbol{Q}_d - 2\alpha \left(\boldsymbol{C}_{\boldsymbol{q}} \dot{\boldsymbol{q}} + \boldsymbol{C}_t \right) - \left(\beta^2 \right) \boldsymbol{C} \end{bmatrix} \tag{3.1}$$

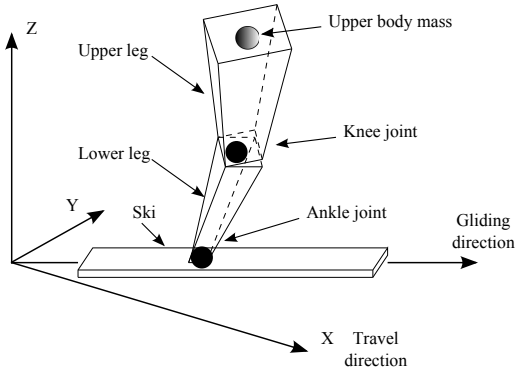

Figure 3.2. Simplification of the leg in the second skier model. The dark circles represent the positions of the joints of the lower limbs and the shaded circle represents the mass of the rest of the skier's body.

Equation 3.1 remains similar to Equation 2.29 presented in Chapter 2. Similarly, the vector of generalized coordinates conserves the same structure. Equation 3.2 shows the vector of generalized coordinates in the extension of the skier model.

$$\boldsymbol{q} = \begin{bmatrix} \boldsymbol{q}_1^{\mathrm{T}} & \boldsymbol{q}_2^{\mathrm{T}} & \boldsymbol{q}_3^{\mathrm{T}} \end{bmatrix}^T \tag{3.2}$$

The Euler angle sequence used remains ZXY, Figure 3.3 shows the location and orientation of the body reference systems.

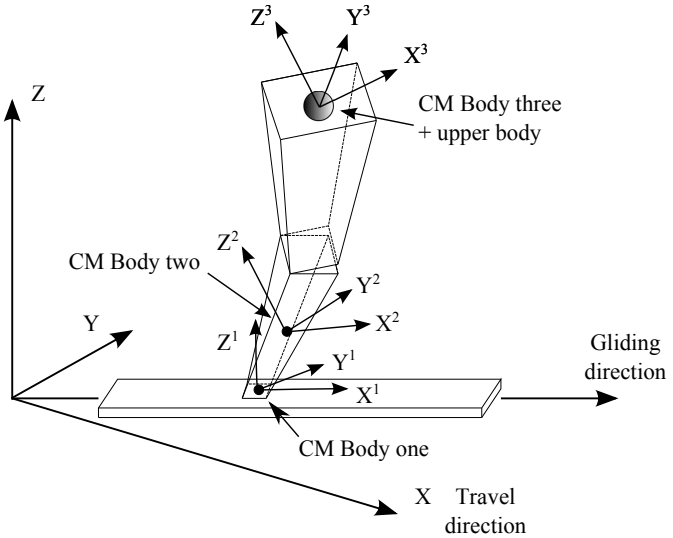

Figure 3.3. Body reference system location and orientation. Consideration of the initial orientation of the body reference systems used in the second skier model.

Treating the knee as a revolute joint and replicating the real angular movement performed by the skier's leg represents new challenges. As the rotational movements of the lower leg with respect to the ski have to be prescribed and have to reproduce those taken from the motion capture system, constraints $C14$, $C15$, $C16$, and $C17$ represented in Equations (2.17), (2.18), (2.19), and (2.21), respectively, were substituted as follows:

$$C14 = \varphi^2 - \varphi^2_{fitted} \tag{3.3}$$

$$C15 = \theta^2 - \theta^2_{fitted} \tag{3.4}$$

$$C16 = \psi^2 - \psi^2_{fitted} \tag{3.5}$$

where φ^2_{fitted}, θ^2_{fitted}, and ψ^2_{fitted} are the prescribed Euler angles that the body reference system has to follow.

And in the case of the revolute joint representing the knee joint:

$$C17 = \theta^3 - \theta^3_{fitted} \tag{3.6}$$

where, θ^3_{fitted} is the reference value that the angle θ^3 has to follow.

With Equations (3.3), (3.4), and (3.5), the spherical joint that represents the ski–ankle joint is defined completely. And Equation (3.6) provides the angular movement of the knee while the skier is transitioning from gliding to pushing.

Consequently, after describing a set of 17 constraint equations, the resulting number of DoF of the model is one.

Mass matrix of the system

The construction of the mass matrix of the system is based on theoretical information found in the literature. The inertia components of the different body parts included in the model (lower and upper leg) are taken from previous studies that collected these physiological data. More detailed information can be found in the work of Yeadon [85].

Vector of generalized forces

Figure 3.4 presents the external forces on the model and their direction of application.

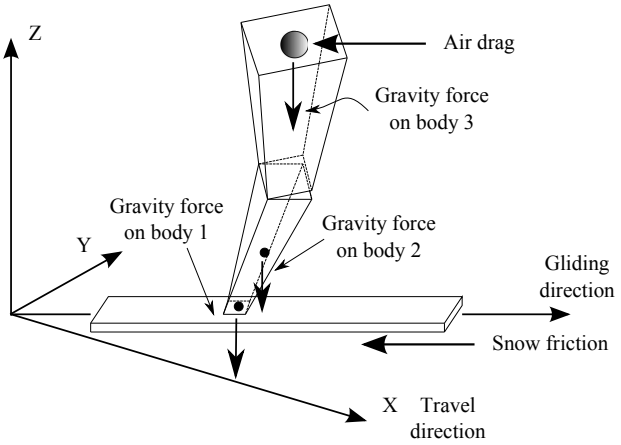

Figure 3.4. External forces considered in the skier model.

As it can be seen, the number and nature of forces applied in the skier modeled were not changed in comparison with the model presented in Figure 2.12.

Parameters used in the model

Table 3.1 presents the detailed parameters used to produce the results in this paper.

Table 3.1. Parameters used in the second skier model

Parameter	Value	Units
Mass of the skier	80	kg
Weight of the skis plus force bindings	24	N
Length upper leg	0.4288	m
Length lower leg	0.4489	m
Height of the skier	1.83	m
Coefficient of friction	0.15	
Air drag coefficient	1	
Integration time	0 to 0.55	s
ρ_{air} @ -5°C	1.316	$\mathrm{kg\,m^{-3}}$
Skating angle φ^1	16.5	°

3.3 Data analysis

The data needed some prepossessing to make it suitable for use in the model. Firstly, the data belonging to the selected propulsion phase was isolated from the rest of the measurements. This was done by analyzing the marker positions attached to both skis and the positioning of the center of mass of the skier with respect to each ski. Finally, a comparison of the measured force from each binding clarified which leg was pushing and which one was gliding. Only the position and force data of the leg performing the propulsion was taken.

Secondly, as the multibody model needs to use the position of the selected lower limb markers to extract the respective Euler angles of the leg parts, it was important to guarantee that these functions representing the Euler angles were smooth, continuous and differentiable up to the second degree. A Fourier fitting process also applied by Fintelman et al. in the speed skater model [19], was used to convert the discrete data into continuous functions. In this chapter, more detail is given to the fitting process because four new discrete variables are introduced to drive the model.

Finally, to verify that the fitted continuous functions represented the discrete data well, the Pearson correlation coefficient, the analysis of residuals, and the Bland–Altman plots were used to test the goodness of fit.

Figure 3.5 present the resultant force raw data and the resultant curve from the fitting process. Additionally, Figure 3.6 shows the resultant residuals after the fitting process showing that a large percentage of differences encountered in the fitted function are between -10 and 10 N. This is a quantitative indication on how good the fitting process might be considered.

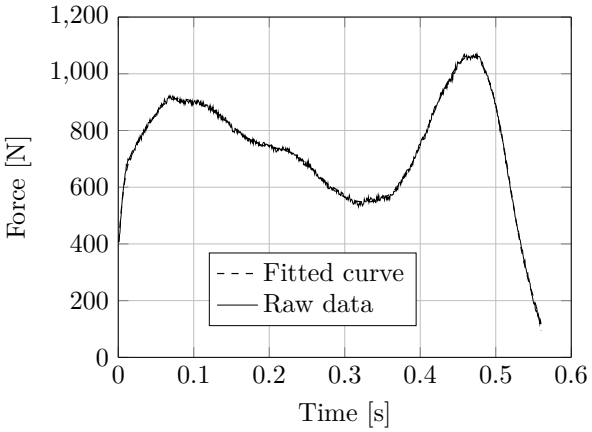

Figure 3.5. Comparison of the raw total ski force data and fitting results.

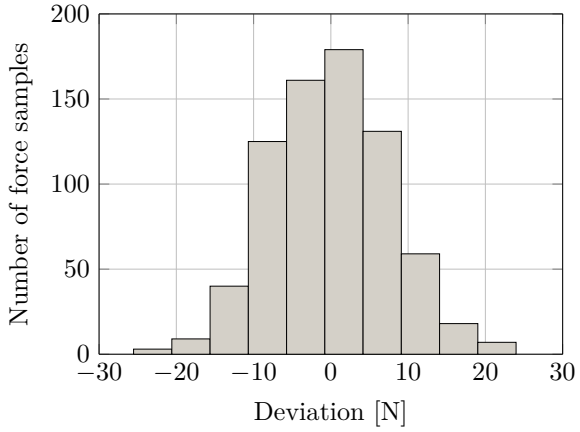

Figure 3.6. Histogram of the residuals related to the fitting process of the total ski force.

It is also important to show the fitted data used as an input in the model. Figure 3.7 presents the graphical representation of the measured Euler angles representing the orientation of the leg during the analysis and the curve produced by the fitting process. To quantify the difference between the raw and fitted data, the histogram of the residuals of the deviations is also constructed for these curves. Figure 3.8 presents the residual product of this fitting process. Also, the good agreement of the raw vs. fitted data can be seen here indicated by the residuals of the deviations being close to zero.

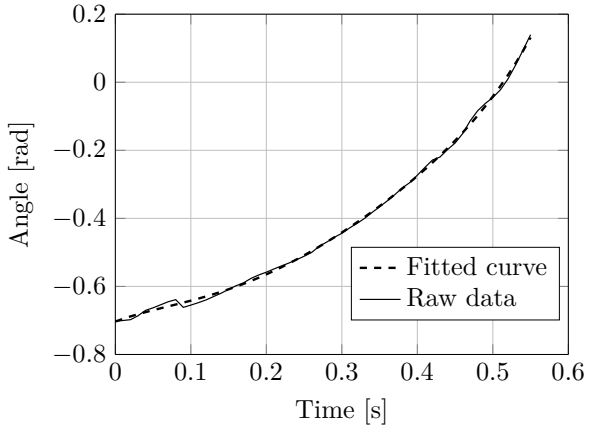

Figure 3.7. Comparison of the raw kinematic data and fitting results of the Euler angle θ^2 used to represent the orientation of the leg.

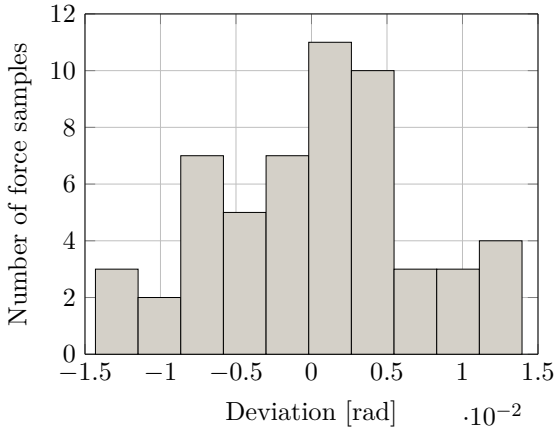

Figure 3.8. Histogram of the residuals related to the fitting process of the kinematic data for the Euler angle θ^2.

In this part of the study, it is not possible to show error bars on the uncertainties of the measurements. The force and position measurements for different test runs cannot be compared because of the high variability of the skier's movement in the trial, the lack of a well–established reference point for comparison and the multiple changes that the skier could introduce with slight changes in technique. Each measurement has to be taken as an individual set of data that could be used in the model. However, the force measurement system is validated and showed minimal differences to reference systems in various test situations, which can be seen in the work by Ohtonen et al. [54].

3.4 Results

After inputting the positions measured during the propulsion phase as a reference, the first important simulation output to show is the comparison of the measured and modeled trajectories of three specific topological points on the leg. This comparison validates the response of the model that uses movement simplifications for the leg joints, meaning that it is possible to keep the generality of the leg movements with the assumptions made.

Figure 3.9 shows the X–Y plane projection of the position of these simulated and measured points, and Figure 3.10 presents the X–Z plane projection.

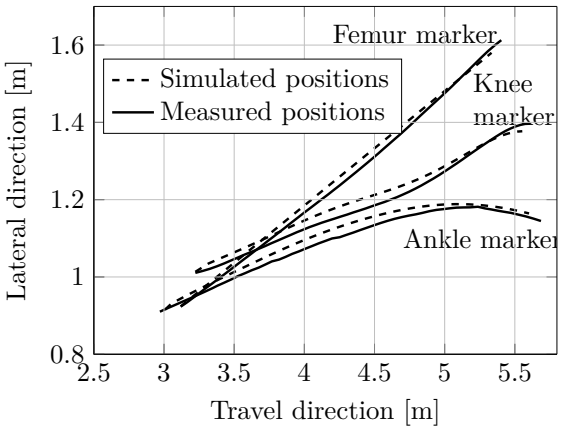

Figure 3.9. Plane X–Y: projection of the measured and simulated points for one skiing stroke.

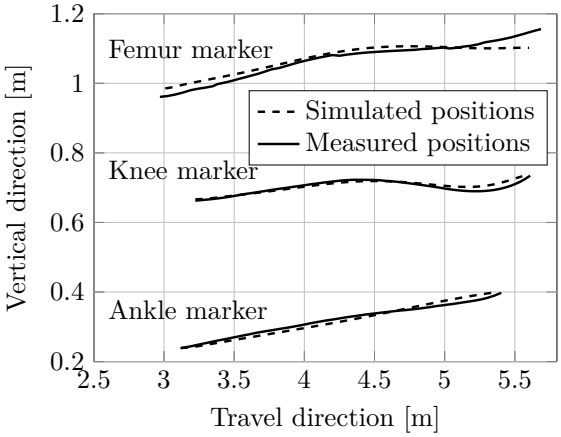

Figure 3.10. Plane X–Z: projection of the measured and simulated points for one skiing stroke.

A simple visual inspection reveals the similarities between the trend of the measured and simulated points on the lower leg. A difference exists in the trajectory of the points: one reason is that even though the markers of the data acquisition movement are attached to the body, they still have some relative movement that affects the measurement of the position of those points. This was determined when the assumed constant distance between the reference markers was investigated. These marker errors are a common issue to deal with in movement analysis experiments. As presented by Andersen [4], where close accuracy of the measurement is needed, corrective actions have to be enforced.

In Table 3.2, the Pearson correlation coefficient is used to find out how well the simulated data describes the experimental data. The closer this value is to one, the better the description of the phenomena is by the simulated data. It can be seen that the values obtained for each case are in good agreement with the expected results.

Table 3.2. Pearson correlation coefficient of the position simulated results

	Ankle marker	Knee marker	Femur marker
Plane X–Y	0.9537	0.9927	0.9997
Plane X–Z	0.9724	0.9338	0.9410

A comparison between the measured and calculated forces is shown in Figure 3.11. Although differences are expected to occur because of the assumptions and simplifications made, the results are still in agreement with the measured data.

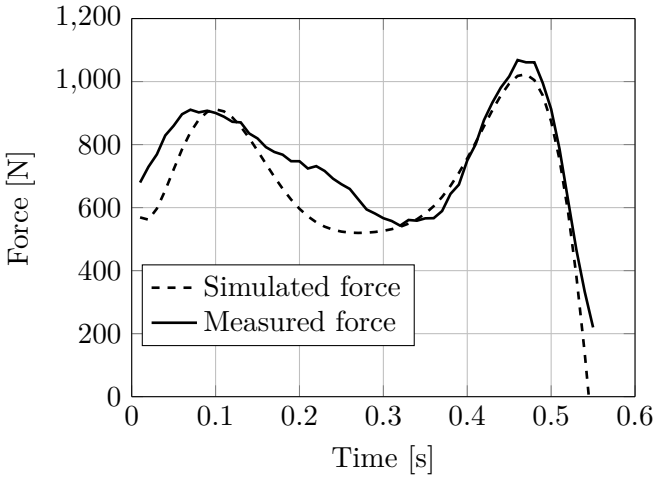

Figure 3.11. Comparison of the simulated and measured resultant total ski forces for one skiing stroke.

In Figure 3.11, a simple inspection shows that the simulated force follows a trajectory similar to the measured force. For the present case, the shapes of the curves are very similar, with a dwell around $t = 0.35$ s and a clear push around $t = 0.47$ s (with an overall Pearson correlation of 0.94). The mean values are approximately the total weight of 785 N of the skier and the maximum difference between the measured and calculated values is about 263 N, occurring at around 0.27 s.

As the Pearson correlation coefficient by itself is not enough to assess the agreement between the experimental and simulated set, Figure 3.12 introduces the Bland-Altman plot of the comparison of the two time series data representing the resultant force. The Blant–Altman plot quantifies the agreement between two quantitative measurements by studying the mean difference and constructing limits of agreements [8, 23].

From Figure 3.12, it can be seen that despite a negative bias, most of the points are within the 95% confidence interval. This shows that there is a difference between the methods compared. However, the fact that most of the points are concentrated within the confidence interval can be considered as an acceptable agreement between the simulated results and the measured data.

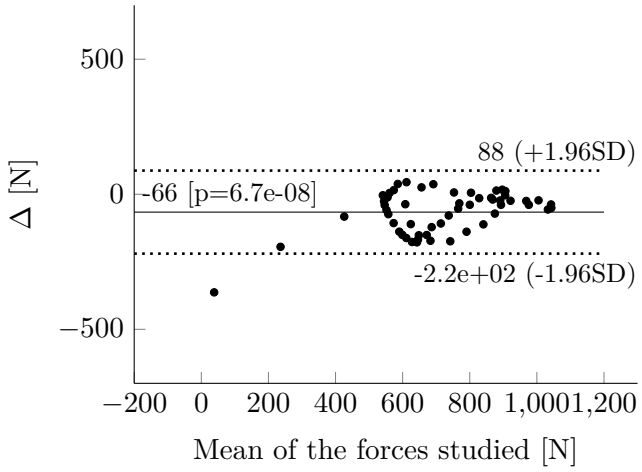

Figure 3.12. Bland–Altman plot showing the 95% limit of agreement between the measured and simulated resultant force.

This level of proximity in the results might be considered as one of the key aspects towards certifying the validity of the proposed model.

Finally, the experimental and simulated resultant forces are projected onto the $\boldsymbol{X}$, $\boldsymbol{Y}$, and $\boldsymbol{Z}$ axes to obtain the propulsive, lateral, and vertical force components which are shown in Figures 3.13, 3.14, and 3.15, respectively.

In the propulsion force in Figure 3.13, the shape is close to the one obtained by Fintelman et al. [19] in the speed skater model. Additionally, it can be seen that both the measured and the simulated forces, follow a similar path with coincident positions of peak values.

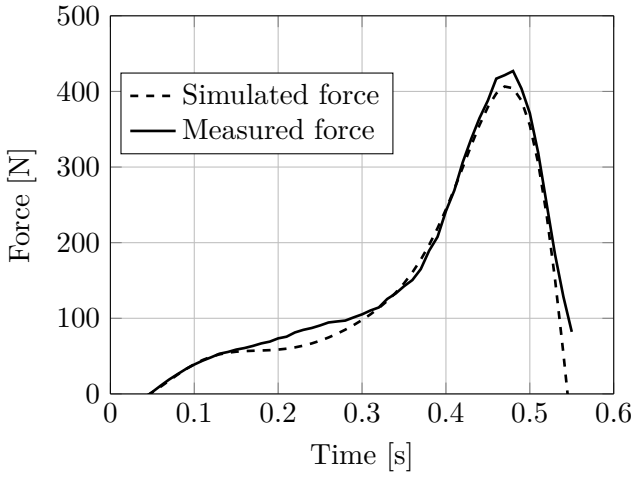

Figure 3.13. Simulated and experimental propulsion force for the selected active phase.

A similar case occurs when comparing the lateral forces. Figure 3.14 demonstrates how much the shape of both experimental and simulated curves resemble each other.

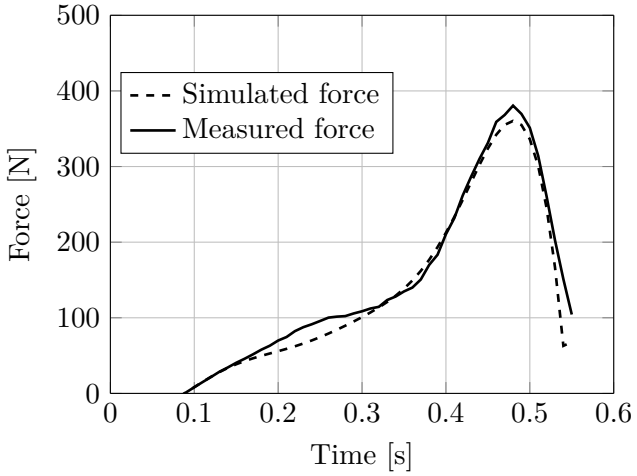

Figure 3.14. Simulated and experimental lateral forces for the selected active phase.

Figure 3.15 shows the vertical component of the leg force. It is noticeable that this force influences the general shape of the total leg force and it is larger, almost the double, than the propulsion force.

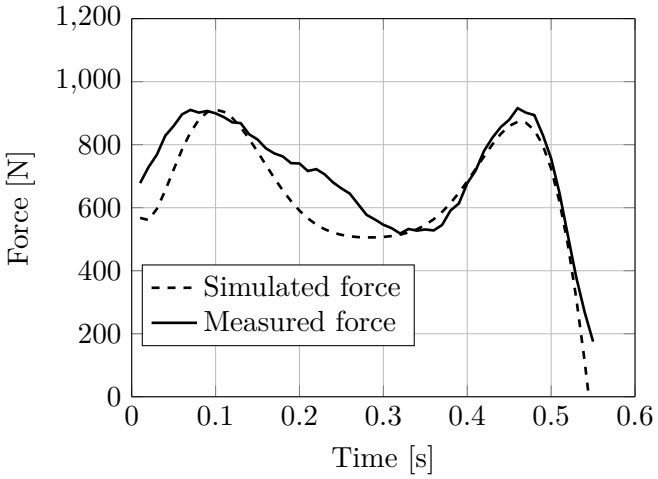

Figure 3.15. Simulated and experimental vertical forces for the selected active phase.

The information provided by the components of the resultant force is obvious when looking at their shapes. Propulsion and lateral forces clearly indicate the propulsion moment represented by the peak at the end of the movement. The vertical force contains the information of three important phases during the stroke.

These phases could be defined as follows: the initial touch of the ski represented by the first peak value, the gliding phase denoted by the valley of the curve, and finally, the propulsion phase described by the second peak value towards the end of the curve.

3.5 Discussion

Simulation models can be used in training, technique research, and the development of new equipment. Additionally, the advantages of human models are countless in the investigation of injuries in sports.

This study presented a mechanical model for a skier performing the skating technique in cross–country skiing. The selections of the joints used to model the human movements are, at the same time, simple to implement but also general enough that they cover a wide range of movements included in the natural physiology of the leg. To present an additional advantage of simulation models, Figure 3.16 shows a timed visualization of the sequence of leg movements during the propulsion phase.

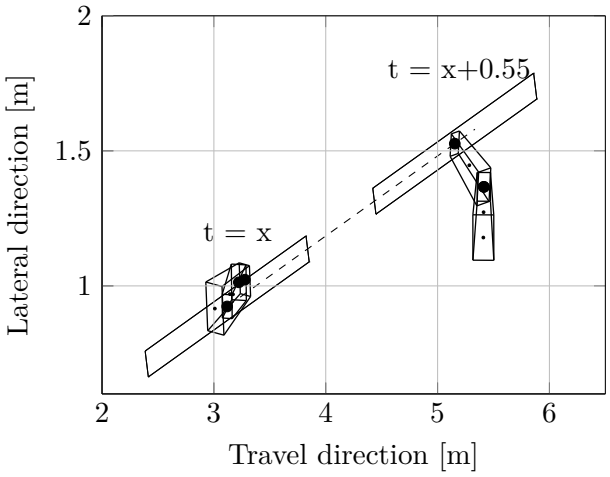

Figure 3.16. Leg extension sequence obtained from the multibody skier model. The subsequent time frames are 0.55 seconds representing the start and end of the leg extension cycle.

Visualizations facilitate the analysis and add relevant information that a mere numeric chart or table cannot present openly to the user. Visualization and movement animation are well–recognized features used more and more in biomechanics study cases. For example, in the visualization figure, it is simple to observe the bodies forming the leg, the position of the joints and the travel direction of the ski. Also, the flexion and rotation movements can be identified. Another important aspect of this model is the fact that certain parameters that have a high impact on the technique can be changed easily. Track steepness, athlete data, snow friction, and air drag can be changed very quickly, and a new simulation set is ready to be performed.

The researcher considered it convenient to implement once again the anthropometric data uncovered by Yeadon [85] in the model. This type of statistical representation relies on the simplicity that the researcher wants to achieve. Counting on a model that minimizes the amount of input data and continues to give close enough results approximates this research to what a simple model should be. Movement and force representation, movement details on the joints of the lower leg during the execution of the phase, and a wide range of visualization speeds guarantee that the customization of the post-processing will fit the requirements of the user.

As the model presented had the objective of resembling the trajectory of certain representative points during a single stride and of determining the forces exerted by the skier on the ski from them, the simplifications and assumptions made were adequate to accomplish the task. However, the model may be adjusted and

customized for more detailed applications and other areas of study. For example, the only parameter assumptions made in the present case were related to the determination of the snow friction and air drag. These parameters were tuned in an iterative form but always kept within the limits proposed in the literature.

It is important to mention the limitations of the present model. This study focuses on modeling one skiing stroke without the use of poles. Although this might seem a significant limitation, it is instead the starting point of a more complete modeling system where a complete race could be simulated or reproduced. Advances in wireless technology and miniaturization will, in the near future, enable taking information related to force production, speed or rhythm automatically from athletes during a competition. This information and the results can be used to enhance the accuracy of the simulation model towards the point where the simulation of a race can become reliable and several scenarios could be analyzed.

Currently, the limited availability of position measuring devices for longer runs with enough accuracy affects the development of other simulation attempts directly. It could be possible to extend the amount of data collected for one short experiment. However, the variability of the skier's movement while performing the technique rapidly prevents the idealization of the model.

It is proposed as a future step to work towards the development of this type of reliable equipment, to elaborate more general models, and factoring in simulations for the athlete's fatigue. Working on the development of user–friendly interfaces where the coaches, practitioners, and public in general could benefit from these models without the participation of a multibody specialist.

One specific task where this simulation tool can be used is in understanding how the propulsion force is produced taking advantage of the measured kinematic data. In the skate skiing technique is a key factor in achieving speed and fluidity. As maintained by Rusko [63], there exist many elements to be controlled while skate skiing – some of them are done intuitively and others can be learned and reinforce by training.

This tool would allow producing information to be used in the development stage of athletes. For example, the technique of a young or aspiring athlete can be compared with that of a top level athlete, enabling the detection of important differences by using a simulation tool. Additionally, a baseline of the practitioner's parameters can be generated to be compared later as the practitioner improves, and force variations caused by modifications in the leg movement of the athlete can be simulated quickly without the need for field measurements.

3.6 Conclusions

A simulation tool that could help coaches or researchers in general during the training phase can expedite improvement and serve as a means to evaluate the performance of athletes. This study demonstrated the possibility of using simplified multibody models to simulate the human movement specifically in winter sports such as cross–country skiing.

Even though this is a simple model where the upper mass of the skier's body was positioned in the point representing the femur, the results obtained on the calculated motion and forces are in good agreement with those measured.

Extending the model with the usage of poles to analyze poled cross–country skiing is a challenging direction for future work.

Chapter 4

Assessment of the skier technique's evolution

To assess how well the results from one measurement system can follow the results of a gold standard system, or how an execution technique has evolved, an efficient comparison tool has to be adopted. Comparing the results of a variable obtained from different measurement systems might involve a series of adjustment steps. Actions like cropping, linear trend removal, offset removal, and amplitude scaling belong to the tool–set of research teams. However, part of the work to implement these techniques is still manual, laborious, and varied. This variety turns the data post-processing into a lengthy and complex task [71].

The majority of the research studies omit detailed information on their data handling process. As an example, in certain studies such as those based on camera–recorded movements, researchers study the position of specific body landmarks frame by frame [83]. This represents a gigantic amount of work.

For this study, the raw gait data was available from two different motion capture systems. A high–speed camera-based system with skin–attached markers and an inertial measurement unit system. To simplify the extent of the procedural application proposed in this chapter, the knee flexion–extension angle, from the known range of gait kinematic variables, served as the test signal. The dynamic time warping (DTW) technique, initially developed for the recognition of spoken speech [66], is tested as a tool to arrange and compare these test signals in an automated fashion.

The specific objective of this contribution is to investigate DTW as a technique to provide comparable knee joint flexion–extension angle data collected at different walking speeds and with different acquisition systems. The researcher compared the flexion–extension knee joint angles measured at different walking speeds. On

a general point of view, the objective of this apart is to adapt a tool to efficiently compare time–based sequences prone to be used in an automatized fashion with minimum manual intervention. For this purpose, a single subject design protocol following the guidelines proposed for gait studies [37] was implemented.

4.1 Dynamic time warping implementation

DTW is a technique able to handle nonlinear fluctuations due to the speaking rate variation in the analysis and recognition of speech [64]. It is also able to find an optimal global alignment between time series, becoming the most commonly used measure to quantify dissimilarities between sequences [59]. These important characteristics make it suitable for analyzing gait or human movement temporal series data that may vary in speed or time. DTW can also be applied in other fields than speech recognition. From analyzing gene expressions to recognizing hand signatures [3, 60], DTW has demonstrated its relevance.

DTW has been used in prior studies to recognize walking, climbing and descending stairs using data acquired with a single inertial sensor unit [34]. To the best of the author's knowledge, this method still needs work in the analysis of gait and ski data across different measurement systems or between trials acquired with the same measurement system.

DTW minimizes the distance between two time series, no necessarily equal in length, by calculating an optimal warping path P. This warping path maps the series' points with same shape to each other. DTW considers the two time series or sequences in the form: $X = \{x_1, x_1, \ldots, x_n\}$ and $Y = \{y_1, y_2, \ldots, y_m\}$, with $n \in [1 : N]$ and $m \in [1 : M]$ and N and M representing the length of X and Y, respectively. The warping path can be denoted as $p = (p_1, \ldots, p_L)$, where each element of p is represented as an ordered pair $p_l = (n_l, m_l)$. In the warping path, $l \in [1 : L]$, being L the length of the warping path constrained to the interval $L \in [max(N, M), M + N - 1]$.

Figure 4.1 shows the target points on each time sequences that DTW tries to align.

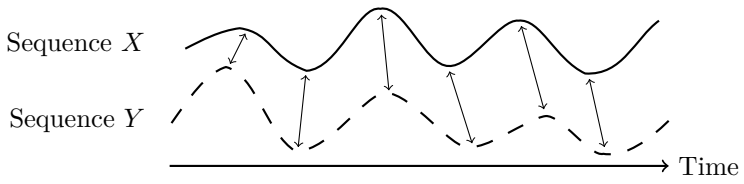

Figure 4.1. Time alignment of two time–dependent sequences. Adapted from [48].

A cost function or local distance measure is used to calculate a matrix of accumulated cost between the different points of the analyzed curves. After constructing the accumulated cost matrix, the minimum cost path or warping path that is not always unique is derived, fulfilling the constraints of the boundary condition, monotonicity and step size condition.

4.2 Experiment configuration

The two motion capture systems used in this study were Vicon Nexus [1] and Xsens MVN BIOMECH [2]. The Vicon Nexus system utilizes a set of high–speed cameras and retro–reflective markers attached to the subject to collect position data of anatomical landmarks. The data is later used by the system to calculate joint angles, velocities, accelerations, and other related kinematic variables. In contrast, the Xsens system is based on measuring acceleration and the angular rate of body segments with inertial sensors. The acceleration and angular rate data are then fused to obtain joint angle data [29].

The Vicon Motion system set up consisted on thirty–four 14 mm retro-reflective markers which were attached to the test subject according to the Plug–in Gait full body model. An eight–camera system (Vicon T40, Oxford, UK) was used to record marker positions at 120 Hz. The marker trajectories were first low–pass filtered using a fourth order Butterworth filter with a cut–off frequency of 12 Hz, and joint angles were then calculated using Plug–in–gait model (Vicon Nexus). The standard Vicon calibration procedure was applied prior to performing the measurements.

In the case of the Xsens setup, 17 IMUs were attached to the subject. To minimize the movement of wires during walking, a lycra body suit was used. Additionally, the sensors were placed on bony surfaces as recommended to minimize measurement errors, and the sampling frequency of 120 Hz was used to match that used by the Vicon system. N–pose–type calibration was used to express segment kinematics in the global frame, and it was done after each five trials to minimize measurement errors caused by the drifting of the sensor data.

The Vicon and Xsens systems were synchronized via the standard synchronization protocol provided by Xsens in its instruction manuals. The master system was set to be Xsens while Vicon remained a slave system during all of the measurements.

After setting up the equipment, a healthy male subject performed 27 walking trials at different speeds over a runway of approximately six meters. Each trial started with at least three seconds of standstill in which the test subject did not move. To minimized the common drift errors in IMU systems, an N–pose–type recalibration was performed after every five trials.

4.3 Analysis of the data

The systems' output data was filtered to work only with the knee joint angle values, i.e. the knee flexion and extension angles. Additionally, axis alignment orientated the main reference axes in which the systems represented their data. These two actions guarantee the same angle representation for the studied flexion–extension.

The baseline offset in the measurement data of the different systems was corrected. This offset is suspected to exist because the angular calculation method and initial calibration protocol used by the two systems are different; however, no additional tests were performed to validate this assumption. The initial knee joint angle when the subject is standing still should be approximately 180 degrees (leg fully extended). The offset was calculated such that the closest signal from any of the two systems to 180 degrees was considered to be the reference configuration. The other system's reference configuration was moved by the amount indicated in the offset.

After correcting the offset between the two systems, the knee joint flexion–extension angle data was normalized with the DTW normalization technique. In the next section, the DTW implementation procedure is presented. This form of implementation was taken from [67] and is one of many other forms that can be found in the literature.

All of the studies were conducted using the software MATLAB for Windows (MATLAB, 2013). A custom-made script was written to read the Xsens system native .mvnx format and the Vicon system .c3d format as well as to generate the alignment.

4.4 Results

After orienting each of the systems' axes to match the measurement of the flexion–extension angles of the knee joint, the data obtained for a typical trial looks like the sequences shown in Figure 4.2.

Next, the offset between both signals was accounted for and compensated. As previously mentioned, this compensation was made in all of the cases by aligning the sequences to the one with a starting point close to 180°. Other offset compensation techniques may be applied, such as the baseline removal. However, as a healthy subject is likely to have a knee angle close to this value when standing still, the research team used this simple approach.

Once the offset was corrected, the DTW analysis was performed according to the methodology outline in the method section. Figure 4.3 shows the aligned sequences after applying DTW. It can be observed how well the curves aligned after the procedure.

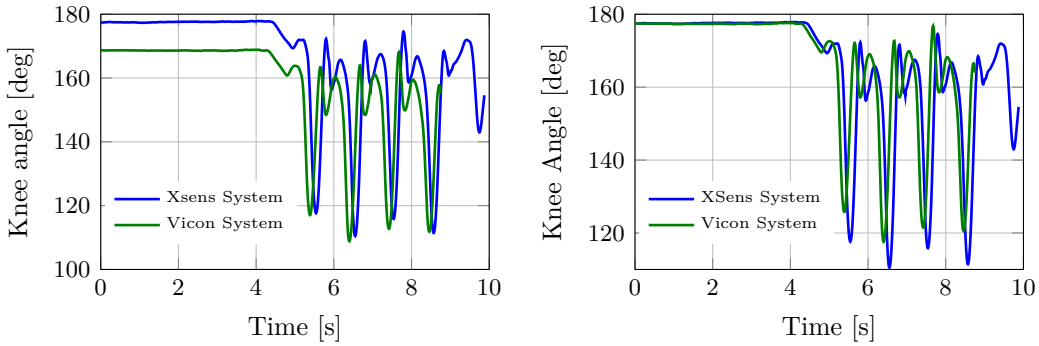

(a) Before offset removal.

(b) After offset removal.

Figure 4.2. Example time sequences obtained from Vicon and Xsens systems. Right leg knee flexion–extension angle.

After the alignment, as an exercise, several pieces of statistical data were calculated by extracting important points from the studied sequences e.g., maximum knee flexion angle. Statistical analyzes can be also automated together with the application of the DTW algorithm. Selecting an adequate method to analyze the data, allows for determining if two or more sets of data can be considered statistically equal, how one variable correlates to another, or how the athlete's technique has change from a quantitatively point of view.

In this example, Figure 4.4 shows the mean of the maximum knee angle found in the complete set of trials.

With the statistical data easily obtained from the aligned sequences, a common analysis such as the one-way ANOVA [30]. ANOVA is a method commonly used to test the differences among means by analyzing the variances. ANOVA gives indications whether the means of the groups are different or statistically equal. Table 4.1 shows the results of the F–value for each comparison set, and the probability of observing an F–value larger than the F–value obtained in the study are also presented.

Table 4.1. One-way ANOVA results of the flexion–extension angle differences.

Variable	One-way ANOVA	
	F-value $df = 3.2$	p-Value
Left knee flexion–extension	2.964	0.061787
Right knee flexion–extension	1.743	0.186568

If it is of interest to compare the leg movements to analyze how different the athlete executes the technique, DTW presents a straightforward method to do it.

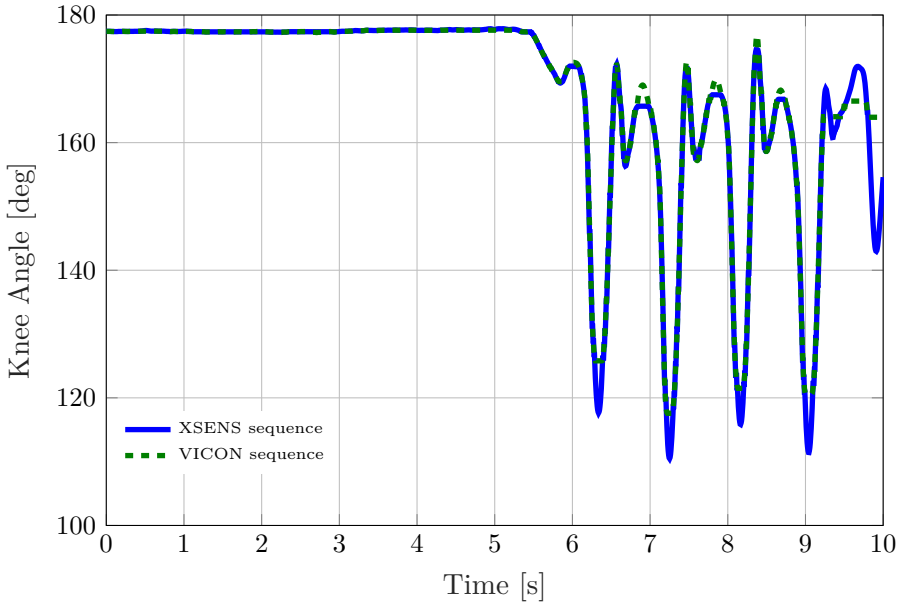

Figure 4.3. Resultant sequence alignment after DTW. Right leg knee flexion–extension angle.

In Figure 4.5, DTW was applied to compare the right and left knee angle values of the test subject obtained from the Xsens data. Graph 4.5–a presents the raw initial values, and graph 4.5–b shows the results of applying DTW with no extra manual intervention.

4.5 Discussion

The post–processed results on the two sets of flexion–extension angle sequences demonstrated that DTW provides comparable data across different measurement systems with minor manual processing. The list of necessary tasks to post–processed the experiments results is as follows:

- Orient results according to the same reference system.
- Correct baseline offset.
- Perform DTW algorithm.
- Perform automated statistical analysis.

Figure 4.2 showed that apparently dissimilar curves might be obtained when using different systems or inclusive the same system to measure the same variable without

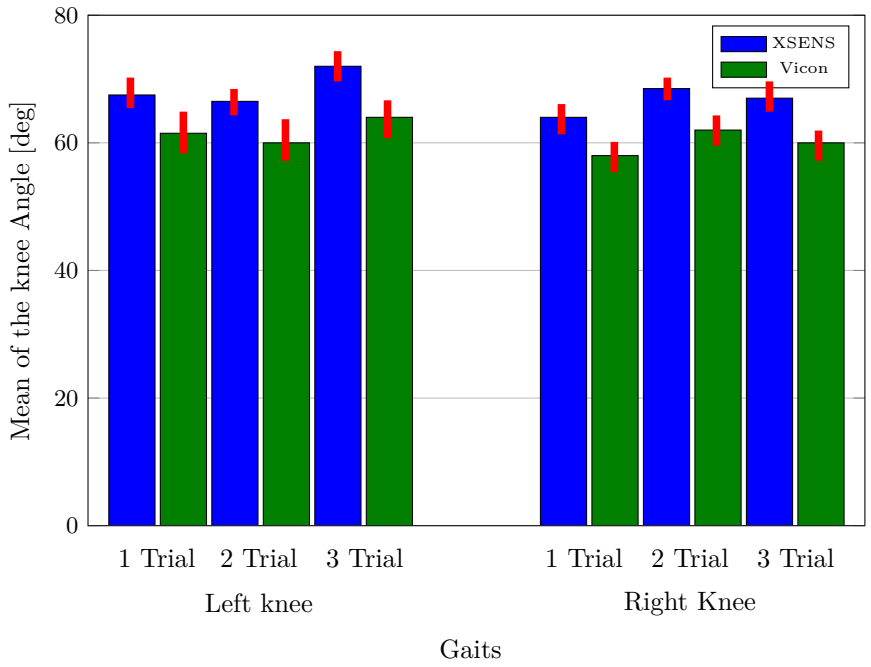

Figure 4.4. Mean of the maximum knee angles and standard deviations (in red). The data is divided into three gait cycles to present the maximum angle for the left and right knee.

using a suitable post–processing method. Often, a dedicated post processing procedure is performed to make sequences comparable. One method is to divide the sequences into isolated gait segment cycles and proceed with the adjustment. In contrast, a straightforward method outlined here can be used to compare the full measurement data.

Figure 4.3 shows the typical outcome for all experiments conducted in this study. It was observed that in all of the cases, the sequences were aligned successfully, and after that, any statistical posterior analysis can be performed directly on the normalized data. Even in testing data, the arrangement of the right and left knee angles is proven, to work with almost no manual intervention.

In addition, a posterior one–way ANOVA test was carried out determine if any of the differences between the means are statistically significant. For the one-way ANOVA test, the maximum flexion–extension angles and the time when they occur were identified. Table 4.1 displays the results of the ANOVA analysis. The probability values obtained in the analysis are low enough to reject the null hypothesis using the common significance level of 0.05. However, in the case of the means of both sets, the means of the left knee flexion–extension angle seems

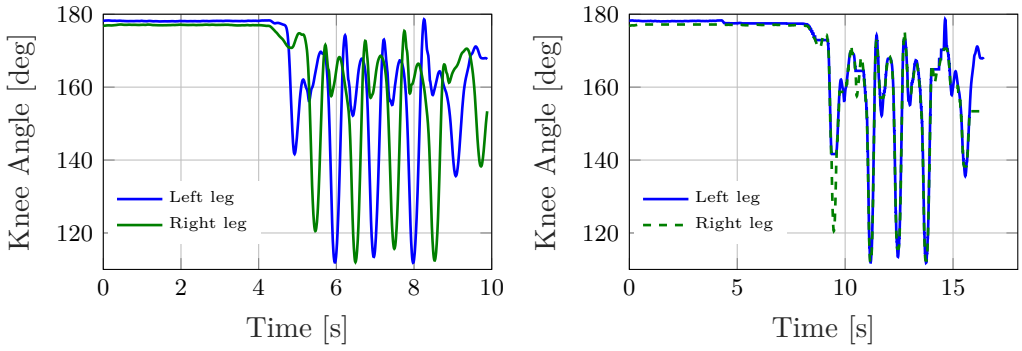

(a) No DTW application. (b) DTW applied.

Figure 4.5. Application of DTW to normalize right and left leg knee angles.

to belong to the same group, while in the case of the right knee flexion–extension angle the means seem not to be equal.

As the experiment is based on two simultaneous measurements of one subject performing all the trials, it is rapidly shown that there exist an important difference in the results of both systems. As it was shown in Figures 4.3 and 4.4, Xsens consistently showed larger flexion values than those obtained by Vicon.

Figure 4.5 compares data from the Xsens system for one example trial. the results show consistency in the flexion angle measurement.

4.6 Conclusions

This chapter demonstrated one application of the dynamic time warping technique in the study of the human body movement analysis. Several time series sequences of the flexion–extension angles measured with two different measurement systems served as input data to test the implementation of the DTW method. It was shown that implementing DTW, originating from the speech pattern analysis, was suitable for the automated post–processing stage of the analysis without affecting the nature of the experiment. As DTW mainly requires the use of a distance measure function for sequence alignment, the Manhattan distance worked in 100 % of the cases in this study. The comparison between measurement data from DTW treated Vicon and Xsens was easily assessed highlighting differences between the two systems. For the present set of studies, it could be quickly seen that the results of the left knee flexion–extension angles obtained from both systems can be considered statistically equal. That was not the case of the right knee flexion–extension angles. One of the causes of this difference might be attributed to magnetic distortion found in the test area. As Xsens

relies on magnetic measurements to estimate the orientation of its sensors, any magnetic interference can disturb the results and make them useless. With aims of incorporating fast automated analysis in portable instruments wore by the ski practitioner, the researcher considers that DTW as a tool to compare sets of data, fits the objectives presented in this chapter.

Chapter 5

Ski pole kinematics

In the preceding chapters, the cross–country skiing modeling was approached excluding the effect of the ski poles. Nevertheless, ski poles play a relevant role in the discipline. It was described that in some cross–country techniques, the skier relies mainly on the poles to achieve the forwards propulsion. That is the case of the double poling technique of the classic ski style. The question raised at the moment is how to include the poles in the modeling process?

Studies similar to those carried out by Cignetti [12] show the importance of using ski poles and their coordination with the overall movement of the skier. The differences between athletes are noticeable when detailing the movement coordination and the kinematics in the execution of the technique. Due to the cyclic nature of cross–country skiing, the kinematics of the skier can be based on cycles as fundamental study units. Some benchmarking measurements used by researchers are based on cycle duration, cycle speed, cycle length, ski thrust duration, ski glide duration, ski thrust duration, and recovery phase duration [16].

To study the kinematics and dynamics of the ski pole action in particular, the methods used to study the skier's movement can be used. Camera–based methods based on infrared cameras or high speed camera recording are popular among research groups [16]. However, the instrumentation of these methods is complex and their application is limited by the spatial setup of the test site. Camera–based methods are expensive and it is inaccessible to most ski practitioners interested in the conclusions that can be drawn from data provided by camera systems.

The need for extending cross–country ski studies beyond the confined conditions imposed by camera based systems motivated researchers to look at other alternatives. One of the systems increasingly utilized in human movement research is the one based on IMUs. IMUs are less accurate than infrared camera systems,

but their advantages supersede those of camera–based systems. These inertial measurement systems are portable, light, and can be carried in any race situation without interfering with the skier's technique.

In this chapter, the kinematics of the ski poles will be approached in the following manner. Firstly, the findings related to the recognition of an important phase of the ski pole kinematics, the pole plant, will be introduced. The pole plant refers to that phase of the pole movement in which the tip of the pole is in contact with the ground, thus closing the kinematic loop snow–skier–pole–snow. During this phase, the skier might take advantage of the forces produced by the contact between the ski pole and ground. The second point of view is related to the orientation of the ski pole during the pole plant phase. Knowing the ski pole plant, the orientation of the pole at this moment, and the axial forces that the ski–snow contact produces, it is possible to estimate the propulsive reaction forces from these contacts. The development of this chapter is the result of a seven-month exchange visit to the Laboratory of Dynamics of Human Motion of the University of Michigan in the US.

5.1 Pole plant phase determination

To estimate the pole plant phase from the IMU reading, it is necessary to perform a deep analysis of the information gathered from IMUs and their kinematic relationships. The main idea at this stage, is to be able to determine the pole plant start and end with the use of the sole IMUs information. Several methods have been used in the past and recently to closely determine these instances. In the following paragraphs, few comments will be given to some of these methods and a new way of defining these instances will be proposed and tested.

The methods to determine the pole plant phases can be listed into three basic groups: force sensors, camera–based inspection methods, and acceleration analysis methods. One of the first researchers to study the forces produced in cross–country skiing was P. Komi in the 1980s [32]. Komi conducted his research under the premise of accounting for the leg and pole forces separately in order to determine their contribution to the forward progression. To measure the forces produced by the ski poles, Komi used long force platforms installed onto the ski tracks, which allowed him to determine the ski pole force components and their action instances directly. Force platforms such as those used by Komi provide almost direct force measurement with the drawback of the installation and calibration they require. The time and effort to set up the system is considerable and highly dependent on the calibration. This system was used also by Vähäsöyrinki et al. in a ski tunnel under controlled conditions [81]. Vähäsöyrinki's findings resemble to those by Komi.

Other research teams have installed strain gauges and piezoelectric force sensors to measure the pole forces and thus detect their actuation time. That is the case of the studies by Holmberg [25], Stöggl [74], and Street [77]. Strain gauges and piezoelectric force sensors provide the researchers with more portable equipment to perform their experiments. They are comparatively easier to set up and calibrate, and the measurement range is increased notably with respect to the fixed force platform systems.

In the case of camera–based and IMU systems, the former are often used as a means of validating for the latter. Because of the inherent inaccuracy of the systems based on IMUs, it becomes necessary to provide them with a form of valid comparison to assess the proposed detection algorithm. It can be seen in studies, such as the one by Fasel et al. [16], where the ability to detect spatio–temporal parameters on the skier, and more specifically on the ski poles, is verified by using infrared camera systems. Myklebust [50] used a similar concept to study the differences between the V1 and V2 technique of cross–country skiing.

These two studies [16, 50] present the first attempts to estimate the kinematics of ski poles using IMUs and utilize different approaches to estimate the pole plant and pole lift instants. As mentioned in the previous paragraphs, knowing the contact events of the poles will allow determining the behavior of the ski pole orientation during this phase, and consequently, the components of the pole forces promoting forward propulsion can be determined. Fasel and Myklebust did not estimate of the ski pole angles during the contact phase, and studies where the orientation information can be found are based mainly on camera systems, as detailed in the introduction of this dissertation.

To determine the pole plant and lift, Myklebust [50] used the jerk and span of the raw acceleration, i.e. the first and second derivative of the raw acceleration, respectively. The jerk in this case can be understood as a jump–discontinuity in the acceleration, the effect of which can be seen when touching or leaving the ground contact. Fasel approaches the problem by analyzing the acceleration peaks measured during the pole contact. Fasel's approach is simpler because no extra calculations are needed to identify the moment of the pole plant and lift. One important aspect to highlight is that neither of the approaches is suitable for automation. Manual work is needed to locate the peaks representing the contact instants.

The method used in this work exploits the kinematics of the ski pole. Considering only the classic ski and skate skiing techniques, the ski poles present two types of movements: swing or actuated–inverted pendulum movements. During the swing phase, the ski pole is subjected to the arbitrary movements controlled by the skier. However, the arbitrariness of these movements could be better explained by implying that the skier performs some sort of natural arm optimization [56, 87] in

the ski pole movement in the air. During the snow–pole contact, the kinematics of an inverted pendulum can be used to propose some hypotheses which enable estimating the instants of the pole plant and lift. In the next sections, a brief description of the inverted pendulum kinematics will be presented to define the foundations of the method proposed.

5.2 Ski pole as an inverted pendulum. Pole plant and lift

The kinematics of the inverted pendulum problem has been widely approached and taught in mechanical engineering courses around the world. The methods used to study the inverse pendulum kinematics span almost all of the formulations in classic mechanics. For this specific case, the inverse pendulum kinematics is described by analyzing the accelerations from two specific points on the ski pole: one located close to the hand grip and the other located at the tip. The exact positioning of these points is shown in Figure 5.1 together with the coordinate reference system used to represent the part of the pole kinematics relevant to this case.

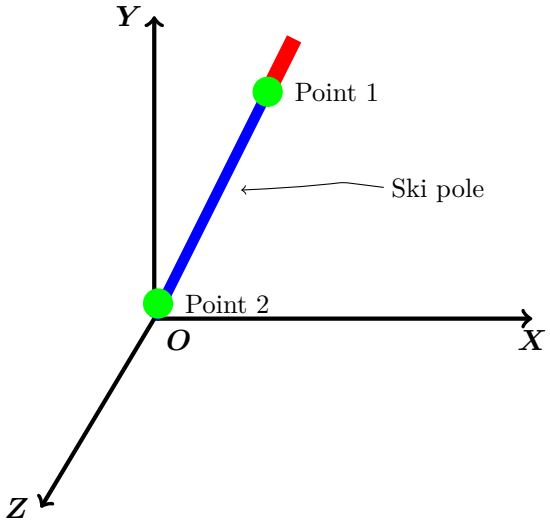

Figure 5.1. Location of the points on the ski pole used to explain the kinematics approach to the pole plant and lift detection problem. Point 1 is located at the ski pole hand grip and point 2 is located at the pole tip.

Taking $\boldsymbol{O}$ as the origin of the coordinate reference system, it is possible to calculate the linear velocity and linear acceleration of both points as follows:

$$\boldsymbol{v}_{p1} = \boldsymbol{v}_O + \boldsymbol{\omega} \times \boldsymbol{r}_{p1/O} \tag{5.1}$$

$$\boldsymbol{v}_{p2} = \boldsymbol{v}_O + \boldsymbol{\omega} \times \boldsymbol{r}_{p2/O} \tag{5.2}$$

$$\boldsymbol{a}_{p1} = \boldsymbol{a}_O + \dot{\boldsymbol{\omega}} \times \boldsymbol{r}_{p1/O} + \boldsymbol{\omega} \times \boldsymbol{\omega} \times \boldsymbol{r}_{p1/O} \tag{5.3}$$

$$\boldsymbol{a}_{p2} = \boldsymbol{a}_O + \dot{\boldsymbol{\omega}} \times \boldsymbol{r}_{p2/O} + \boldsymbol{\omega} \times \boldsymbol{\omega} \times \boldsymbol{r}_{p2/O}. \tag{5.4}$$

In Equations (5.1) to (5.4), $\boldsymbol{v}_{p1}$ and $\boldsymbol{v}_{p2}$ are the linear velocities of points 1 and 2, $\boldsymbol{v}_O$ is the linear velocity of the origin of the reference system, $\boldsymbol{\omega}$ is the angular velocity of the ski pole, $\boldsymbol{a}_{p1}$ and $\boldsymbol{a}_{p2}$ are the linear accelerations of points 1 and 2, respectively, $\boldsymbol{a}_O$ is the linear acceleration of the origin of the coordinate systems, $\dot{\boldsymbol{\omega}}$ is the angular acceleration of the pole, $\boldsymbol{r}_{p1}$ and $\boldsymbol{r}_{p2}$ represent the position vectors of points 1 and 2 measured from the origin of the coordinate reference system, respectively.

For the following parts, it is important to remind that the variables measured directly by the IMUs are the linear acceleration (including inertial accelerations and gravity) and the angular velocity. Any other variable derived directly from those previously mentioned is subjected to a cumulative error which introduces noise in the calculations. For this approach, the use of derived variables will be limited to just one: the angular acceleration.

During the inverted pendulum movement (pole contacting the ground), the vectors $\boldsymbol{v}_O$ and $\boldsymbol{a}_O$ are zero. This simple characteristic of the movement of the pole during contact brings to the surface an important simplification which allows proposing the following evident relationships:

- The linear velocities of the points differ only by a factor related to the ratio between $\boldsymbol{r}_{p1}$ and $\boldsymbol{r}_{p2}$. Figure 5.2 shows graphically this particular condition recurring during the pole–ground contact. Equation (5.5) expresses this ratio,
$$\frac{\|\boldsymbol{v}_{p1}\|}{\|\boldsymbol{v}_{p2}\|} = \frac{\|\boldsymbol{r}_{p1}\|}{\|\boldsymbol{r}_{p2}\|} \tag{5.5}$$
- The values of the linear accelerations calculated using Equations (5.3) and (5.4) should be close the linear acceleration measured by the IMUs except for the effect of the gravity acceleration, which can be subtracted from the IMUs measurement.

Using these two hypotheses, the estimates of the pole plant and pole lift instants should yield coherent results suitable for the purposes of the ski pole study. The

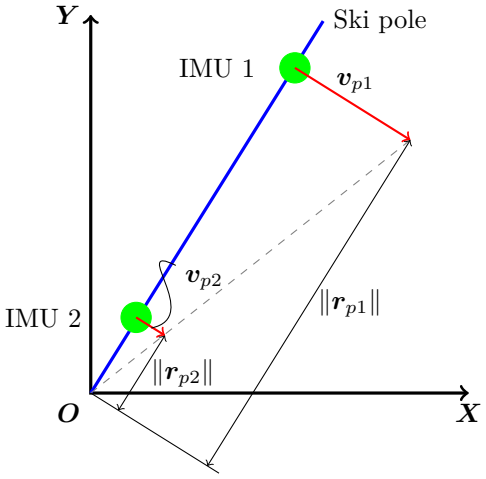

Figure 5.2. Linear velocities calculated using sensors' information during the inverted pendulum phase.

first hypothesis presents the advantage of utilizing variables measured directly from the sensor and the mounting of the sensor on the pole. It minimizes the inclusion of the the error produced when integrating or differentiating the angular velocity. The drawback of this approach is that the ratio $\|\boldsymbol{r}_{p1}\|/\|\boldsymbol{r}_{p2}\|$ might vary during the contact movement depending on the ski pole movement, and setting a fixed value to evaluate the contact condition might be misleading. The second hypothesis provides a direct comparison of a calculated value with a direct measured value. This condition eliminates the ratio variability presented in the first hypothesis; However, it is necessary to differentiate the angular velocity to obtain one of the terms needed in the equation. As mentioned recently, differentiating the angular velocity introduces errors caused mainly by the noise present in the sensor readings.

To validate the effectiveness of these approaches in determining pole plant and lift instants, camera–based systems are usually used. These systems bring associated manual work that might introduce errors into the validation of the contact points, and they might lead to erroneous conclusions when assessing the effectiveness of the method. For this case, a contact button installed at the very tip of the pole is used. Every time that the ski pole hits or leaves the ground, the push–button will immediately detect this situation without manual intervention. The details of the equipment used for the experiment and their setup will be described in the following sections.

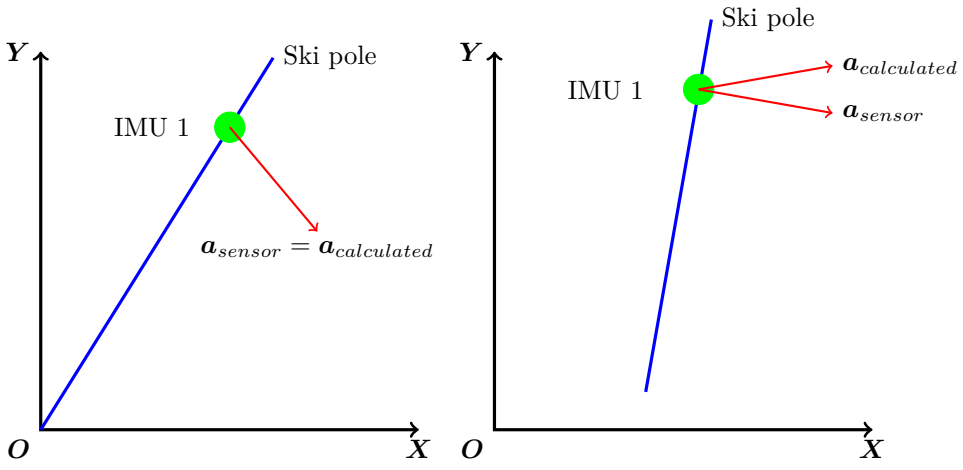

(**a**) Inverted pendulum phase (**b**) Swing phase

Figure 5.3. Relation of the linear acceleration measured by the sensor and calculated using Equation (5.3) during the inverted pendulum and Swing phases.

5.3 Signal treatment and estimation of the pole orientation

The data measured by the sensors is noisy and biased. Additionally, using the data unsmoothed may increase errors when calculating integrals or derivatives from the acceleration or angular velocity signals. When searching for high accuracies in the outcome of new processing algorithms, noise can hinder the comparison between the outcomes from the proposed algorithm and the system used to validate the former.

To minimize errors, two actions were taken: Firstly, the sensors used in this experiment were previously calibrated to reduce the bias error and cross axis sensitivity errors according to the internal procedures existent in the Laboratory of Dynamics of Human Motion [31]. Due to the controlled conditions maintained during the tests, no concerns arose from possible radiometric, temperature, or sensitivity errors. Lastly, to eliminate the noise, which is characterized by its high frequency, a first order Butterworth filter with a cutoff frequency of 10Hz is used.

To determine the orientation of the ski pole (roll and pitch angles), the method published by McGinnis et al. [39] is used. This method is a modified complementary filter which is able to extract the true quantities from the acceleration and angular velocity readings. Although the acceleration and angular velocity values are directly read by the IMUs, these readings are formed by a linear combination of the real value, white noise, bias and/or gravity in the case of the acceleration.

As mentioned by McGinnis et al., the goal of the technique is to use the measured

linear acceleration to estimate the bias and noise on the gyroscope readings and remove them from the measured angular velocity, leaving only the true angular velocity ($\boldsymbol{\omega}$) which will be used to calculate the orientation of the sensor in the form of a direction cosine matrix $\boldsymbol{C}_{G/I}$.

5.4 Experimental setup

Three types of experiments were conducted to validate the accuracy of the complementary filter algorithm in controlled conditions, how accurately the ski pole plant and lift phases were detected, and to determine the orientation of the ski pole while being in contact with the ground. Thus, the propulsive force components can be estimated with the use of a load cell. The same setup configuration was used throughout the experiments presented in this chapter.

5.4.1 Validation of the accuracy of the complementary filter implementation under controlled conditions

A controlled experiment was performed to learn about the techniques and behavior of the filter. The experiment consisted of provoking inverse pendulum controlled movements of the ski pole where the ski pole was oscillated from the vertical position to an incline position of ±15.12°. This is shown in Figure 5.4. According to this setup, the ski pole oscillation should have a total travel of 30.24°.

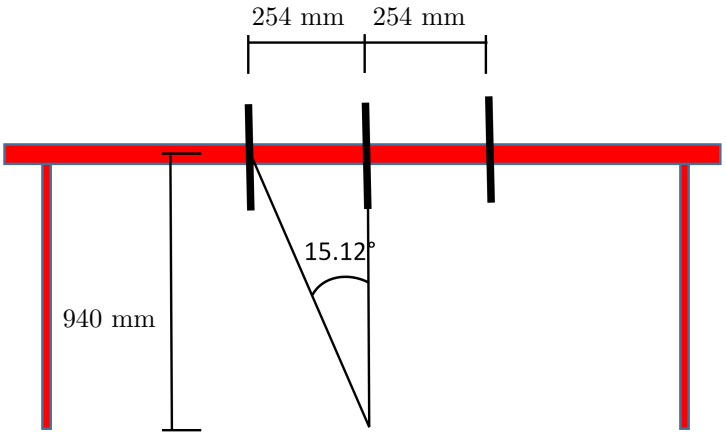

Figure 5.4. Inverted pendulum experiment setup.

For this experiment, two YEI 3-Space sensors (Yost Engineering, Portsmouth, Ohio) were attached to the had grip and tip area as shown in Figure 5.5.

(a) Hand grip mounted sensor.

(b) Tip mounted sensor.

Figure 5.5. YEI 3-Space sensors mounted on a) hand grip area and b) tip area. The tip area is considered the closest point of the pole to the ground when in contact. To avoid the relative movement between the sensors and the body of the ski pole, an adhesive tape is used in the position where the sensors are mounted. Then, sensors are fixed to the body using a pair of zip–ties.

These sensors are capable of measuring angular rates up to 2000 °/s with a 16–bit resolution, and a 0.03 °/s/$\sqrt{\text{Hz}}$ noise floor. The acceleration has an adjustable range up to 24 G's, with a 14–bit resolution and a 650 μg/$\sqrt{\text{Hz}}$ noise floor.

The sensors' calibration data were previously obtained by the researchers in the laboratory of Dynamics of Human Motion [31]. Then, the measured data written on the internal flash memory on each sensor were retrieved using a USB connection and a MATLAB code developed by the laboratory researchers for this purpose. All of the data processing was done successively in MATLAB. At this point, the interest was focused on the travel angle captured by the hand grip sensor. The angle read by this sensor should be close to the theoretical travel angle for which the experiment was designed. One of the results of these experiments can be seen in Figure 5.6.

5.4.2 Ski pole plant and lift instant extraction from IMU data

To validate the hypotheses proposed in section 5.2, the same sensor setup used in section 5.4.1 setup was used. The experiments consisted of performing several Nordic walk trials on a flat surface of approximately six meters. The author served as test subject in all of the cases presented in this section.

The sensor systems employed in the experiment lacked proper synchronization software. This obligates the users to develop their own synchronization routines to

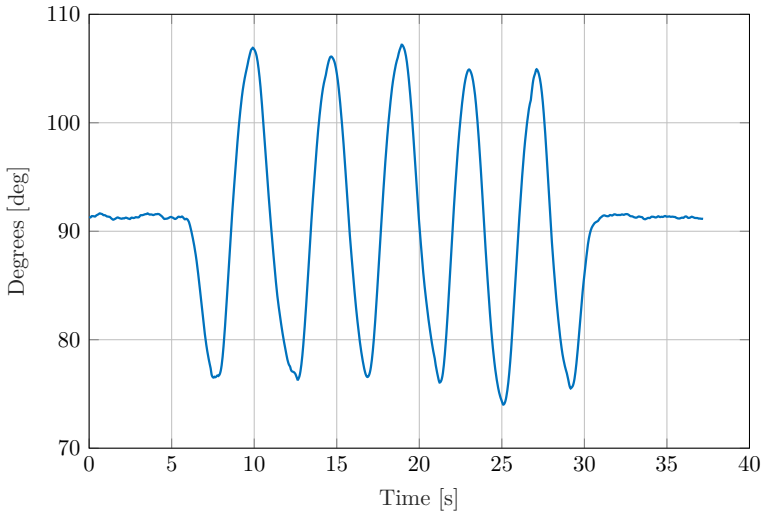

Figure 5.6. Ski pole orientation obtained from the hand grip IMU reading and processed by the complementary filter algorithm.

match the data measured from the IMUs. In this experiment, the synchronization action was induced by tapping the ski pole three times against the ground at the beginning and end of the walking trial. Tapping the ski poles produces visible peaks which serve as synchronization points. Using three taps reduces the synchronization algorithm to a manual task which involves a simple time axis alignment between the signals.

5.5 Results

After applying the algorithm proposed by McGinnis, it was found that averaging the start and end point values of the experiment and subtracts them, a difference of $91.37° - 91.31° = 0.06°$ is obtained. The mean of the difference of the maximum and minimum peak angles in the ski pole oscillation was found to be 30.245°, which presents a difference of 0.05° with respect to the theoretical expected value. The results present an angle determination free from the typical drift found in angle calculations using the angular velocity measured by the gyroscope.

Figure 5.7 presents the acceleration measurement from the hand grip IMU of one of the trials. At first sight, the figure seems to convey little information; however, if we focus on the signal peaks, we can distinguish three sectors. The first sector corresponds with the initial synchronization tapping (three in total), the second sector belongs to the walking action, and finally, in the the last sector we find the last synchronization tapping.

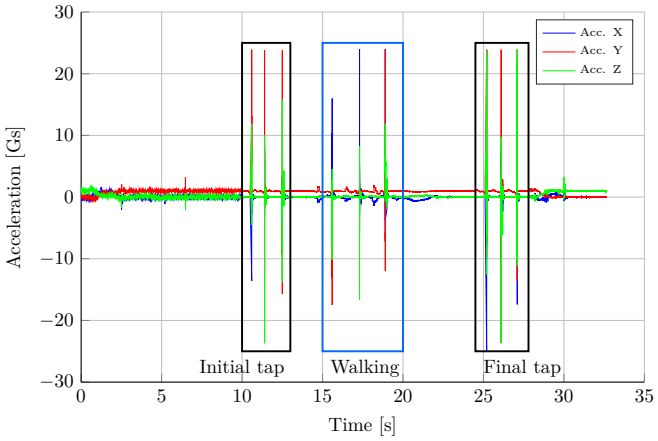

Figure 5.7. Sample of a Nordic walk experiment. Values of the acceleration measured by the hand grip IMU represented in the sensor reference system.

Although it might be evident that sectors 1 and 3 are the synchronization moments, what happens during walking is not clear. The magnitude of the acceleration peaks during walking minimizes the part of the signal of interest. Analyzing the sensor axis information separately will make proving the contact hypotheses difficult.

Instead, if we choose the magnitude of the acceleration measured in the sensor reference system, then the information it conveys will be much clearer. This can be seen in Figure 5.8.

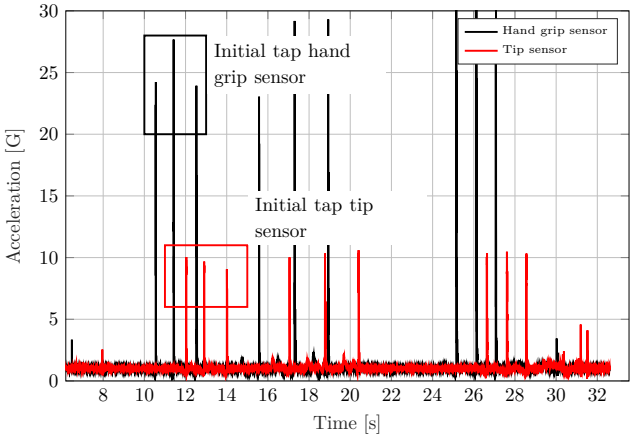

Figure 5.8. Magnitude of the acceleration measured in both sensors mounted on the ski pole. The aim of using the magnitude of the acceleration is to detail the pole plant and lift behavior on these curves instead of using separate signals which are highly dependent on the sensor orientation.

Using these clear tapping points, the manual synchronization is performed and the resultant signals match perfectly. This can be observed in Figure 5.9. Additionally, it is possible to easily identify the following parts of the walking: pole plant characterized by the highest peak in the walking sector, pole cycle defined between two pole plants, and pole lift, which cannot be detected visually, but the time span when it occurs is rapidly located, pole contact occurring between the pole plant and lift and the flying phase between the pole lift and the next pole plant.

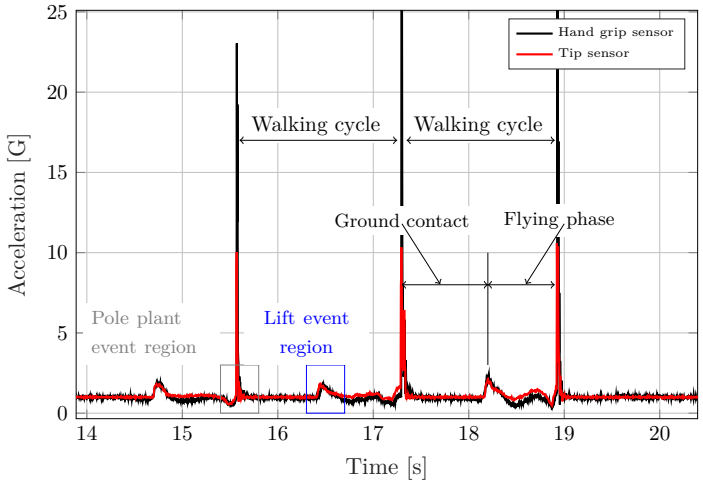

Figure 5.9. Signals from hand grip and tip sensors synchronized. Some of the important characteristics in the walking action are found.

Knowing that the beginning of the pole plant is represented by the highest peak during walking, it is possible to impose the hypotheses proposed in section 5.2 to find the pole lift instant. Additionally, these hypotheses will help us discard any extra high peak that might appear during the activity due to other factors such as the pole hitting any other surface or the body of the test subject.

Before showing the results of applying the hypotheses presented in section 5.2, it is important at this point to present the method used to validate the contact points. Other studies used a motion capture system based on cameras to determine the contact instants of the ski pole. In this case, a push–button attached to the tip of the ski pole is used. The push–button setup is shown in Figure 5.10

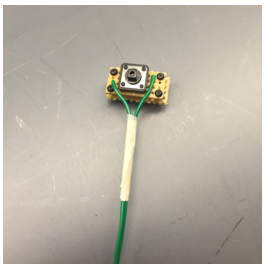

(a) Configuration of the push–button used.

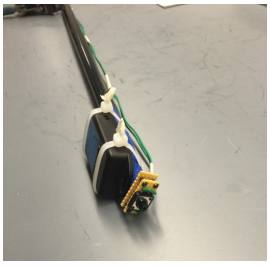

(b) Push–button installed in the pole tip area.

Figure 5.10. Push–button setup to detect the contact phases of the ski pole during the experiments.

Every contact action of the ski pole against the ground passed through the push–button assembly. When the ski pole is in contact with the ground, the push–button sends an active signal to the data–logging system which is responsible for acquiring this data at a frequency of approximately 100 Hz. The data logging systems comprise an Arduino UNO board and an SD card shield capable of storing up to 2 gigabytes of information. The system was powered with a 9 V battery. Figure 5.11 presents the details of this system setup.

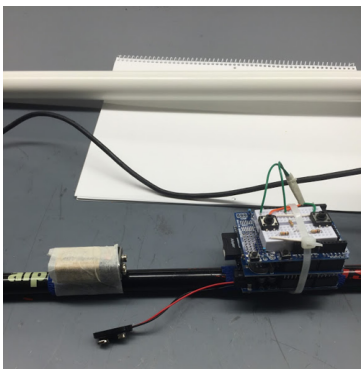

Figure 5.11. Details of the data–logging systems used to acquire the push–button data.

The data obtained from this push–button data–logging system is easily retrieved by reading the SD card in a computer. The data collected only comprises the time stamp and situation of the push–button – activated or not. Figure 5.12 visualizes an example of the data. To minimize the mechanical bouncing when using this type of mechanical push–button, a combination of a software debouncing algorithm and additional hardware elements were used.

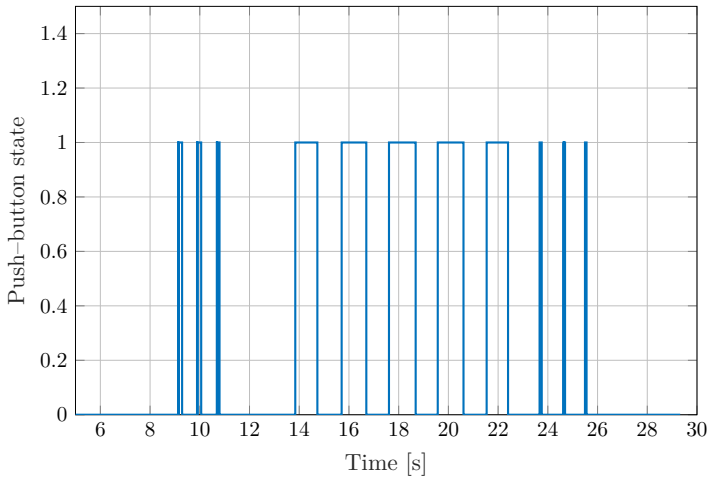

Figure 5.12. Example signal obtained from the push–button setup. There are only two states in these measurements: non–active and active.

Next, in Figure 5.13, two signals are superimposed: the push–button signal and the magnitude of the acceleration measured by the hand grip sensor. This graph of superimposed signals is important to the determination of the pole–plant and pole list–off instants.

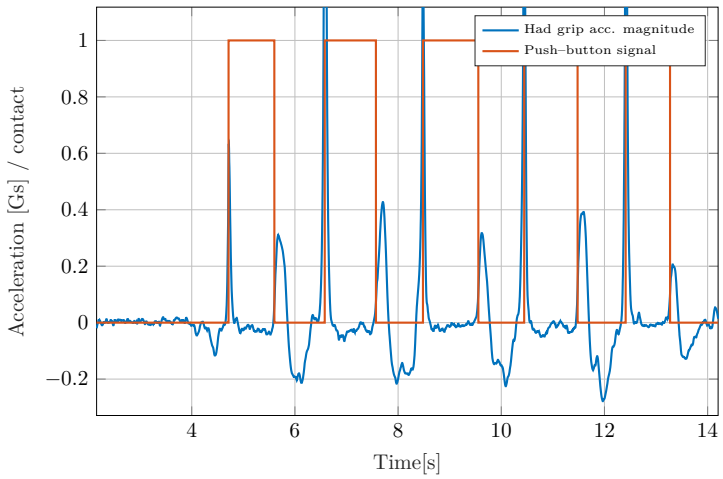

Figure 5.13. Comparison of the push–button signal and the signal obtained from the IMU setup.

5.6 Discussion

The complementary filter used here has already been validated in several dynamic applications [38, 40, 41]. The test done in this experiment had the purpose of getting familiar with the application of the filter. With the values obtained using the complementary filter, it was possible to account for the roll and pitch angles obtained during the inverted pendulum movement of the ski pole. The yaw angle remains unknown as there is no possibility to orientate the global reference system with respect to the the vertical axis aligned with the gravity. Because of the absence of a fixed global horizontal axis, as the one defined by the magnetic pole when using magnetometers, the solutions to the problem of transforming the sensor reference system to the global reference system are infinite.

Another important objective of the experiments performed was to validate one specific hypothesis found in the literature. In the research performed by Fasel et al. [16], the pole lift instant was considered to be at the peak at the end of the contact phase. However, Figure 5.13 shows that the contact is lost before the instant proposed in [16].

Pole–ground contact detection is important to account for the ski pole forces correctly. Applying the hypotheses proposed in section 5.2, it is possible to start drawing specific conclusion for each of these hypotheses and their applicability to determine pole plant and pole lift contact instants.

As mentioned previously when the linear velocity assumption was introduced in section 5.2, the description of the plant and lift instants would be determined by the linear velocity ratio. One of the drawbacks of utilizing this method was that the value of this ratio could vary during the inverted pendulum movement, making a strong conclusion difficult to draw.

Figure 5.14 illustrates that the behavior of the ratio during the pole–plant phase, characterized by the high level of the push–button signal, is difficult to differentiate from the swing phase. Besides, during the pole–plant, the velocity ratio changes instead of being constant, as ideally hypothesized.

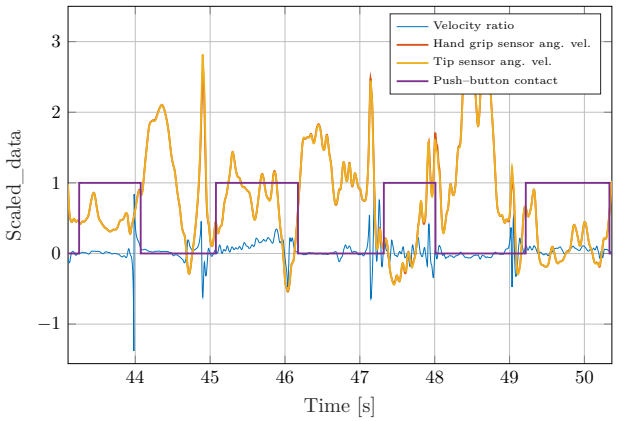

Figure 5.14. Detail of the accelerations, push–button data, and velocity ratio measured by the sensors during the walking trial.

For the case of the acceleration hypothesis, the results obtained are more promising. The initial thought of utilizing two sensors, one at the pole tip and another at the hand grip to gather the necessary information to determine contact instants was tested. Figure 5.15 displays that during the pole plant phase, both accelerations are quite similar to each other. At this point, it is presumable to utilize just one sensor to detect the pole plant and lift phases if the hypothesis related the the acceleration presented in section 5.2 is met. It is evident that using a sensor near the tip of the ski pole could present some disadvantages such as the inherent inconvenience of the location. The hand grip sensor, instead, is conveniently positioned in a secure location, and it can be used to determine the pole plant and lift instants.

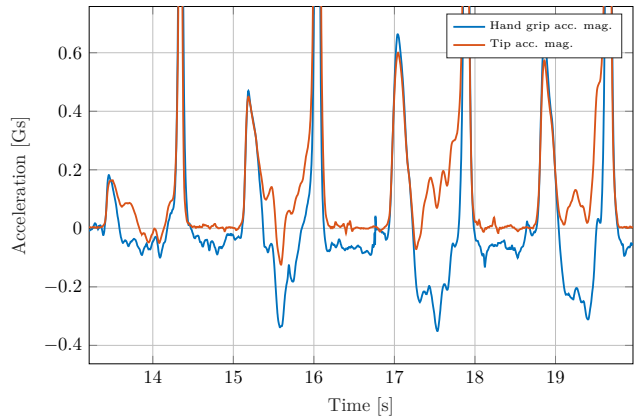

Figure 5.15. Detail of the accelerations measured by the hand grip and tip IMUs during the walking trial.

Figures 5.16 and 5.17 show the results of applying the second assumption to the experiment. Although the assumption of equality between the calculated linear acceleration and the measured sensor acceleration during the pole plant phase is far from being a perfect match, there exists a correlation between theses two signals during the pole plant phase.

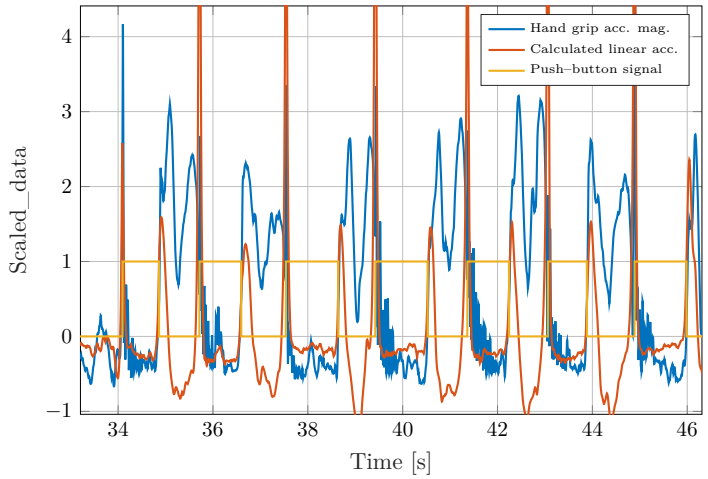

Figure 5.16. Verification of the second hypothesis using the hand grip IMU.

Actually, as can be seen in Figure 5.17, the change in the push–button signal corresponds closely to the instant where both signals (calculated and measured acceleration) start drifting apart. The problem now is to identify this point for each pole plant phase.

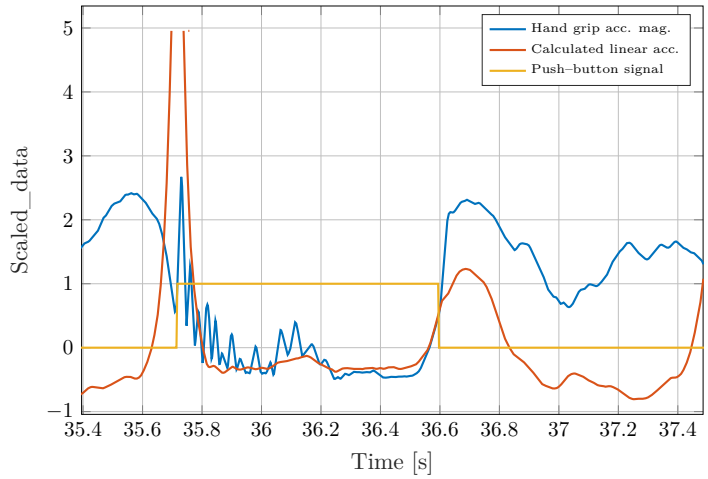

Figure 5.17. Verification of the second constraint: details of one walking cycle.

To accomplish the automatic selection of the closest point to the push–button down signal, the following condition is added: the automatic algorithm will calculate for the difference between the calculated and measured acceleration signals. A arbitrary threshold will be imposed which will make the value of this difference zero if the threshold value is not met. Another possibility would be to look for the intersection point between the calculated and measured signals in the interval formed by the flat zone of the measured acceleration signal and the first of the characteristic double peaks formed by the calculated signal.

Figure 5.18 shows the graphic results of imposing the automatic detection algorithm via a threshold condition. It is found that the mean of the difference between the computation of the constraint and signal button difference was about 7 ms and its standard deviation is 25.8 μs out of the tests selected for the estimation.

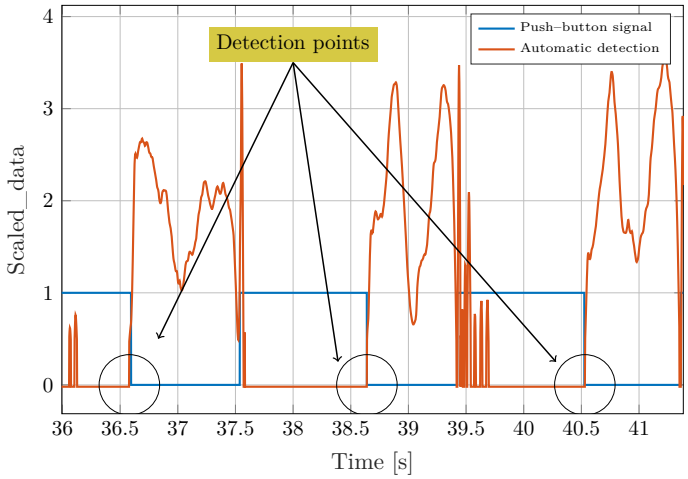

Figure 5.18. Results of imposing the threshold condition the calculated and measured acceleration differences.

Figures 5.19 and 5.20 show the results of using the complementary filter to determine the pitch and roll angle. Figure 5.20 details the typical behavior of the pith and roll angle during the pole plant phase. While the roll angle might stay close to the initial angle at the beginning of the movement, the pitch angle presents the larger variation.

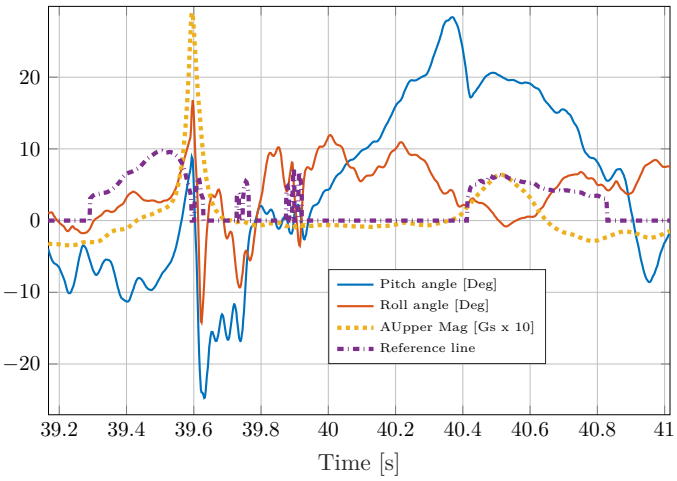

Figure 5.19. Pitch and roll angles shown with the correspondent acceleration and reference signal to estimate the pole lift instant.

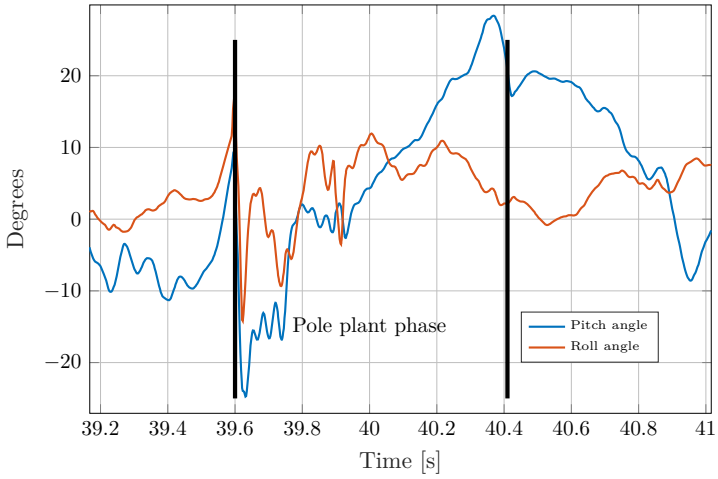

Figure 5.20. Pitch and roll angles shown isolated from the rest of the signals.

5.7 Conclusions

The behavior of the complementary filter was consistent during the experiments performed to estimate the partial orientation (roll and pitch) and the pole–ground contact instants. In the case of the two main skiing techniques existent in cross–country skiing, classic and skating, roll and pitch angle are considered as the main angles providing the most information to calculate ski pole force components. The yaw, not accounted in this experiments, is important from an athlete's execution

technique point of view. There is no doubt of the influence of the technique in obtaining larger propulsion forces; However, this topic was not planned to be addressed at this moment.

Different methods found in the literature deal with algorithms to estimate pole–ground contact instants. Each one of them provides advantages and their results might be said to be close to the vicinity of the real contact and lift instants. In this dissertation, another method was provided based on exploiting a few kinematic relationships of the parameters directly read by the IMUs. The first supposition where two sensors were used to estimate the contact instants based on their linear velocity ratio led to unsatisfactory results. The second approach, where the measured acceleration was compared against a calculated acceleration, provided better results. These results were compared with those produced by a contact detection system based on a push–button installed at the tip of the pole. The push–button system detected precisely the contact instants of the poles and it can be said that it provides a reliable source to compare the results obtained in the experiments. After the application of the hypothesis based on accelerations, it was found a difference of approx. 7 ms between the push–button system and the proposed algorithm. This difference in the contact detection is improved when compared with the results obtained by applying the method presented by Fasel et al. [16] of 14 ms or those found by using the algorithm developed in Myklebust, Losnegard and Hallén [50] of 12 ms.

Chapter 6

Conclusions

This dissertation presents the findings of studies on the dynamics of cross–country skiing – specifically the skate technique. The content of this work introduces in their chapters three main concepts applicable to the development of the study of skiing dynamics. The study field includes the utilization of the multibody dynamics theory, the application of speech analysis techniques, and the manipulation of information acquired from IMU sensors.

The mix of approached in this dissertation yields a wealth of knowledge that might be used to fill in information gaps in the field of skiing and develop the sport further. The dissertation may also contribute to the creation of a more complete evaluation system based on computer simulations.

This dissertation presents the following key conclusions:

- The dynamics of the cross–country skate skiing technique can be simulated using the multibody systems theory.
- The evolution of an athlete's performance can be quantified by applying techniques used in speed recognition, such as the DTW technique.
- IMUs can be used to estimate the skier's pole orientation and floor contact period during the execution of the technique.

For the first key conclusion, two models were developed. The aims of the models were to replicate the movement of the center of mass of the skier using a reduced number of bodies to represent the skier and to estimate the propulsion force exerted by the skier's leg. For both models, several assumptions were made regarding the interrelation between the skier's body parts, the ski–snow contact and the skier's

body mass distribution to simplify the simulation of the full body dynamics. In the first model, the constraints representing the lower leg joints were selected such as these constraints did not reproduce exactly the natural movements of the leg joints. Instead, a series of composed movements were proposed to match the skier's leg movement, and thus, to achieve the natural movement of the center of mass of the skier. For the second model, the constraints representing the lower leg joints were selected to match the joint's natural behavior. The ski was considered to move in a straight line on the snow, although in reality, the travel of the ski on the snow is non–rectilinear. Regarding the mass distribution of the skier, the lower leg was considered to have, in both models, its real mass while the mass of the rest of the body was considered to be located on the top of the femur. The results obtained in both models can be considered closed to the data measured via camera–based systems for the body movement and force measurement systems for the leg propulsion forces. For the center of mass of the skier, the position simulation results are close to the results measured by camera–based systems, and the model was able to produce results with a difference of 10.78% with respect to the measured velocity. The second model was able to replicate the leg propulsive force with a Pearson correlation coefficient of 0.94.

The second key conclusion is related to how it would be possible to compare two sets of data to evaluate the evolution of the execution of the skiing activity. This apart introduces a novel technique, applied frequently in the field of speech recognition, to compare two sets of data based on time. This technique is suitable as it disregards the meadurement technology, the effects of unequal acquisition rate sampling, the amount of data acquired, and time interval differences. After the application of the implementation algorithm, DTW produces two reorganized data sets which can be compared directly without further manipulation. The ease of automation in the application of the DTW to the skier's data series opens the door for more advance evaluation systems where a diagnosis of the evolution of athletes' technique could be assessed to detect the main differences which make one athlete perform better.

Finally, the IMU technology was used to estimate pole–ground contact events and the orientation angles of the ski pole during a Nordic walking trial. A simple setup allowed for the accurate estimation of two of the most important ski pole angles: pitch and roll. These angles, in conjunction with the use of an axial force measurement system, and the pole–ground contact detection, will allow us to estimate the skier's poling forces during the execution of the technique. This piece of information adds a great deal to the study of how the skier can benefit from the ski pole forces and which are the characteristics of an effective poling action and. Little has been done in this regard, and the findings of the experiments in this dissertation can be used further to develop the use of these inexpensive sensors for determining the positive evolution of the poling technique.

6.1 Suggestions for future work

This dissertation contributes to the scientific and sports literature related to skiing techniques. This information can be used further to develop certain, little examined areas not only in the field of skiing but also in other closely related fields. However, much experimental and theoretical research is still required. Below are a few suggestions for future works for researchers interested in the topic.

- A more extended dynamic model of a skier's body could benefit the study of specific cases, such paralympic athletes and the effect of the different parts of the human body on the different skiing techniques.
- Detail dynamic models of the skier's body and specific joints such as the knee joint could help to study more in detail the causes of injuries in athletes and practitioners. The combination of these dynamic models and finite element concepts could improve the scientific level of the study of these injuries, and researchers could even simulate different scenarios.
- The effect of the ski–snow interaction as well as the impact of clothing on skier's performance could benefit from extended dynamic models.
- The algorithms used to estimate positions and orientations from the information produced by IMU systems need to be refined more. This is necessary to take full advantage of the long–term acquisition capabilities of these IMU systems.

[1] Vicon Motion Systems LTD. UK., 2015.

[2] XSens Technologies., 2015.

[3] Aach, J., and Church, G. M. Aligning gene expression time series with time warping algorithms. *Bioinformatics 17*, 6 (2001), 495–508.

[4] Andersen, C. R. Determination of rigid body registration marker error from edge error. *Journal of Biomechanics 42*, 7 (2009), 949–951.

[5] Babiel, S. Studies on intra-individual variability of selected cross-country skiing techniques. *European Journal of Sport Science 3*, 3 (2003), 1–10.

[6] Bilodeau, B., Boulay, M. R., and Roy, B. Propulsive and gliding phases in four cross-country skiing techniques. *Medicine and Science in Sports and Exercise 24*, 8 (1992), 917–25.

[7] Blajer, W. Augmented Lagrangian formulation: Geometrical interpretation and application to systems with singularities and redundancy. *Multibody System Dynamics 8*, 2 (2002), 141–159.

[8] Bland, J. M., and Altman, D. G. Statistical methods for assessing agreement between two methods of clinical measurement. *Lancet 1*, fig 1 (1986), 307–310.

[9] Bruzzo, J., Schwab, A. L., Mikkola, A., Ohtonen, O., and Linnamo, V. A simple multibody dynamic model of cross-country ski-skating. In *ASME, International Design Engineering Technical Conferences IDETC2013* (2013).

[10] Canclini, A., Pozzo, R., Moriconi, B., and Cotelli, F. 3D and 2D kinematic analysis of classical technique in elite cross country skiers during a world cup race (S. Caterina 1995) and world championships (Ramsau 1999). *Proceedings ICSS 2000 – Austria*, Ramsau 1999 (2000), 3–9.

[11] Chen, L., and Qi, Z.-H. A 2-dimensional multi rigid bodies skiing model. *Multibody System Dynamics 21*, 1 (2009), 91–98.

[12] Cignetti, F., Schena, F., Zanone, P., and Rouard, A. Dynamics of coordination in cross-country skiing. *Human Movement Science 28*, 2 (2009), 204–217.

[13] Colbeck, S. C. The kinetic friction of snow. *Joumal of Glaciology 34*, 116 (1988), 78–86.

[14] Cuadrado, J., Cardenal, J., and Bayo, E. Modeling and Solution Methods for Efficient Real-Time Simulation of Multibody Dynamics. *Multibody System Dynamics 1* (1997), 259–280.

[15] Ekström, H. Force interplay in cross-country skiing. *Scandinavian Journal of Sports Sciences 3*, 2 (1981), 69–76.

[16] Fasel, B., Favre, J., Chardonnens, J., Gremion, G., and Aminian, K. An inertial sensor-based system for spatio-temporal analysis in classic cross-country skiing diagonal technique. *Journal of Biomechanics 48*, 12 (9 2015), 3199–3205.

[17] Federolf, P., Reid, R., Gilgien, M., Haugen, P., and Smith, G. The application of principal component analysis to quantify technique in sports. *Scandinavian Journal of Medicine and Science in Sports 24*, 3 (2014), 491–499.

[18] Filippi Oberegger, U., Kaps, P., Mössner, M., Heinrich, D., and Nachbauer, W. Simulation of turns with a 3D skier model. *Procedia Engineering 2*, 2 (2010), 3171–3177.

[19] Fintelman, D. M., Braver, O. D., and Schwab, A. L. A simple 2-dimensional model of speed skating which mimics observed forces and motions. In *Multibody dynamics ECCOMAS, Brussels, Belgium* (2011).

[20] Flores, P., Ambrósio, J., Claro, J. P., and Lankarani, H. M. *Kinematics and Dynamics of Multibody Systems with Imperfect Joints*, vol. 34. 2008.

[21] Flores, P., Pereira, R., Machado, M., and Seabra, E. Investigation on the Baumgarte stabilization method for dynamic analysis of constrained multibody systems. In *Eucomes 08, the Second European Conference on Mechanism Science* (2009).

[22] Full, R. J., Koditschek, D. E., and Full, R. J. Templates and anchors: neuromechanical hypotheses of legged locomotion on land. *The Journal of Experimental Biology 2*, 12 (1999), 3–125.

[23] Giavarina, D. Understanding Bland Altman analysis. *Biochemia Medica 25*, 2 (2015), 141–151.

[24] Gilgien, M., Spörri, J., Chardonnens, J., Kröll, J., and Müller, E. Determination of external forces in alpine skiing using a differential global navigation satellite system. *Sensors 13*, 8 (2013), 9821–9835.

[25] Holmberg, H. C., Lindinger, S., Stöggl, T., Eitzlmair, E., and Müller, E. Biomechanical analysis of double poling in elite cross-country skiers. *Medicine and Science in Sports and Exercise 37*, 5 (2005), 807–818.

[26] Holmberg, J., and Wagenius, P. A biomechanical model of a double-poling skier. In *International Society of Biomechanics XIXth Congress : the human body in motion, 6-11 July 2003, Dunedin New Zealand, Dunedin, N.Z.* 2003.

[27] Holmberg, L. J., and Lund, A. M. Using double - poling simulations to study the load distribution between teres major and latissimus dorsi. In *In Science and Nordic Skiing, Linnamo, V., Komi, P.V. and Müller, E. (Eds.), Meyer and Meyer Sport, Oxford, UK.* Meyer and Meyer Sport, Oxford, UK, 2007, pp. 81–89.

[28] Holmberg, L. J., and Lund, A. M. A musculoskeletal full-body simulation of cross-country skiing. *Proceedings of the Institution of Mechanical Engineers, Part P: Journal of Sports Engineering and Technology 222*, 1 (2008), 11–22.

[29] Kalman, R., and others. A new approach to linear filtering and prediction problems. *Journal of Basic Engineering 82*, 1 (1960), 35–45.

[30] Kaltenbach, H.-M. *A Concise Guide to Statistics.* 2012.

[31] King, K. *The Design and Application of MEMS Inertial Measurement Units for the Measurement and Analysis of Golf Swings.* PhD thesis, University of Michigan, 2008.

[32] Komi, P. V. Force measurements during cross-country skiing. *International Journal of Sports Biomechanics 3*, 4 (1987), 370–381.

[33] Krichko, K. China's Stone Age Skiers and History's Harsh Lessons - The New York Times.

[34] Little, C., Lee, J. B., James, D. A., and Davison, K. An evaluation of inertial sensor technology in the discrimination of human gait. *Journal of Sports Sciences 31*, 12 (2013), 1312–1318.

[35] Liu, C. K., and Popović, Z. Synthesis of complex dynamic character motion from simple animations. *ACM Transactions on Graphics 21*, 3 (2002), 408–416.

[36] Lund, A. M., and Holmberg, J. L. Which are the antagonists to the pectoralis major muscle in 4th gear free-style technique, cross-country skiing? In *In Science and Nordic Skiing* (2007), V. Linnamo, P. Komi, and E. Müller, Eds., Meyer and Meyer Sport, Oxford, UK, pp. 112–118.

[37] Lützner, C., Voigt, H., Roeder, I., Kirschner, S., and Lützner, J. Placement makes a difference: Accuracy of an accelerometer in measuring step number and stair climbing. *Gait & Posture 39*, 4 (4 2014), 1126–1132.

[38] Mcginnis, R., Cain, S., Mcginnis, R. S., Arbor, A., Arbor, A., Cain, S. M., and Mclean, S. G. Validation of Complementary Filter Based IMU Data Fusion for Tracking Torso Angle and Rifle Orientation.

[39] McGinnis, R. S. *Advancing Applications of IMUs in Sports Training and Biomechanics*. PhD thesis, 2013.

[40] McGinnis, R. S., Cain, S. M., Tao, S., Whiteside, D., Goulet, G. C., Gardner, E. C., Bedi, A., and Perkins, N. C. Accuracy of femur angles estimated by IMUs during clinical procedures used to diagnose femoroacetabular impingement. *IEEE Transactions on Biomedical Engineering 62*, 6 (2015), 1503–1513.

[41] McGinnis, R. S., and Perkins, N. C. A highly miniaturized, wireless inertial measurement unit for characterizing the dynamics of pitched baseballs and softballs. *Sensors 12*, 9 (2012), 11933–11945.

[42] McKenne, K. Introduction to Cross Country Skiing [Blog] Cross Country Ski Technique, 2014.

[43] Meyer, F., Le Pelley, D., and Borrani, F. Aerodynamic drag modeling of alpine skiers performing giant slalom turns. *Medicine and Science in Sports and Exercise 44*, 6 (2012), 1109–1115.

[44] Millard, M., Kubica, E., and McPhee, J. Forward dynamic human gait simulation using a SLIP target model. *Procedia IUTAM 2* (2011), 142–157.

[45] Millet, G. Y., Hoffman, M. D., Candau, R. B., Buckwalter, J. B., and Clifford, P. S. Cycle rate variations in roller ski skating: effects on oxygen uptake and poling forces. *International journal of sports medicine 19*, 8 (1998), 521–5.

[46] Millet, G Y, Hoffman, M D, Candau, R B, and Clifford, P. S. Poling forces during roller skiing: effects of grade, 1997.

[47] Moxnes, J. F., and Hausken, K. A dynamic model of Nordic diagonal stride skiing, with a literature review of cross country skiing. *Computer Methods in Biomechanics and Biomedical Engineering 12*, 5 (2009), 531–551.

[48] Müller, M. Dynamic Time Warping. In *Information Retrieval for Music and Motion*. Springer Berlin Heidelberg, Berlin, Heidelberg, 2007, pp. 69–84.

[49] Müller, W. The physics of ski jumping. *2005 European School of High-Energy Physics* (2006), 269–277.

[50] Myklebust, H., Losnegard, T., and Hallén, J. Differences in V1 and V2 ski skating techniques described by accelerometers. *Scandinavian Journal of Medicine & Science in Sports 24*, 6 (2014), 882–893.

[51] Nilsson, J., Jakobsen, V., Tveit, P., and Eikrehagen, O. Skiing. *Sports Biomechanics 2*, 2 (2003), 227–236.

[52] Nilsson, J., Jakobsen, V., Tveit, P., Eikrehagen, O., and Nilsson, J. Skiing: Pole length and ground reaction forces during maximal double poling in skiing. *Sports Biomechanics 2*, 2 (2003), 227–236.

[53] Nilsson, J., Tinmark, F., Halvorsen, K., and Arndt, A. Kinematic, kinetic and electromyographic adaptation to speed and resistance in double poling cross country skiing. *European Journal of Applied Physiology 113*, 6 (6 2013), 1385–1394.

[54] Ohtonen, O., Lindinger, S., Lemmettylä, T., Seppälä, S., and Linnamo, V. Validation of portable 2D force binding systems for cross-country skiing. *Sports Engineering 16*, 4 (2013).

[55] Ohtonen, O., Lindinger, S., and Linnamo, V. Effects of gliding properties of cross-country skis on the force production during skating technique in elite cross-country skiers. *International Journal of Sports Science and Coaching 8*, 2 (2013), 407–416.

[56] Okadome, T., and Honda, M. Trajectory formation in sequential arm movements: a critical investigation of optimization approach to human movement control. In *IEEE International Conference on Systems, Man, and Cybernetics* (1992), IEEE.

[57] Pellegrini, B., Bortolan, L., and Schena, F. Poling force analysis in diagonal stride at different grades in cross country skiers. *Scandinavian Journal of Medicine & Science in Sports 21*, 4 (8 2011), 589–597.

[58] Pellegrini, B., Zoppirolli, C., Bortolan, L., Zamparo, P., and Schena, F. Gait models and mechanical energy in three cross-country skiing techniques. *The Journal of Experimental Biology 217* (2014), 3910–3918.

[59] Petitjean, F., Ketterlin, A., and Gançarski, P. A global averaging method for dynamic time warping, with applications to clustering. *Pattern Recognition 44*, 3 (2011), 678–693.

[60] Piyush Shanker, A., and Rajagopalan, A. N. Off-line signature verification using DTW. *Pattern Recognition Letters 28*, 12 (2007), 1407–1414.

[61] Poulakakis, I., and Grizzle, J. W. Monopedal running control: SLIP embedding and virtual constraint controllers. *IEEE International Conference on Intelligent Robots and Systems* (2007), 323–330.

[62] Rosenberg, R. Why Is Ice Slippery? In 1859 Michael Faraday postulated that a thin film of liquid covers the surface of ice - even. *Physics Today 58* (2005), 50–55.

[63] Rusko, H. *Cross Country Skiing*. Blackwell Science, Malden, Mass., 2003.

[64] Sakoe, H., and Chiba, S. Dynamic programming algorithm optimization for spoken word recognition. *IEEE transactions on acoustics, speech, and signal processing 26*, 1 (1978), 43–49.

[65] Schiehlen, W. *Multibody Systems Handbook*, 1 ed. Springer-Verlag Berlin Heidelberg, 1990.

[66] Schwesig, R., Leuchte, S., Fischer, D., Ullmann, R., and Kluttig, A. Inertial sensor based reference gait data for healthy subjects. *Gait & posture 33*, 4 (4 2011), 673–8.

[67] Senin, P. Dynamic Time Warping Algorithm Review. Tech. rep., 2008.

[68] Seo, K., Watanabe, I., and Murakami, M. Aerodynamic force data for a V-style ski jumping flight. *Sports Engineering 7*, 1 (2004), 31–39.

[69] Shabana, A. A. *Dynamics of Multibody Systems*. Cambridge University Press, 1998.

[70] Shabana, A. A. *Computational Dynamics*. John Wiley & Sons, 2001.

[71] Simon, S. R. Quantification of human motion: Gait analysis - Benefits and limitations to its application to clinical problems. *Journal of Biomechanics 37*, 12 (2004), 1869–1880.

[72] Smith, G. A., and Holmberg, H.-C. Nordic skiing biomechanics and physiology. In *XXVIII International Symposium of Biomechanics in Sports* (2010).

[73] Smith, G. A., Nelson, R. C., Feldman, A., and Jeffrey, L. Analysis of VI Skating Technique of Olympic Cross-Country Skiers. *International Journal of Sport Biomechanics 5*, 2 (1989), 185–208.

[74] Stöggl, T., and Holmberg, H.-C. Force interaction and 3D pole movement in double poling. *Scandinavian Journal of Medicine & Science in Sports 21*, 6 (2011), 393–404.

[75] Stöggl, T., and Karlöf, L. Mechanical behaviour of cross-country ski racing poles during double poling. *Sports Biomechanics 12*, 4 (11 2013), 365–380.

[76] Stöggl, T. L., and Holmberg, H. C. Double-Poling Biomechanics of Elite Cross-country Skiers: Flat versus Uphill Terrain. *Medicine and Science in Sports and Exercise 48*, 8 (2016), 1580–1589.

[77] Street, G. M., and Frederick, E. C. Measurement of skier-generated forces during roller-ski skating. *Journal of Applied Biomechanics 11*, 3 (1995), 245–256.

[78] Supej, M., Sætran, L., Oggiano, L., Ettema, G., Šarabon, N., Nemec, B., and Holmberg, H. C. Aerodynamic drag is not the major determinant of performance during giant slalom skiing at the elite level. *Scandinavian Journal of Medicine and Science in Sports 23*, 1 (2013), 38–47.

[79] Theile, T., Szabo, D., Luthi, A., Rhyner, H., and Schneebeli, M. Mechanics of the ski-snow contact. *Tribology Letters 36*, 3 (2009), 223–231.

[80] UHP. Chinese or Norwegian: the History of Skiing - The Ultimate History Project.

[81] Vähäsöyrinki, P., Komi, P. V., Seppälä, S., Ishikawa, M., Kolehmainen, V., Salmi, J. A., and Linnamo, V. Effect of skiing speed on Ski and pole forces in cross-country skiing. *Medicine and Science in Sports and Exercise 40*, 6 (2008), 1111–1116.

[82] Vuokatti. Vuokatti city Website, 2013.

[83] Whittle, M. Clinical gait analysis: A review. *Human Movement Science 15*, 3 (1996), 369–387.

[84] Wittenburg, J. *Dynamics of multibody systems*. Springer Berlin Heidelberg, 2008.

[85] Yeadon, M. R. The simulation of aerial movement–II. A mathematical inertia model of the human body. *Journal of Biomechanics 23*, 1 (1990), 67–74.

[86] Yeow, D. Speed Skating Daily: Men's 500m [Blog] Daniel Yeow Blog, 2010.

[87] Zadravec, M., and Matjačić, Z. Planar arm movement trajectory formation: an optimization based simulation study. *Biocybernetics and Biomedical Engineering 33*, 2 (2013), 106–117.

[88] Zory, R., Vuillerme, N., Pellegrini, B., Schena, F., and Rouard, A. Effect of fatigue on double pole kinematics in sprint cross-country skiing. *Human Movement Science 28*, 1 (2009), 85–98.

ACTA UNIVERSITATIS LAPPEENRANTAENSIS

745. ROTICH, NICOLUS KIBET. Development and application of coupled discrete and continuum models in solid particles classification. 2017. Diss.

746. GAST, JOHANNA. The coopetition-innovation nexus: Investigating the role of coopetition for innovation in SMEs. 2017. Diss.

747. KAPOOR, RAHUL. Competition and disputes in the patent life cycle. 2017. Diss.

748. ALI-MARTTILA, MAAREN. Towards successful maintenance service networks – capturing different value creation strategies. 2017. Diss.

749. KASHANI, HAMED TASALLOTI. On dissimilar welding: a new approach for enhanced decision-making. 2017. Diss.

750. MVOLA BELINGA, ERIC MARTIAL. Effects of adaptive GMAW processes: performance and dissimilar weld quality. 2017. Diss.

751. KARTTUNEN, JUSSI. Current harmonic compensation in dual three-phase permanent magnet synchronous machines. 2017. Diss.

752. SHI, SHANSHUANG. Development of the EAST articulated maintenance arm and an algorithm study of deflection prediction and error compensation. 2017. Diss.

753. CHEN, JIE. Institutions, social entrepreneurship, and internationalization. 2017. Diss.

754. HUOTARI, PONTUS. Strategic interaction in platform-based markets: An agent-based simulation approach. 2017. Diss.

755. QU, BIN. Water chemistry and greenhouse gases emissions in the rivers of the "Third Pole" / Water Tower of Asia". 2017. Diss.

756. KARHU, PÄIVI. Cognitive ambidexterity: Examination of the cognitive dimension in decision-making dualities. 2017. Diss.

757. AGAFONOVA, OXANA. A numerical study of forest influences on the atmospheric boundary layer and wind turbines. 2017. Diss.

758. AZAM, RAHAMATHUNNISA MUHAMMAD. The study of chromium nitride coating by asymmetric bipolar pulsed DC reactive magnetron sputtering. 2017. Diss.

759. AHI, MOHAMADALI. Foreign market entry mode decision-making: Insights from real options reasoning. 2017. Diss.

760. AL HAMDI, ABDULLAH. Synthesis and comparison of the photocatalytic activities of antimony, iodide and rare earth metals on SnO2 for the photodegradation of phenol and its intermediates under UV, solar and visible light irradiations. 2017. Diss.

761. KAUTTO, JESSE. Evaluation of two pulping-based biorefinery concepts. 2017. Diss.

762. AFZALIFAR, ALI. Modelling nucleating flows of steam. 2017. Diss.

763. VANNINEN, HEINI. Micromultinationals - antecedents, processes and outcomes of the multinationalization of small- and medium-sized firms. 2017. Diss.

764. DEVIATKIN, IVAN. The role of waste pretreatment on the environmental sustainability of waste management. 2017. Diss.

765. TOGHYANI, AMIR. Effect of temperature on the shaping process of an extruded wood-plastic composite (WPC) profile in a novel post-production process. 2017. Diss.

766. LAAKKONEN, JUSSI. An approach for distinct information privacy risk assessment. 2017. Diss.

767. KASURINEN, HELI. Identifying the opportunities to develop holistically sustainable bioenergy business. 2017. Diss.

768. KESKISAARI, ANNA. The impact of recycled raw materials on the properties of wood-plastic composites. 2017. Diss.

769. JUKKA, MINNA. Perceptions of international buyer-supplier relational exchange. 2017. Diss.

770. BAYGILDINA, ELVIRA. Thermal load analysis and monitoring of doubly-fed wind power converters in low wind speed conditions. 2017. Diss.

771. STADE, SAM. Examination of the compaction of ultrafiltration membranes with ultrasonic time-domain reflectometry. 2017. Diss.

772. KOZLOVA, MARIIA. Analyzing the effects of a renewable energy support mechanism on investments under uncertainty: case of Russia. 2017. Diss.

773. KURAMA, ONESFOLE. Similarity based classification methods with different aggregation operators. 2017. Diss.

774. LYYTIKÄINEN, KATJA. Removal of xylan from birch kraft pulps and the effect of its removal on fiber properties, colloidal interactions and retention in papermaking. 2017. Diss.

775. GAFUROV, SALIMZHAN. Theoretical and experimental analysis of dynamic loading of a two-stage aircraft engine fuel pump and methods for its decreasing. 2017. Diss.

776. KULESHOV, DMITRII. Modelling the operation of short-term electricity market in Russia. 2017. Diss.

777. SAARI, JUSSI. Improving the effectiveness and profitability of thermal conversion of biomass. 2017. Diss.

778. ZHAO, FEIPING. Cross-linked chitosan and β-cyclodextrin as functional adsorbents in water treatment. 2017. Diss.

779. KORHONEN, ILKKA. Mobile sensor for measurements inside combustion chamber – preliminary study. 2017. Diss.

780. SIKIÖ, PÄIVI. Dynamical tree models for high Reynolds number turbulence applied in fluid-solid systems of 1D-space and time. 2017. Diss.

781. ROMANENKO, ALEKSEI. Study of inverter-induced bearing damage monitoring in variable-speed-driven motor systems. 2017. Diss.

782. SIPILÄ, JENNI. The many faces of ambivalence in the decision-making process. 2017. Diss.

783. HAN, MEI. Hydrodynamics and mass transfer in airlift bioreactors; experimental and numerical simulation analysis. 2017. Diss.